Volume 21, Number 2

August, 1966

SOVIET ATOMIC ENERGY

АТОМНАЯ ЭНЕРГИЯ
(ATOMNAYA ÉNERGIYA)

TRANSLATED FROM RUSSIAN

CONSULTANTS BUREAU

SOVIET ATOMIC ENERGY

Soviet Atomic Energy is a cover-to-cover translation of *Atomnaya Énergiya*, a publication of the Academy of Sciences of the USSR.

An arrangement with Mezhdunarodnaya Kniga, the Soviet book export agency, makes available both advance copies of the Russian journal and original glossy photographs and artwork. This serves to decrease the necessary time lag between publication of the original and publication of the translation and helps to improve the quality of the latter. The translation began with the first issue of the Russian journal.

Subscription
(12 Issues): $95

Single Issue: $30
Single Article: $15

Order from:

CONSULTANTS BUREAU
227 West 17th Street, New York, New York 10011

SOVIET ATOMIC ENERGY

A translation of *Atomnaya Énergiya*

Volume 21, Number 2 August, 1966

CONTENTS

CONTENTS

(continued)

NOTE

The Table of Contents lists all material that appeared in the original Russian journal. Items originally published in English or generally available in the West are not included in the translation and are shown in brackets. Whenever possible, the English-language source containing the omitted items is given.

The Russian press date (podpisano k pechati) of this issue was 7/30/1966. Publication therefore did not occur prior to this date, but must be assumed to have taken place reasonably soon thereafter.

CHEMICAL PROPERTIES OF ELEMENT 104

I. Zvara, Yu. T. Chuburkov,
R. Tsaletka, T. S. Zvarova, M. R. Shalaevskii,
and B. V. Shilov

UDC 541.9:541.27

Using a method of rapid continuous separation of elements of the side groups III and IV of the D. I. Mendeleev Periodic System, developed by the authors of this work, the properties of the chlorides of curium, californium, hafnium, and the isotope 104^{260} were compared.

The isotope 104^{260} had until now been identified only by physical methods. It was established that its chemical properties differ from those of the actinide elements and are close to those of hafnium. An independent confirmation of the atomic number of the new nucleus was obtained, and it was simultaneously demonstrated that the element 104 is a member of group IV. In the experiments, 12 atoms of the isotope 104^{260} were recorded.

In [1] it was reported that when Pu^{242} is irradiated by accelerated Ne^{22} ions, the spontaneous fissioning isotope 104^{260}, with a half-life of ~ 0.3 sec, is formed. Physical methods were used to determine the atomic number and mass number of the isotope synthesized. It was demonstrated that the excitation function has the form expected for the reaction $Pu^{242}(Ne^{22}, 4n)104^{260}$. The value of the effective cross section at the maximum ($2 \cdot 10^{-34}$ cm^2 at a particle energy of 113-115 MeV) is close to the value predicted on the basis of empirical principles. In control experiments with other targets and bombarding particles, in which 104^{260} could not be formed, the isotope with the properties indicated above was not observed.

Considering the difficulty of studying the products of nuclear reactions with such low yields (approximately one atom in five hours of operation of the accelerator), the authors of [1] emphasize the importance of conducting chemical experiments for additional identification and a simultaneous study of the chemical properties of the new element.

According to the well-known actinide hypothesis [2], in the series of transuranium elements, there is a filling of the atomic 5f-electron shell, which leads to an analogy of the properties of these elements to the lanthanides. Element 103 should possess 14 5f-electrons. Element 104 should be the next member of the 6d-transition series, i.e., an analog of hafnium, and conseqeuntly, should differ sharply in chemical properties from the transuranium elements up to 103, synthesized in recent years.

For a chemical identification of element 104, the authors of this work undertook an attempt to compare the properties of the chlorides of curium, californium, hafnium, and the new element.

Earlier the authors of this work had developed a method of rapid continuous separation of the elements of the side groups III and IV of D. I. Mendeleev's Periodic System in the form of the gaseous chlorides [3, 4]. The products of nuclear reactions, flying out of a rather thin target on account of recoil, are chlorinated by reaction with $NbCl_5$ or $ZrCl_4$ in the vapor phase. The chlorides of the radioactive isotopes of zirconium and hafnium obtained are transported by the gas flow to a radiation detector. In this case, under the selected conditions, the chlorides of elements of group III are retained on the walls of the gas tract and on special filters on account of adsorption. The apparatus designed permits chemical operations with recoil atoms close to the irradiated targets, directly in the chamber of the cyclotron. The process of analysis is continuous and is conducted in a fraction of a second from the moment of formation of the atom.

Chemical experiments with the isotope 104^{260} were conducted on the multicharged ion accelerator of the United Institute of Nuclear Research. A target of PuO_2 (700 $\mu g/cm^2$), applied on aluminum foil, was used. Plutonium of the same composition as in [1], containing 97% of the isotope Pu^{242}, was used. The target was irradiated with Ne^{22} ions with an energy of 114 MeV at a beam intensity of $\sim 2 \cdot 10^{12}$ particles/sec.

Translated from Atomnaya Énergiya, Vol. 21, No. 2, pp. 83-84, August, 1966. Original article submitted May 18, 1966.

A mixture of $NbCl_5$ and $ZrCl_4$ vapors (3 : 1) was used as the chlorinating agent and carrier, with a total partial pressure of ~ 0.2 mm. The basic component of the gas mixture (by volume) was nitrogen, at a pressure of ~ 1.5 atm.

The fragments of spontaneous fission were indicated with mica detectors [5], which were washed with the stream of gas transporting the chlorides of elements of group IV. Directly before the experiment, the detectors were treated to remove the accumulated background from the spontaneous fission of the uranium impurity in the mica [6]. They were placed in a paraffin-cadmium shield, so as to reduce the possibility of fission of uranium under the influence of the neutron radiation of the accelerator.

Two series of experiments were conducted. In the first series the temperature of the gas tract was at a level of 220-250°C. The time of passage of the gas flow from the target to the detector was equal to ~ 0.2 sec; the duration of motion of the gas along the detector was ~ 1.2 sec (the area of the detectors was 1400 cm^2). No more than 0.4 sec was required for the chlorination and transport of the isotopes Hf^{170} and Hf^{171} to the detector; there were no losses of hafnium in the chemical process. At the same time, there was a separation of the isotopes of curium, californium, and scandium, with a purification factor of ~ 50. At an integral flux of $4 \cdot 10^{18}$ particles onto the target, i.e., in ~ 600 h of irradiation, four acts of fission were recorded, which is approximately 10 times lower than the effect expected from the isotope 104^{260}. Estimates of the possible background (spontaneous and forced fission of uranium impurities) give a value of no more than one event in the entire series of experiments.

In the second series of experiments, the temperature of the gas tract was raised to 300-350°C. The time of recording was 0.7 sec. In the presence of an integral flux of $6 \cdot 10^{17}$ particles on the target, i.e., in 90 h, eight acts of fission were recorded, which corresponds to the expected effect. The coefficient of purification from curium, californium, and scandium remained at the previous level. The distribution of all 12 acts of fission according to time intervals does not contradict the half-life 0.3 ± 0.1 sec, determined in [1] according to approximately 100 events.

The results cited show that the isotope synthesized is not similar to the heavy actinide elements in its chemical properties, and in certain properties of the higher chloride it is close to hafnium.

Thus, an independent identification of the atomic number of the nucleus studied was made by a chemical method, confirming the conclusion drawn in [1]. At the same time, it was demonstrated that the element 104 is a member of Group IV of the Periodic System.

The authors would like to express deep gratitude to Corresponding Member of the Academy of Sciences of the USSR, G. N. Flerov, for formulating the problem, for his numerous discussions, and his constant attention and support during the performance of the work; and are also grateful to V. P. Perelygin and S. P. Tret'yakova for their aid in the work with mica detectors, to L. K. Tarasov, M. Krzhivanek, Ya. Maly, I. V. Kolesov, and T. D. Zaitseva for their aid in developing the method, to K. A. Gavrilov for preparing the targets, and to the group operating the Y-300 accelerator for providing the work of the machine.

LITERATURE CITED

1. G. N. Flerov et al., Atomnaya Énergiya, 17, 310 (1964).
2. G. Seaborg, in the Collection: The Actinides [Russian translation], Editors G. Seaborg and J. Katz, Moscow, Izd. Inostr. Lit. (1955), p. 594.
3. I. Zvara et al., Radiokhimiya, 8, 77 (1966).
4. I. Zvara et al., Preprint of the United Institute of Nuclear Research, R-25-48, Dubna (1966).
5. P. Price and R. Walker, Phys. Letters, 3, 113 (1962).
6. A. Kapustsik et al., Preprint of the United Institute of Nuclear Research, R-2705, Dubna (1966).

USE OF NONURANIUM DILUENTS FOR PLUTONIUM IN LARGE FAST BREEDER REACTORS

A. I. Leipunskii, O. D. Kazachkovskii, S. B. Shikhov, L. N. Yurova, V. V. Khromov, A. N. Shmelev, and V. K. Sukhoruchkin

UDC 621.039.526:621.039.543.466

The authors study the physical characteristics of fast breeder reactors with cylindrical and ring-shaped cores, and also the characteristics of infinite lattices of heterogeneously-arranged large fuel cassettes distributed in the breeding-zone material.

It is shown that there are certain reactors with optimum doubling period.

In fast breeder reactors, there is a tendency to use fertile material (U^{238}, Th^{232} or their compounds) as diluent of the main fissile isotope in the core for the production of secondary fuel.

In reactors with a cylindrical core surrounded on all sides by the breeding zone, this achieves higher reproduction factors (RF) than those of reactors with other (nonfertile) diluents.

With a nonfertile diluent for the plutonium, the reproduction factor of the core (RFC) is equal to zero, while the reproduction factor of the screen (RFS) falls rapidly with increasing core size (the relative number of neutrons emitted into the screen goes down).

This fact limits the interest taken in nonfertile plutonium diluents, even if they have several advantages over fertile material (stability under high burnup and high temperatures, simplicity or cheapness of processing, etc.).*

The strict requirements which must be imposed on nonfertile diluents considerably narrow the range of choice. They must possess low elastic and inelastic slowing-down cross sections for fast neutrons, and also low capture cross sections for fast neutrons. Such a diluent is called "inert." In choosing it, we must confine ourselves either to weakly capturing nuclei (zirconium and its compounds) or to magic nuclei (Sr^{88}, Ba^{138}, etc.). But even in this case, attempts to use high powers (and hence large volumes) for the core lead to much lower RF than those for reactors with U^{238} as plutonium diluent.

Let us take an example. A fast breeder reactor with thick enough breeding zone of U^{238}, with a uranium–plutonium alloy in the core, a sodium heat-exchanger and stainless steel as structural material, has about the same RF (about 2)† for core volumes V_a ranging from 250 to 1000 liters.

If the plutonium diluent in the core is zirconium, then, with other conditions unaltered and $V_a = 250$ liters, RF = 1.7, while with $V_a = 1000$ liters, RF = 1.3. If we take iron as diluent, then with $V_a = 250$ liters, RF = 1.6, but with $V_a = 1000$ liters, RF = 1.2. Inert diluents (barium and strontium) give RF = 1.85 when $V_a = 250$ liters, RF = 1.60 when $V_a = 1000$ liters.

Thus, even if we use efficient diluents (with magic nuclei), the RF decreases markedly when we go from small to large cores.

It is therefore of interest to seek a reactor of high power, but such that even a "poor," noninert diluent shall be positioned so that the RF is close to that of a fast reactor of the same power with plutonium diluted by uranium.

It is clearly necessary for this purpose that the mean number of collisions suffered by a fission neutron before its capture by U^{238} shall be as small as possible. This requirement is satisfied, for example, by reactors with thin

*The idea of using nonfertile plutonium diluents in fast reactors was first suggested by O. D. Kazachkovskii [1].

†Without allowing for losses associated with the actual construction of the apparatus.

Translated from Atomnaya Énergiya, Vol. 21, No. 2, pp. 84-92, August, 1966. Original article submitted March 30, 1966.

TABLE 1. Characteristics of Cylindrical Reactor with Core of Heat Power W = 1000 Mw (H/D=0.5; coolant, sodium)

Mean energy density of core Q, Mw/liter	Core diameter, m	Radial coefficient of nonuniformity of heat emission in core, K_r	Critical charge of plutonium P_{f^9}, kg	Plutonium concentration in diluent c_9, wt. %	$\bar{\nu}^9_{eff}$	α	$+\Delta RF_{U^8} = (\bar{\nu}^8_f - 1)\frac{(f)_8}{(cf)_9}$	$\Delta RF_{can} = \frac{\Sigma_{c\,can}}{\Sigma_c f^9}$	RF	T_2, years	
										$T_{p.c.} \ll T_c$	$T_{p.c.} = 0.5$ years,
0,660	1,62	1,54	832	10	2,60	0,135	0,039	0,280	1,13	11,4	13,0
1,08	1,36	1,50	627	15	2,62	0,127	0,052	0,315	1,20	7,4	9,5
1,51	1,22	1,44	521	22	2,64	0,122	0,064	0,336	1,26	6,0	8,6
1,73	1,16	1,41	485	26	2,65	0,122	0,072	0,350	1,28	5,6	8,7

ring-shaped cores (with nonuranium) diluent of the plutonium) surrounded on the inside and on the outside by inner and outer breeding zones, and also by heterogeneous reactors made of fuel cassettes of small diameter with non-uranium diluent, regularly in a medium with breeding zone composition.

Below we shall give design calculations for such reactors; in studying heterogeneous reactors, we have limited ourselves to looking for optimum lattices. In both cases, optimization is of the doubling period T_2 [2], which is proportional to the time required to produce as much secondary plutonium as the total amount occurring in all the stages of the fuel cycle (in the core, in the breeding zones, at the processing plant, etc.), allowing for irreversible losses during processing.

In calculating the doubling times, we use the same quantities which primarily determine the fuel component of the cost of electrical power. The characteristics of a reactor which has optimum doubling time often differ little from those of a reactor with optimum fuel component of power production cost.

Results of Calculations

Let us consider a hypothetical plutonium breeder with nuclear density $3 \cdot 10^{22}$ nuclei/cm^3, with multigroup cross sections close to the cross section of barium, mixed with a material which strongly absorbs fast neutrons – the material of the fuel cans. (Such a material might, for example, be tantalum [3].) Let us assume that in all the variants the fuel can thickness is 0.3 mm.

Let us also assume that the chosen nonuranium diluent can achieve high fuel burnup – 100 kg/ton fuel.

As the fertile material of the breeding zones we took UC. The volume fractions of the materials in the breeding zones were: $\varepsilon_{UC} = 0.6$, $\varepsilon_{Na} = 0.25$, $\varepsilon_{constr} = 0.15$. The thickness of the outer breeding zone was taken as 60 cm, allowing for the extrapolated boundaries. The energy density Q(Mw/liter) was calculated with the same temperature limitations on the fuel elements for all variants, and the same heating and maximum velocity of the sodium heat exchanger, which were taken as those given in [2].

The calculations were performed in the multigroup p_1 approximation based on a system of constants [3]. The properties of the two-dimensional geometry of the reactors (the effects of the ring-shaped reflectors) were allowed for by the method of conditional separation of variables as described in [4]. The thermophysical calculations were carried out by means of a "complex" program [5]. The critical concentrations, the RF, and T_2 were calculated for the mean fission-product concentration for the run.

So as to get the effect of the ring-shaped cores and lattices in as pure a form as possible, T_2 was calculated on the assumption that, during the processing time of the core fuel $T_{p.c}$, $T_{p.c} \ll T_c$, the core operating period – this corresponds to optimistically rapid processing. However, in the calculations on the ring-shaped zones, we also considered the value $T_{p.c} = 0.5$ years.

For fuel elements from the breeding zone the processing time $T_{p.b}$ was taken as 0.5 years in every case.

To calculate T_2 we needed the average amount of plutonium remaining constantly in the screen: this was calculated by the "movable-screen" model [6], the fertile material from the breeding zone being discharged via the first row of cassettes next to the core, containing an average of 1 wt.% secondary plutonium. We took account of losses of plutonium during processing (1.5 wt.%). In all the variants, the thermal power of the core rings, W, was 1000 Mw.

TABLE 2. Characteristics of Reactors with Ring-Shaped Cores of Heat Power W = 1000 Mw (H = 0.58 m, coolant, sodium)

Internal radius of ring core r_1, m	Thickness of ring core Δr, m	Radial coefficient of nonuniformity of heat emission in core, K_r	Mean energy density of core Q, Mw/liter	Critical charge of plutonium P_{f9}, kg	Plutonium concentration in diluent c_9, wt. %	$\bar{\nu}^9_{eff}$	α	$+\Delta RF_{U^8}$	ΔRF_{can}	RF	T_2, years	
											$T_{p.c.} \ll T_c$	$T_{p.c.} = 0.5$ years
0	0,58	1,41	1,73	485	26	2,65	0,122	0,072	0,350	1,28	5,6	8,7
0,15	0,40	1,23	1,98	460	29	2,65	0,125	0,107	0,319	1,33	4,9	8,1
0,25	0,30	1,11	2,20	477	33	2,65	0,126	0,147	0,271	1,42	4,1	7,1
0,50	0,19	1,04	2,35	606	44	2,65	0,126	0,214	0,200	1,56	3,5	6,8
1,00	0,11	1,02	2,40	913	58	2,65	0,128	0,292	0,137	1,72	3,9	7,7

The results of the calculations are given in Tables 1 and 2. The reactors dealt with in these tables were critical with the mean fuel isotope composition for the run, allowing for the appropriate amount of fission products, but not allowing for the higher plutonium isotopes.

As the core size decreases, the relative neutron leakage from the core increases and the neutron spectrum hardens. This causes some increase in the mean number of plutonium fission neutrons per captured neutron, $\bar{\nu}^9_{eff}$.

Owing to the increase in the relative neutron leakage, there is an increase in the quantity $(\nu_f^8 - 1) \times \frac{(f)_8}{(cf)_9}$, determined by U^{238} fissions in the breeding zone. The plutonium concentration in the diluent simultaneously increases.

An important factor is the number of neutrons captured in the fuel can for every neutron captured by the plutonium, ΔRF_{can} (since the capture cross section of the can is assumed to be high).

As the power density increases, there is a fall in the volumetric proportion of plutonium-enriched fuel and an increase in the fuel element surface per unit volume, so that the volumetric proportion of the can increases. This effect causes a more rapid increase in the plutonium concentration in the core, and therefore in general there is an increase in ΔRF_{can}, which is compensated for by a corresponding decrease in the relative capture in the diluent ($\Delta RF_{can} + \Delta RF_{dil} \approx$ const).

In Table 1 the value of RF was calculated without allowing for the higher plutonium isotopes at the average concentration of fission products during the run:

$$RF = \nu^9_{eff} - 1 + \Delta RF_{U^8} - \Delta RF - J/(cf)_9,$$

where ΔRF includes all parasitic neutron captures (diluent, can, sodium, fission products), and $J/(cf)_9$ is the relative leakage of neutrons from the breeding zone.

Table 1 shows that with decrease in the size of a compressed core [7] the RF increases, mainly owing to the contribution from U^{238} fission and the increase in ν^9_{eff}. Increase in power density per unit mass of plutonium in the fuel cycle, corresponding to a decrease in the critical charge and a simultaneous increase in the RF with decrease in the volume of the core, leads to a monotonic decrease in T_2. The value of K_r decreases at the same time as the volume.

Further improvement of the reactor indices is impossible, because $\bar{Q} = 1.730$ Mw/liter is the limiting value for $K_r = 1.41$ and the temperature limitations assumed (if we consider only a cylindrical core with given heat power for given H/D).

If we go from a cylindrical core to a ring-shaped one, additional possibilities appear for improving the characteristics of a reactor with given diluent.

Table 2 gives the characteristics of such a reactor. The value of Δr is chosen so that the heat power of the core remains at a given level, while criticality is achieved by appropriate choice of enrichment. In all variants, the height of the ring remains approximately the same as for a maximally-stressed cylindrical reactor (H = 58 cm).

TABLE 3. Lattice Characteristics

a, cm	Δ, cm	K_r	RF	c_9, %	T_2, years	$\bar{\nu}^9_{eff}$	α
10	10	1,00	1,23	30	5,9	2,47	0,178
	20	1,02	1,60	55	3,4	2,53	0,161
	30	1,04	1,78	78	3,6	2,58	0,136
	40	1,06	1,86	83	4,0	2,64	0,124
15	10	1,01	1,01	22	—	—	—
	20	1,04	1,41	33	3,6	—	—
	30	1,07	1,60	42	3,2	—	—
	40	1,10	1,69	47	3,2	—	—
20	10	1,02	0,86	19	—	2,49	0,170
	20	1,05	1,25	29	5,3	2,50	0,156
	30	1,10	1,45	37	3,3	2,57	0,140
	40	1,13	1,54	42	3,2	3,62	0,128

From Table 2 it will be seen that the principal effects which reduce T_2 for a cylindrical core when its mean power density increases continue to act with increase of r_1.

There is now an increase in the relative neutron leakage into the internal and external breeding zones; this is manifested by a corresponding increase in RF. The value of c_9 thus increases montonically. As regards the neutron spectrum in the core, it is substantially unaffected: this is reflected in the constancy of $\bar{\nu}^9_{eff}$ and α. The negative contribution to the RF made by neutron absorption in the can (ΔRF_{can}) decreases monotonically, because the maximum energy density is maintained at a given level and the volumetric proportion of the can is constant, while the value of c_9 increases (i.e., $\bar{\Sigma}_{cf_9}$ increases). As a result, the RF increases with the radius of the ring.

The use of a ring-shaped core with a nonuranium plutonium-diluent enables us to increase the RF to values characteristic for reactors with uranium diluents.

The value of K_r falls relatively sharply and rapidly tends to unity, reflecting the tendency to complete leveling out of heat emission with increasing r_1 (the axial coefficient of nonuniformity K_z is practically constant and equal to 1.16). A consequence of this is that the critical charge is not a monotonic function of the ring radius. As Q_{max} is the same in ring-shaped cores and $P_{f9} \sim c_9 V_a = c_9 \frac{W}{Q_{max}} K_r K_z$, it follows that P_{f9} decreases owing to the rapid leveling out of heat emission as we cross from a cylinder to a ring. On further increase of the ring radius, K_r continues to decrease increasingly slowly and tends to unity, while P_{f9} increases, in general, in proportion to c_9 (Table 2).

Owing to the decrease in K_r and the increase in r_1, $\bar{Q}$ increases in a ring-shaped core, approaching Q_{max}. As a result, on going from a cylindrical to a ring-shaped core, T_2 at first continues to fall owing to the decrease in critical mass and the growth of $\bar{Q}$ and RF; but with further increase in the ring radius, $\bar{Q}$ reaches its limiting value and T_2 rises in correspondence with the rise in critical mass.

Thus, there is a core, with optimum T_2, in which the chosen diluent is most efficiently utilized. In the given case, this is a ring with internal radius $r_1 = 50$ cm and thickness $\Delta r \approx 20$ cm.

TABLE 4. Effects of Pu^{240} and Pu^{241} on RF of Reactors with Ring-Shaped Cores ($r_1 = 50$ cm)

Δr, cm	RF without allowance for Pu^{240} and Pu^{241}	RF with allowance for mean concentrations of Pu^{240} and Pu^{241}	$\Delta RF_{240+241}$	$(\overline{\nu_f \sigma_f} - \overline{\sigma}_{cf})_{240}$
10	1,68	1,80	0,12	0,724
20	1,43	1,53	0,10	0,625
30	1,23	1,32	0,09	0,544

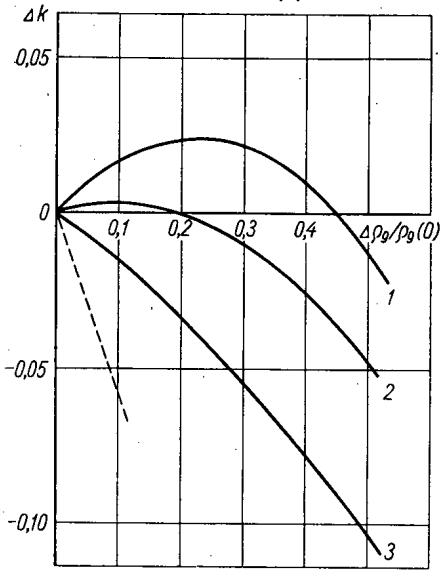

Fig. 1. Reactivity versus relative depth of burnup $\Delta\rho_9/\rho_9(0)$ of principal fissionable isotope in lattices optimum with respect to T_2, allowing for accumulation of secondary plutonium in the fertile material. 1) Lattice with a = 10 cm, Δ = 20 cm; 2) a = 15 cm, Δ = 30 cm; 3) a = 20 cm, Δ = 40 cm. ----) Curve of reactivity without allowance for accumulation of secondary plutonium.

If the processing time for the core material is increased to 0.5 years (as assumed in Tables 1 and 2), an optimum energy-density effect appears [2]. From Table 1 it follows that for a cylindrical core, T_2 is a minimum for some intermediate value $\bar{Q} \approx \bar{Q}_{opt}$.

The optimum-ring effect is also observed with $T_{p.c}$ = 0.5 years (see Table 2). In addition, on going from $T_{p.c.} \ll T_a$ to $T_{p.c.}$ = 0.5 years, the doubling time increases in all the variants. *

Let us now consider a lattice containing cylindrical heat-emitting cassettes arranged in a certain array in an infinite medium with breeding-zone composition. Such a lattice could serve as a basis for a heterogeneous fast reactor, in which leveling out of heat emission is achieved (for example) by shaping the plutonium concentration in the nonuranium diluent. In this case, we encounter the problem of choosing an optimum lattice.

As before, we shall carry out optimization with respect to T_2.

Note that a closely-spaced lattice cannot be optimum, because its RF is small owing to the small amount of uranium which it contains, and therefore T_2 is large. On the other hand, in too widely spaced a lattice c_9 will be large in the diluent, and thus T_2 will also be large. Thus there must be a lattice with optimum T_2.

Table 3 gives calculations on lattices with various cassette radii a and breeding-zone thicknesses between cassettes Δ. The program for the calculation included the usual boundary condition $d\Phi_K/dr = 0$ at the boundary of the equivalent cylindrical cell; the calculation was performed in the same way as for the previous case, in the multigroup p_1 approximation. The maximum heat evolution in a cassette was calculated for the same temperature limitations as in the calculations on ring-shaped systems. The height was taken as equal to that of the ring core (H = 58 cm) with the same axial coefficient of nonuniformity (K_Z = 1.16). We used one-dimensional cylindrical geometry for a lattice of infinite height with the above boundary conditions.

From Table 3 it will be found that the effect of increased hardness in the neutron spectrum inside a fuel cassette is here associated with relative decrease of its area, as shown by the decrease in α and increase in $\bar{\nu}^9_{eff}$ for increasing Δ and fixed a. In this case the reproduction factor increases, reaching a value characteristic for reactors with metallic uranium as plutonium diluent.

The nonuniformity of heat emission inside a casette increases, approaching the value found in a cassette immersed in an infinite breeding medium (since the cell boundary is an ideal "neutron mirror," the non-uniformity can increase when the boundary is further from the cassette). The heat emission is a maximum at the center of the fuel cassette. The mean energy density correspondingly falls, in conformity with the assumed temperature limitations.

From the data in Table 3 we can conclude that there is a tendency for an optimum value of T_2 to exist, this being particularly clear for cassettes with a = 10 cm.

Effects of Pu^{240} and Pu^{241}

The assumed burnup fraction (100 kg/ton) ensures appreciable accumulation of Pu^{240} and Pu^{241} averaged over a core run (~ 16% Pu^{240} and 3% Pu^{241} in Pu^{239}). Pu^{241} is, of course, a more efficient fuel than Pu^{239} (in the

*It is interesting to note that the optimum thickness of a ring-shaped core is practically independent of the power if the internal radius of the ring is large enough (for fixed core composition). Furthermore, other conditions being constant, the doubling time also varies little with the power of the optimum ring.

TABLE 5. Investigation of Döppler Effect and Sodium Coefficient in Reactors with Ring-Shaped Cores (r_1 = 50 cm)

Δr, cm	$\frac{dk_{eff}}{dt} / _{Na}$ ×10⁶, 1/°C *	$\frac{dk_{eff}}{dt} / _{Na_a}$ ×10⁶, 1/°C †	$\frac{dk_{eff}}{dt} /$ Döppl ×10⁶, 1/°C	Components of reactivity coefficient due to Döppler effect		
				$\frac{dk_{eff}}{dt} / _{Pu}$ ×10⁶, 1/°C	$\frac{dk_{eff}}{dt} / _{can}$ ×10⁶, 1/°C	$\frac{dk_{eff}}{dt} / _{U^8}$ ×10⁶, 1/°C
10	−0,973	+0,079	−2,40	+0,48	−0,29	−2,58
20	−0,555	+0,261	−1,85	+0,51	−0,51	−1,83
30	+0,095	+0,733	−1,60	+0,52	−0,68	−1,43

*Change of reactivity for 1°C increase of temperature of sodium in reactor.
†Change of reactivity for 1°C increase of temperature of sodium in core.

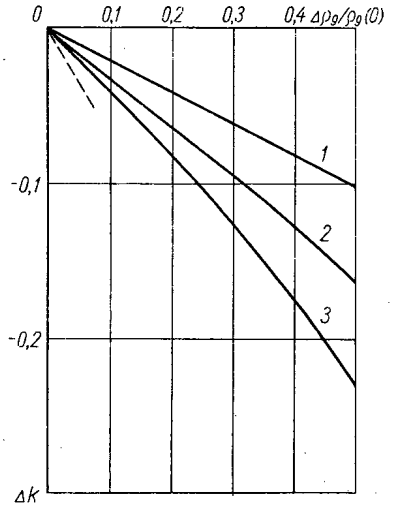

Fig. 2. Reactivity versus relative depth of burnup $\Delta\rho_9/\rho_9(0)$ of principal fissionable isotope in ring reactors, with allowance for accumulation of secondary plutionium in breeding blanket (r_1 = 50 cm). 1) Thickness of ring-shaped core Δr = 10 cm; 2) 20 cm; 3) 30 cm. ----) Reactivity curve without allowance for accumulation of secondary plutonium.

above reactors, Pu^{241} is approximately 1.2 times more efficient than Pu^{239}, i.e., $\frac{(\overline{\nu_f\sigma_f} - \bar{\sigma}_{cf})_{241}}{(\overline{\nu_f\sigma_f} - \bar{\sigma}_{cf})_{239}} \approx 1{,}2$). Pu^{240} has a wide diffuse fission cross section threshold, stretching from ~ 0.2 MeV, where the fission cross section of over-threshold neutrons is ~ 1.5 barn, i.e., greater by a factor of 3 than the fission cross section of U^{238}, while the number of neutrons per fission event is $\nu_f \approx 3$.

We can thus reckon that Pu^{240} is a fairly good fuel in fast reactors, and that its contribution to the reactivity and RF increases with the hardness of the neutron spectrum in the core. Because of these advantageous qualities, Pu^{240} is especially effective when we go from cylindrical to ring-shaped cores, or for very widely spaced lattices.

From Table 4 it follows that, in these variants, the additional contribution to the RF from Pu^{240} and Pu^{241} ($+\Delta RF_{240+241} = \frac{(\overline{\nu_f\Sigma_f} - \bar{\Sigma}_{cf})_{240}}{\bar{\Sigma}_{cf239}} + \frac{(\overline{\nu_f\Sigma_f} - \bar{\Sigma}_{cf})_{241}}{\bar{\Sigma}_{cf239}}$) is about 0.11 for a ring-shaped core. For optimal lattices the corresponding contribution to the RF is 0.05.

The RF of 1.56 given in Table 2 for the variant with r_1 = 50 cm, Δr = 19 cm, increases owing to Pu^{240} and Pu^{241} to 1.66, while that for the variant with r_1 = 100 cm, Δr = 11 cm, increases to 1.84.*

When we go to thinner rings, the neutron spectrum in the core ring is distorted, so that the numbers of high-energy and low-energy neutrons increase (the spectrum becomes, as it were, "spread out"); as a consequence, $\bar{\nu}^{239}_{eff}$ and $\bar{\nu}^{241}_{eff}$ alter hardly at all, and thus the contribution of Pu^{241} to the RF varies little with the ring thickness. However, the quantity $(\overline{\nu_f\sigma_f} - \bar{\sigma}_{cf})_{240}$ does change appreciably, also causing an appreciable growth in the contribution of Pu^{240} and Pu^{241} as the ring becomes thinner.

*Note that the values of the RF allowing for Pu^{240} and Pu^{241} were calculated for the critical core composition (isotopes averaged over run), including the corresponding concentrations of Pu^{239}, Pu^{240}, Pu^{241}, and fragments.

TABLE 6. Investigation of Döppler Effect and Sodium Coefficient in Lattices with Optimum T_2

a,cm	Δ,cm	$\frac{dk_{eff}}{dt} / _{Na}$ ×10⁶, 1/°C	$\frac{dk_{eff}}{dt} / _{Na_a}$ ×10⁶, 1/°C	$\frac{dk_{eff}}{dt} / _{Döppl}$ ×10⁶, 1/°C	Components of reactivity coefficient due to Döppler effect		
					$\frac{dk_{eff}}{dt} / _{Pu}$ ×10⁶, 1/°C	$\frac{dk_{eff}}{dt} / _{can}$ ×10⁶, 1/°C	$\frac{dk_{eff}}{dt} / _{U^8}$ ×10⁶, 1/°C
10	20	+4,014	+1,280	—4,210	+1,000	—0,336	—4,870
15	30	+1,688	+0,163	—3,173	+0,705	—0,395	—3,470
20	40	—0,985	—1,197	—2,247	+0,533	—0,458	—2,320

Changes in Reactivity during Irradiation

Attempts to obtain the greatest possible height of burnup when using stable plutonium diluents are frustrated by difficulties associated with the necessity to compensate for the greater reactivity margin. With ring-shaped zones or heterogeneous lattices, the problem is made easier, because the fertile material is closer to the fuel inside the ring or fuel cassette (of size comparable to the path length of the neutrons). In these circumstances, an important part is played by accumulation of secondary fuel in the fertile material, which is most concentrated in just those layers which adjoin the main bulk of the fuel. As a result, in given conditions the reactivity does not alter during burnup, but even increases until the burnup becomes so high that the deciding factor becomes the decrease in the mass of the main fuel. This also simplifies the difficult problem of compensating the reactivity at high burnup. This effect is observed in lattices (Fig. 1). For the optimum lattices under consideration, the greatest positive "overshoot" of reactivity occurs for the variant with $a = 10$ cm. The reactivity reaches its initial value at 45% burnup of the originally loaded fuel. The optimum lattice with $a = 15$ cm already has lower positive reactivity overshoot, while for the optimum lattice with $a = 20$ cm the reactivity decreases to its initial value.

In ring-type reactors, the influence of secondary plutonium accumulation in the breeding zone on the reactivity changes is also quite appreciable (Fig. 2); however, in this case there is no positive reactivity overshoot. Nevertheless, if we allow for accumulation of secondary plutonium, for an optimum ring ($r_1 = 50$ cm, $\Delta r = 20$ cm) the reactivity change during a run is approximately halved.*

It must be noted that the problem of compensating for the reactivity fall due to high burnup in ring-shaped cores is much more easily solved than is the case for large cylindrical cores, provided that we allow for replacement of the row of cassettes in the breeding zone nearest the core by cassettes from the core. In a ring-shaped core, one such row will compensate for very much more reactivity than in a large cylinder.

Sodium Temperature Coefficient and Döppler Temperature Coefficient

When (Table 5) we consider the sodium temperature coefficient of the core reactivity in reactors with ring-shaped cores, we find that this coefficient is positive and decreases with the ring thickness. Its positive sign is due to the increase in the fission cross section of Pu^{239} with rise in energy in hard-spectrum conditions, and also to the use of cans of strong neutron-absorber (tantalum). The existence of a positive sodium coefficient, it must be admitted, creates additional difficulties in the use of such reactors.

For a ring-core reactor with optimum T_2,

$$\frac{dk_{eff}}{dt}\Big|_{Na_a} = +0.26 \cdot 10^{-6}\ 1/°C\dagger.$$

The chief contributions to the Döppler temperature coefficient are made by Pu^{239} (positive component), the can (negative component) and U^{238} in the breeding zone (negative component).

*We are not considering additional difficulties due to increased heat emission in the layers of the breeding zone which adjoin the core when plutonium accumulates in these layers.

†We considered only density changes in the sodium. Changes in the blocking coefficients were not considered.

For ring-shaped cores with $\Delta r = 30$-10 cm approx., an important part is played by the negative component (U^{238}). For a reactor with ring-shaped core and optimum T_2, when $\Delta r = 20$ cm, $\left.\frac{dk_{eff}}{dt}\right|_{Döppl} = -1.85 \cdot 10^{-6}$ 1/°C.

The resultant temperature coefficient for an optimum ring-shaped core is due to the sodium and Döppler effects, is negative and is equal to $-2.41 \cdot 10^{-6}$ 1/°C.

We also investigated the temperature coefficients for lattices with optimum T_2. The sodium temperature coefficient of a lattice (see Table 6) changes sign from negative (for widely spaced lattices) to positive (for closely spaced lattices). This is due to the fact that, as we go to closely spaced lattices, the negative contribution from neutron leakage decreases, and the positive contribution from U^{238} fission increases.

The reactivity coefficient associated with the Döppler effect is negative, and increases as we go to closely spaced optimum lattices: this is due to the increasinginfluence of U^{238} on the reactivity.

From the above data we can draw the following conclusion: With the use of nonuranium diluents for the plutonium in fast high-power reactors (with large cores), ring-shaped cores and cores with fuel cassettes distributed in a medium with breeding-zone composition have certain specific properties which make them preferable to large cylindrical cores.*

In conclusion, the authors would like to thank I. S. Slesarev, A. M. Kuz'min, M. F. Troyanov, and V. M. Murogov, who helped in the work, and O. N. Gerasimova, who helped in the preparation of this article.

LITERATURE CITED

1. O. D. Kazachkovskii, In: "Proceedings of Second International Conference on the Peaceful Uses of Atomic Energy" (Geneva, 1958), reports by Soviet scientists, Vol. 2, Atomizdat, Moscow (1959), p. 188.
2. A. I. Leipunskii et al., Report No. 369 submitted by the USSR to the Third International Conference on the Peaceful Uses of Atomic Energy (Geneva, 1964).
3. L. P. Abagyan et al., Group Constants for Design Calculations on Nuclear Reactors, Atomizdat, Moscow (1964).
4. V. V. Khromov et al., In: "Some Problems on the Physics and Engineering of Nuclear Reactors," Atomizdat, Moscow (1965), p. 51.
5. I. S. Slesarev et al., Ibid., p. 70.
6. S. B. Shikhov et al., Ibid., p. 85.
7. V. V. Khromov et al., Atomnaya Énergiya, 17, 199 (1964).

*Similar results are obtained with compressed cylindrical cores [7]. In this case, however, a marked radial nonuniformity is observed.

DETERMINATION OF THE BURNOUT OF A FUEL ELEMENT FROM THE ICEBREAKER LENIN ON THE BASIS OF Cs^{137} ACTIVITY WITHOUT CHEMICAL SEPARATION

N. F. Pravdyuk, V. I. Vikhrov,
S. Yu. Pavlov, and V. N. Perevezentsev

UDC 61.039.548

It is proposed to use a scintillation gamma spectrometer for determining the absolute values of fuel element burnout. The burnout is determined from the intensity of the gamma lines of the Cs^{137} (E_γ = 0.66 MeV) accumulated in the fission products.

The report gives the results of investigations of U^{235} burnout as a function of distance along a depleted fuel element of the reactor on the icebreaker Lenin.

The research was conducted in the hot laboratory of the I. V. Kurchatov Atomic Energy Institute.

The most exact method of determining fuel burnout in reactor fuel elements is the mass-spectrometer method. However, the use of this method leads to radioactive contamination of the equipment. One may also use the radiochemical method, in which the quantity determined is the U^{235} loss or the quantity of fission fragments – for example, Cs^{137} or Tc^{99} – that are formed [1]. A disadvantage of this method is that radiochemical work must be done with highly active materials.

In [2] the fuel burnout along the element was measured (without destroying the element) by means of a magnetic Compton spectrometer, and in [3] a gamma spectrometer with a semiconductor detector was used. The burnout was determined from the intensity of the gamma lines of the fission fragments. The measurement results given in [2, 3] are only relative results.

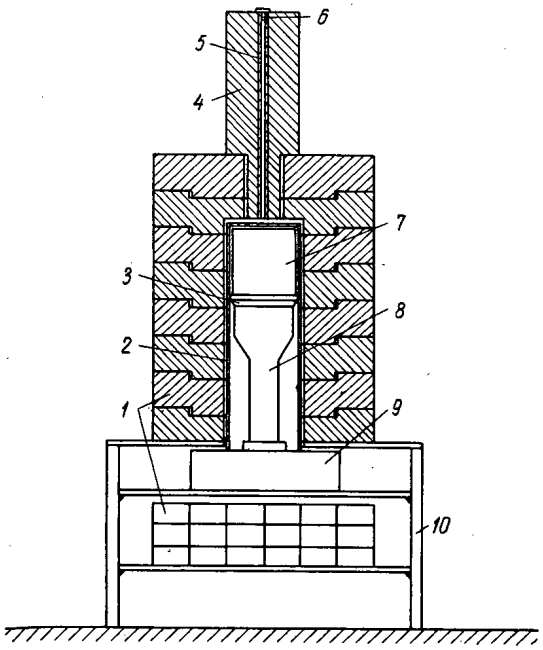

Fig. 1. Diagram of gamma spectrometer: 1) Lead shielding; 2) casing; 3) light guide; 4) collimator; 5) copper pipe; 6) target; 7) NaI (Tl) crystal; 8) FEU; 9) cathode repeater; 10) supporting stand.

In the present study we investigated the burnout of nuclear fuel along a depleted fuel element from cell 5/3 of the reactor of the icebreaker Lenin [4]. The burnout was found from the absolute activity of the Cs^{137} in the fission products without chemically decomposing it. The absolute activity was measured on the basis of the intensity of the gamma lines of the Cs^{137} (E_γ = 0.66 MeV) by means of a scintillation gamma spectrometer. This isotope has a long half-life (30 years), and its fission yield is well known [5]. Because of the long half-life, we can neglect the operating time of the element.

Technique of the Experiment

The fuel element from the reactor of the icebreaker Lenin had operated for 428 effective days, and it had been stored for 575 days after being extracted from the reactor. The nuclear fuel of the element consisted of pellets of uranium dioxide with an enrichment of 5.5%. The operating part of the element was 1580 mm long.

The rod was cut at 11 places in the hot chamber, and two measurement specimens were taken from each

Translated from Atomnaya Énergiya, Vol. 21, No. 2, pp. 92-96, August, 1966. Original article submitted February 1, 1966.

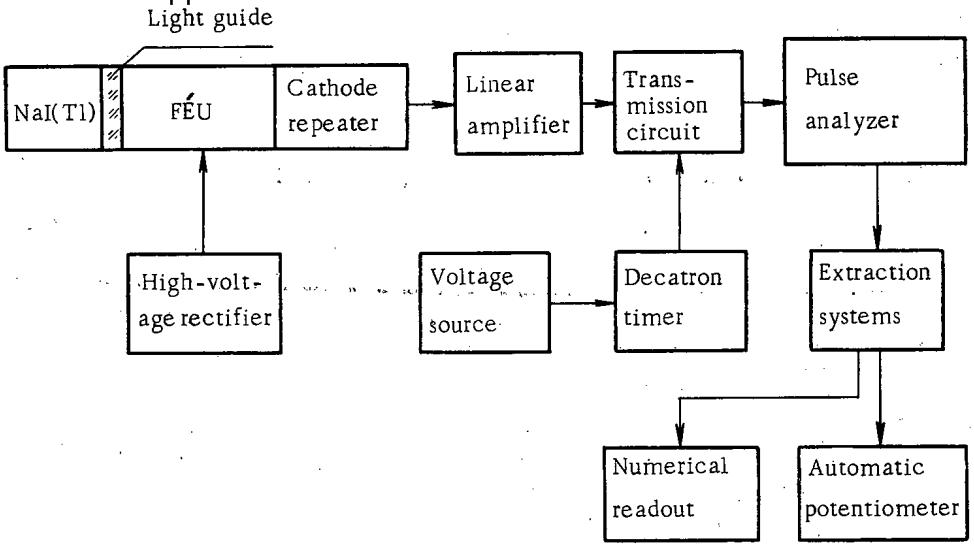

Fig. 2. Block diagram of gamma spectrometer.

TABLE 1. Data on Long-Lived Fission Products of U^{235}

Isotope	$T_{1/2}$	E_γ, MeV	k*	ν†	Remarks
Zr^{95}	65 days	0,757 0,724	0,49 0,49	6,0	—
Ru^{106}	1 year	0,619 0,513	0,10 0,21	0,380	Gamma-line of daughter nucleus Rh^{106} ($T_{1/2}$ = 30 sec)
Sb^{125}	2,7 years	0,175 0,595 0,427	0,06 0,32 0,29	0,023	—
Cs^{137}	30 years	0,662	0,92	6,15	Gamma-line of daughter nucleus Ba^{137m} ($T_{1/2}$ = 2.6 min)
Ce^{141}	282 days	0,081 0,134 0,100	0,04 0,10 0,01	5,39	—
Nb^{95}	35 days	0,768	1,0	—	Daughter nucleus Zr^{95}

*Coefficient taking account of decay scheme.
†Isotope yield upon fission.

TABLE 2. Relative Intensities of Gamma Lines of Long-Lived Isotopes

E_γ, MeV	Ce^{144}			Sb^{125}			Ru^{106}		Cs^{137}	Zr^{95}	
	0,08	0,10	0,134	0,175	0,427	0,595	0,513	0,619	0,662	0,724	0,757
I, rel. units	1,2	3,4	3,4	0,07	0,33	0,34	4,8	2,4	34	7,6	7,6

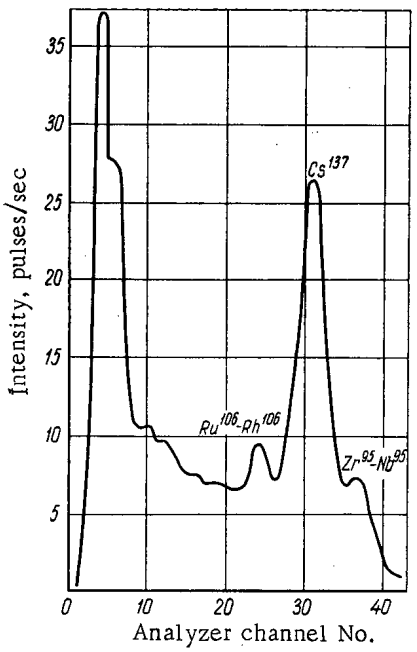

Fig. 3. Instrument gamma spectrum of one of the specimens investigated.

cut location; these were pieces of uranium dioxide measuring 1-3 mm and weighing 10-30 mg. The absolute activity of the Cs^{137} was measured by means of a gamma spectrometer with an 80 × 80 mm NaI (Tl) crystal.

Figure 1 shows the arrangement of the gamma spectrometer, and Fig. 2 is a block diagram of the gamma spectrometer. The gamma detector used an FÉU-56 photomultiplier with good stability and satisfactory resolution.

The information from the AI-100 pulse analyzer was obtained by means of a VD information extraction system, developed by M. P. Sokolov at the I. V. Kurchatov Atomic Energy Institute [6]. The use of the VD system and the decatron timer in the information-gathering equipment improves the accuracy and allows automatic measurement.

The energy resolution of the gamma spectrometer for the photopeak of the Cs^{137} gamma line was 11.0%. The area of the photopeak was determined from the following equation, which utilizes the properties of a Gaussian curve [7]:

$$S_{ph} = 1.064 I_{max} i_{0.5}, \quad (1)$$

where I_{max} is the number of pulses at the maximum of the photopeak; $i_{0.5}$ is the width of the photopeak at half its height.

The efficiency of the gamma spectrometer for gamma quanta with $E_\gamma = 0.66$ MeV was determined both experimentally and by calculation. The efficiency was calculated by the formula

$$\varepsilon(E_\gamma) = P(E_\gamma)\left[1 - e^{-\mu(E_\gamma)d}\right]\Omega_{geom}\left(1 + \frac{1}{2\mu_c l}\right), \quad (2)$$

where $P(E_\gamma)$ is the photofactor [$P(E_\gamma) = 0.75$ when $E_\gamma = 0.66$ MeV]; $\mu(E_\gamma)$ is the total linear coefficient of attenuation of the gamma quanta by the material of the crystal; d is the thickness of the crystal; Ω_{geom} is the geometric solid angle of the collimator; l is the length of the collimator; μ_c is the total linear coefficient of attenuation of the gamma quanta by the material of the collimator. The calculated value of the efficiency was $\varepsilon = 1.5 \cdot 10^{-5}$.

Experimentally the efficiency was determined by means of Cs^{137} sources. A solution of Cs^{137} with a known specific activity was used for preparing three sources (0.1 mCi, 0.25 mCi, and 0.5 mCi). The specific activity of the solution was determined by measuring a number of "weightless" targets with a 4π-geometry flow counter. The experimental value of the efficiency was found to be 1.7×10^{-5}. The error was ±6%.

Analysis of Results

Since the fuel element under investigation had been stored for 575 days, the short-lived isotopes in the fission-product mixture had practically disintegrated. Table 1 shows the data on the long-lived isotopes, which account for most of the gamma activity of the specimens after cooling. Table 2 shows the calculated relative intensities I of the gamma lines of these isotopes, which are needed for analyzing the instrument spectra.

During reactor operation the radioactive isotope Cs^{134} ($T_{1/2} = 2.7$ years), formed by the decay scheme

$$I^{133} \xrightarrow[\beta^-, \gamma]{20.8\,h} Xe^{133} \xrightarrow[\beta^-, \gamma]{5.27\ days} Cs^{133}\ (\text{stable}),$$
$$Cs^{133}(n, \gamma)\, Cs^{134},$$

accumulates in the fission products. An estimate of the intensity contributed by the Cs^{134} gamma line, taking account of the operating time and cooling time of the full element and of the reaction cross section, showed that this contribution was very small in our case. In analyzing the instrument spectra, therefore, we ignored the effect of the Cs^{134} gamma lines.

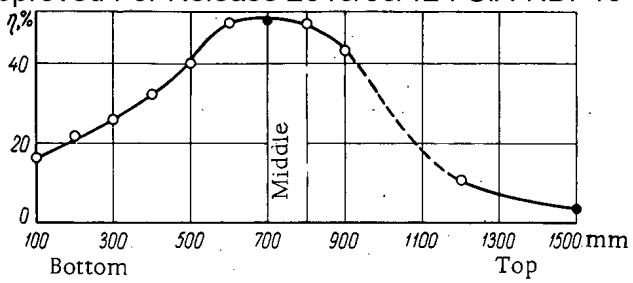

Fig. 4. Distribution of burnout as a function of position along the fuel element.

As an example, Fig. 3 shows the instrument spectrum of one of the specimens investigated. It can be seen from Fig. 3 that the photopeak of the Cs^{137} gamma line (E_γ = 0.66 MeV) is clearly distinguishable. To the right of it we see the combination photopeak of the gamma lines of Zr^{95} and Nb^{95} (E_γ = 0.76 MeV), and to the left of it we see the photopeak produced by Ru^{106} (E_γ = 0.51 MeV). The low-energy part of the spectrum (< 0.3 MeV) was not identified. The resolution of the gamma spectrometer was not sufficient for complete separation of the photopeaks of the gamma lines of Cs^{137}, Ru^{106} (E_γ = 0.619 MeV), and Sb^{125} (E_γ = 0.596 MeV). Therefore, using the intensity values I shown in Table 2, we determined how much the areas of the Ru^{106} and Sb^{105} photopeaks contributed to the area of the Cs^{137} photopeak. Using Equation (1) to calculate the area of the photopeak, we found that this contribution was no more than 4%. In analyzing the results, we took into account the value of the "pedestal" of the Compton distribution of Zr^{95} (E_γ = 0.76 MeV), amounting to 1/10 of the photopeak maximum.

From the results of measurements made on the two specimens from each cut on the fuel element, we found the average area, S_{av}, of the photopeak of the Cs^{137} gamma line per gram of specimen weight. The individual measurements did not deviate more than 6% from the average values. In analyzing the results, we took account of the self-absorption in the specimens. Neglecting self-absorption may produce errors of up to 7%.

The experimental values of S_{av} we obtained and the number of Cs^{137} nuclei accumulated by the end of the irradiation are related by the following equation:

$$N(x,\ t_0) = \frac{S_{av}(x)\, e^{\lambda t_0}}{\varepsilon(E_\gamma)\, k\lambda}, \tag{3}$$

where $e^{\lambda t_0}$ is a coefficient used to allow for the decay during storage; k is the coefficient used to take account of the decay scheme; λ is the decay constant; $\varepsilon(E_\gamma)$ is the efficiency of the gamma spectrometer. The maximum error in the determination of $N(x, t_0)$ was ± 12%. This is a combination of the errors in the determination of S_{av} and $\varepsilon(E_\gamma)$.

The values of $N(x, t_0)$ were used for determining the thermal-neutron flux, from which the burnout was calculated.

Calculation of the Total Thermal-Neutron Flux and the Burnout

The burnout η is the relative decrease in the number of U^{235} nuclei as a result of fission and radiative capture of thermal neutrons:

$$\eta = \frac{\Delta N^{U^{235}}}{N_0^{U^{235}}} = 1 - e^{-\sigma_a^{U^{235}} \Phi_t}, \tag{4}$$

where $N_0^{U^{235}}$ is the initial number of U^{235} nuclei per gram of fuel; $\Delta N^{U^{235}}$ is the absolute decrease in U^{235} nuclei per gram of fuel;

$$\sigma_a^{U^{235}} = \sigma_f^{U^{235}} + \sigma_c^{U^{235}}, \tag{5}$$

where $\sigma_f^{U^{235}}$ is the fission cross section; $\sigma_c^{U^{235}}$ is the radiative-capture cross section; Φ_T is the total thermal-neutron flux.

The isotope Cs^{137} accumulates not only through the fission of U^{235} but also through fast-neutron fission of U^{238} and the thermal-neutron fission of the Pu^{239} that is formed. The relationship between the rate of accumulation of Cs^{137} nuclei per gram of fuel at time t and the number of U^{235}, U^{238}, and Pu^{239} nuclei is expressed by the following equation:

$$\frac{dN(x,\ t)}{dt} = \nu^{U^{235}}\sigma_f^{U^{235}}\varphi_T(x,\ t)\,N^{U^{235}}(t) + \nu^{U^{238}}\sigma_f^{U^{238}}\varphi_f(x,\ t)\,N^{U^{238}}(t)$$

$$+ \nu^{Pu^{239}}\sigma_f^{Pu^{239}}\varphi_T(x,\ t)\,N^{Pu^{239}}(t) - \lambda N(x,\ t), \tag{6}$$

where x is the distance from the lower end of the fuel element; N(x, t) is the number of Cs^{137} nuclei per gram of fuel; ν is the Cs^{137} yield from the fission of each isotope; σ_f is the fission cross section; $\varphi_T(x, t)$ is the thermal-neutron flux; $\varphi_f(x, t)$ is the fast-neutron flux; λ is the Cs^{137} decay constant; $N^{U^{235}}(t)$, $N^{U^{238}}(t)$, and $N^{Pu^{239}}(t)$ are the numbers of U^{235}, U^{238}, and Pu^{239} nuclei per gram of fuel, respectively.

The solution of Eq. (6) for $t = t_0$ is of the following form:

$$N(x,\ t_0) = \frac{\xi[(\Phi_T(x)]\,\nu^{U^{235}}\sigma_f^{U^{235}}}{\sigma_a^{U^{235}}} N_0^{U^{235}} \frac{\sigma_a^{U^{235}}\Phi_T(x)}{\sigma_a^{U^{235}}\Phi_T(x) - \lambda t_0}$$

$$\times [e^{-\lambda t_0} - e^{-\sigma_a^{U^{235}}\Phi_T(x)}], \tag{7}$$

where $N(x, t_0)$ is the number of Cs^{137} nuclei accumulated over a period of time t_0 per gram of fuel (experimental value); t_0 is the operating time of the fuel element; $\Phi_T(x)$ is the total thermal-neutron flux; $\xi[\Phi_T(x)]$ is a coefficient taking account of the accumulation of Cs^{137} through the fission of U^{238} and Pu^{239}.

Knowing the estimated values of the fast-neutron and thermal-neutron fluxes, their ratio, and the values of the cross sections, we can use a few mathematical transformations to express $\xi[\Phi(x)]$ in terms of the total thermal-neutron flux. For our case $\xi[\Phi_T(x)]$ maybe represented in the form

$$\xi[\Phi_T(x)] \approx 1.03 + 43.3 \cdot 10^{-24}\Phi_T(x). \tag{8}$$

The first term is due to the accumulation of Cs^{137} through the fission of U^{235} and U^{238} (the number of Cs^{137} nuclei resulting from fission of U^{235} is taken to be unity), while the second term expresses the accumulation of Cs^{137} as a result of Pu^{239} fission.

Equation (7) is used for determining $\Phi_T(x)$ from the knowledge of $N(x, t_0)$. However, in order to solve Eq. (7) for $\Phi_T(x)$, we must know the value of $\xi[\Phi_T(x)]$. For this purpose we found the approximate value of the total flux $\Phi'_T(x) = \varphi'_T(x)t$ from the equation

$$\frac{dN(x,\ t)}{dt} = \nu^{U^{235}}\sigma_f^{U^{235}}\varphi'_T(x)\,N_0^{U^{235}}e^{-\sigma_a^{U^{235}}\varphi'_T(x)t} \tag{9}$$

with the initial condition $N(x, 0) = 0$, where $\varphi'_T(x)$ is the approximate value of the thermal-neutron flux averaged over the operating time of the fuel element.

The solution of Eq. (9) is of the form

$$N(x,\ t) = \frac{\nu^{U^{235}}N_0^{U^{235}}\sigma_f^{U^{235}}}{\sigma_a^{U^{235}}}(1 - e^{-\sigma_a^{U^{235}}\varphi'_T(x,\ t)}). \tag{10}$$

For $t = t_0$, $\varphi'_T(x)t_0 = \Phi'_T(x)$ and $N(x, t) = N(x, t_0)$. Then,

$$\Phi'_t(x) = -\frac{1}{\sigma_a^{U^{235}}} \ln\left(1 - \frac{N(x, t_0)\,\sigma_a^{U^{235}}}{\nu^{U^{235}} N_0^{U^{235}} \sigma_f^{U^{235}}}\right). \quad (11)$$

Using the values of $\Phi'_T(x)$, we determined the values of $\xi[\Phi_T(x)]$ from formula (8) and substituted them into Eq. (7). Equation (7) is transcendental in $\Phi_T(x)$ and was solved graphically. From the values of $\Phi_T(x)$ found by solving Eq. (7), we determined the burnout by using Eq. (5), with a maximum error of ± 16%. Figure 4 shows the burnout of U^{235} as a function of position along the fuel element. It can be seen that the burnout distribution is strongly skewed, with the maximum displaced toward the bottom of the fuel element. The largest burnout value is 50% and corresponds to a point 700 mm from the bottom. The lowest burnout value is 3.7%, corresponding to the top of the fuel element. For the bottom of the element the burnout value is 16%. The average burnout value for the entire element is about 25%.

Our investigations showed that by using a scintillation gamma spectrometer we could determine the burnout of a fuel element on the basis of the activity of the Cs^{137} in the fission products without chemically decomposing it. For this purpose we can use a scintillation gamma spectrometer with a resolution of the order of 10-12%. This method can be used for determining the burnout after the fuel element has been cooled for a considerable time. The method can be used for determining the relative distribution of burnout as a function of position along the fuel element (with an accuracy of ±16%) and the absolute value of the burnout (with an accuracy of ±16%).

In conclusion, the authors express their gratitude to N. M. Mordvinov for his comments on the results and to A. A. Markov and M. P. Sokolov for their practical assistance in preparing the information extraction system.

LITERATURE CITED

1. A. P. Smirnov-Averin et al., Atomnaya Énergiya, 11, 454 (1961).
2. L. V. Groshev and A. M. Demidov, Atomnaya Énergiya, 13, 458 (1962).
3. M. Higatsberger et al., Report No. 399, presented by Austria at the Third International Conference on the Peaceful Uses of Atomic Energy (Geneva, 1964).
4. I. P. Afrikantov et al., Atomnaya Énergiya, 17, 349 (1964).
5. A. K. Krasin (Ed.), Handbook of Nuclear Physics Constants for Reactor Calculations [in Russian], Moscow, Atomizdat (1960), p. 230.
6. N. P. Sokolov, In: Proceedings of the Sixth Conference on Nuclear Radioelectronics, Vol. 2 [in Russian], Moscow, Atomizdat (1965), p. 102.
7. Yu. A. Egorov, The scintillation method of spectrometry for gamma rays and fast neutrons [in Russian], Moscow, Gosatomizdat (1963).

EFFECT OF THE PARAMETERS OF A RESEARCH REACTOR ON THE FLUX OF THERMAL NEUTRONS IN THE REFLECTOR AND THE COST OF THE FUEL

A. S. Kochenov

UDC 621.039.572 : 621.039.537 + 621.039.54

The influence of the parameters of a research reactor on the thermal-neutron flux in the reflector and the cost of the fuel required is considered. It is shown that, the higher the neutron breeding factor and the smaller the radius of the active zone, the greater is the ratio of the maximum thermal-neutron flux to the reactor power. This ratio is in particular quite large for reactors of the water-cooled, water-moderated type operating with intermediate neutrons. From the point of view of minimum fuel cost in experimental reactors, it is undesirable to choose either very low or very deep burnup.

The development of experimental reactors tends to follow the course of increased thermal-neutron fluxes. At the present time some experiments demand thermal-neutron fluxes of 10^{15} neutrons/cm^2 · sec and more.

The cost of operating modern research power reactors is to a considerable extent determined by the fuel component. Hence optimization of the parameters of high-power research reactors plays an important part in reducing their cost.

In many research reactors the experimental channels are situated in the reflector. In view of this it is interesting to consider the effect of various reactor parameters on the thermal-neutron flux in the reflector and to find what type of reactor gives a maximum ratio of the thermal-neutron flux to the reactor power.

Effect of Reactor Parameters on the Thermal-Neutron Flux

Let us consider a reactor with a spherical active zone and an infinite reflector. If there is no resonance absorption in the reflector, we may write the following relation:

$$\frac{k-1}{k}\cdot\frac{N}{\varepsilon}\nu_f = 4\pi\Sigma_c\int_R^\infty \Phi(r)\,r^2\,dr, \tag{1}$$

where k is the neutron breeding factor in an infinite medium with the composition of the active zone, N is the reactor power, ε is the energy associated with fission, ν_f is the number of neutrons formed in one fission, Φ is the thermal-neutron flux in the reflector, Σ_c is the macroscopic absorption cross section in the reflector, and R is the radius of the active zone.

TABLE 1. Values of J for Reactors with Various Reflectors

Reflector material	ν	J, $\times 10^{-10}$ neutrons/cm^2 · sec · kW
Water	1,0	8,7
Beryllium	1,85	6,8
Heavy water	1,1	5,9
Graphite	1,7	3,3

Translated from Atomnaya Énergiya, Vol. 21, No. 2, pp. 97-101, August, 1966. Original article submitted February 8, 1966.

TABLE 2. Values of J for a Number of Working Reactors

Reactor	J, $\times 10^{-10}$ neutrons/cm²·sec·kW
VVR-M	1,0
MTR	1,35
VVR-2	1,5
HFBR	1,75

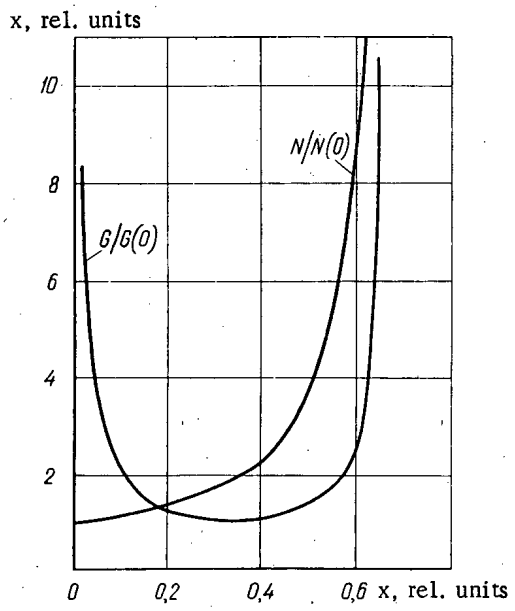

Fig. 1. Effect of the depth of burn-up of U^{235} on the reactor power and U^{235} consumption for a fixed thermal-neutron flux in the reflector. x) Relative depth of burnup for the U^{235}; N) reactor power; N(0)) reactor power for zero mean burnup; G) consumption of U^{235} per unit time; G(0)) consumption of U^{235} per unit time for optimum average burnup.

In the diffusion approximation the thermal-neutron flux is described by the equation

$$D\nabla^2\Phi - \Sigma_c\Phi + q = 0 \qquad (2)$$

(D is the diffusion coefficient, q is the density of thermal-neutron generation) with boundary conditions

$$\frac{1}{\Phi(R)}\cdot\frac{d\Phi}{dr}\Big|_R = \frac{1}{Z\lambda_{tr}}; \qquad (3)$$

$$\Phi(r\to\infty)\to 0. \qquad (4)$$

The density distribution of thermal-neutron sources over the reflector in the two-group approximation takes the form

$$q \sim \frac{1}{r}\, e^{-\frac{r-R}{\sqrt{\tau}}}, \qquad (5)$$

where τ is the age of the thermal neutrons.

Solving Eq. (2) with due allowance for (4) and (5), we obtain

$$\Phi = A\frac{e^{-\frac{r-R}{L}}}{r} + B\frac{e^{-\frac{r-R}{\sqrt{\tau}}}}{r}, \qquad (6)$$

where L is the diffusion length.

From condition (3),

$$B = -\frac{1+R\left(\frac{1}{L}+\frac{1}{Z\lambda_{tr}}\right)}{1+R\left(\frac{1}{\sqrt{\tau}}+\frac{1}{Z\lambda_{tr}}\right)}A. \qquad (7)$$

If the active zone is "black" for thermal neutrons, then Z = 0.71. Since the materials of the reflector are characterized by the inequalities $\lambda_{tr} \ll \sqrt{\tau}$ and $\lambda_{tr} \ll L$, we have

$$B \approx -A. \qquad (8)$$

Thus,

$$\Phi \approx \frac{A}{r}\left(e^{-\frac{r-R}{L}} - e^{-\frac{r-R}{\sqrt{\tau}}}\right). \qquad (9)$$

From condition (1) we find that

$$A = \frac{1}{4\pi}\cdot\frac{\nu_f}{e}\cdot\frac{1}{D\left[1-\frac{\tau}{L^2}+\frac{R}{L}\left(1-\frac{\sqrt{\tau}}{L}\right)\right]}\cdot\frac{k-1}{k}N. \qquad (10)$$

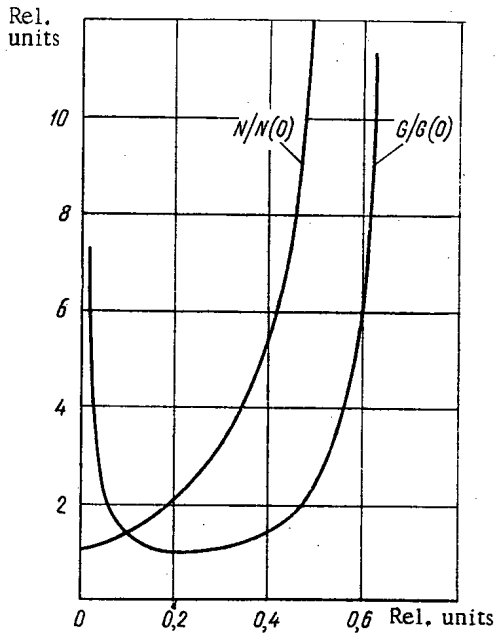

Fig. 2. Effect of the depth of burnup of U^{235} on the reactor power and U^{235} consumption for a fixed thermal-neutron flux in the trap.

Let us find at what distance from the boundary with the active zone the maximum thermal-neutron flux occurs. With an accuracy equivalent to the expansion

$$e^{\frac{r_0-R}{\sqrt{\tau}}\left(1-\frac{\sqrt{\tau}}{L}\right)-1} \approx \frac{r_0-R}{\sqrt{\tau}}\left(1-\frac{\sqrt{\tau}}{L}\right) \qquad (11)$$

the coordinate r of the maximum flux may be determined from the quadratic equation

$$e^{\frac{\sqrt{\tau}}{L}}\left(1-\frac{\sqrt{\tau}}{L}\right)\left(\frac{r_0-R}{\sqrt{\tau}}\right)^2 + \left[e\left(1-\frac{\sqrt{\tau}}{L}\right)\left(1+\frac{R}{L}\right)-1\right]\frac{r_0-R}{\sqrt{\tau}} - \left(1+\frac{R}{\sqrt{\tau}}\right)=0. \qquad (12)$$

Analysis of the coefficients of Eq. (12) shows that for heavy water with $R/\sqrt{\tau} < 3$, and for beryllium, graphite and water with any ratio $R/\sqrt{\tau}$, the thermal-neutron flux is greatest at $\sim\sqrt{\tau}$ from the boundary with the active zone,* i.e.,

$$\frac{r_0-R}{\sqrt{\tau}} \approx 1. \qquad (13)$$

Hence the maximum thermal-neutron flux is equal to

$$\Phi_{max} \approx \frac{A}{R+\sqrt{\tau}}\left(e^{-\frac{\sqrt{\tau}}{L}}-e^{-1}\right). \qquad (14)$$

If we define the "quality" J of a research reactor as the ratio of the maximum thermal-neutron flux to the reactor power [1, 2], then we have from Eqs. (10) and (14):

$$J=\frac{\Phi_{max}}{N} \approx \frac{1}{4\pi}\cdot\frac{\nu_f}{\varepsilon}\cdot\frac{1}{D\left[1-\frac{\tau}{L^2}+\frac{R}{L}\left(1-\frac{\sqrt{\tau}}{L}\right)\right]}\cdot\frac{e^{-\frac{\sqrt{\tau}}{L}}-e^{-1}}{R+\sqrt{\tau}}\cdot\frac{k-1}{k}.$$

The J value attainable with various moderators was calculated theoretically in [1]. The effect of the individual parameters of the reactors on their quality factors was not, however, considered. Equation (15) shows which parameters affect the value of J and to what extent they do this in each case. We see from Eq. (15) that, for a selected reflector material, the quality of the reactor is the higher the greater the neutron breeding coefficient and the smaller the radius of the active zone. For identical reflector materials and equal breeding factors, the radius of the active zone is the smaller the shorter the neutron migration length. Hence it is best to use ordinary water as moderator in the active zone of a research reactor, since in this case the migration length is shortest. We should also not forget that water is a good heat carrier.

For different values of the breeding factor, the relation between the maximum thermal-neutron fluxes in different materials is different. It is interesting, however, to compare the J values for a fairly high breeding factor. Table 1 shows the values of J for various reflector materials, when the composition of the active zone is the same as in the SM-2 reactor (without counting burnup and poisoning) [3].

*For water $L < \sqrt{\tau}$; hence the relation $\frac{r_0-R}{L} \approx 1$.

Despite the fact that the largest value of J occurs for water, the short relaxation length of the flux and the relatively high "impurity" content of fast neutrons makes water a not entirely suitable material for the reflector of a research reactor. From this point of view beryllium and heavy water are better.

Let us compare the data of Table 1 with analogous parameters of some well-known reactors (Table 2).*

Comparison shows that intermediate-neutron research reactors with water, heavy-water, or beryllium moderators and reflectors may have a higher quality than better reactors without traps at present constructed.

Let us consider the variation in thermal-neutron flux at an arbitrary point of the reflector on reducing the radius of the active zone:

$$\frac{d\Phi}{dR}=\frac{\nu_f}{4\pi}\cdot\frac{N}{\varepsilon}\cdot\frac{1}{r}\left\{\frac{-\frac{D}{L}\left(1-\frac{\sqrt{\tau}}{L}\right)}{D^2\left[1-\frac{\tau}{L^2}+\frac{R}{L}\left(1-\frac{\sqrt{\tau}}{L}\right)\right]^2}\,\frac{k-1}{k}\left(e^{-\frac{r-R}{L}}-e^{-\frac{r-R}{\sqrt{\tau}}}\right)\right.$$

$$+\frac{1}{D\left[1-\frac{\tau}{L^2}+\frac{R}{L}\left(1-\frac{\sqrt{\tau}}{L}\right)\right]}\cdot\frac{1}{k^2}\,\frac{dk}{dR}\left(e^{-\frac{r-R}{L}}-e^{-\frac{r-R}{\sqrt{\tau}}}\right)$$

$$\left.+\frac{1}{D\left[1-\frac{\tau}{L^2}+\frac{R}{L}\left(1-\frac{\sqrt{\tau}}{L}\right)\right]}\,\frac{k-1}{k}\left(\frac{1}{L}e^{-\frac{r-R}{L}}-\frac{1}{\sqrt{\tau}}e^{-\frac{r-R}{\sqrt{\tau}}}\right)\right\}. \tag{16}$$

Expression (16) contains three components. The first two are negative for any value of r. The third is negative for small values of r − R and positive for large values. Thus on reducing the radius of the active zone the thermal-neutron flux at small distances from the active zone (in the maximum-flux region) always increases. At large distances from the active zone, however, where the flux is comparatively weak, it may turn out that the absolute value of the positive term is greater than that of the negative.

If we vary the radius of the active zone by varying the fuel concentration, then the effective addition remains practically constant, and in the one-group approximation,

$$\frac{dk}{dR}\approx\frac{dk}{dR_0}=\left(\frac{\pi}{R_0}\right)^2\frac{dM^2}{dR}-\frac{2(k-1)}{R_0}, \tag{17}$$

where R_0 is the effective radius of the active zone and M^2 is the migration area.

The value of the derivative dM^2/dR depends on the composition of the active zone. For an active zone with a water moderator, the value of M^2 remains practically unaltered on changing the fuel concentration. In this case,

$$\frac{dk}{dR}\approx-\frac{2(k-1)}{R_0}. \tag{18}$$

We can easily see from expressions (16) and (18) that, if

$$\frac{2}{k}\cdot\frac{L}{R_0}\left(1+\frac{L}{R+\sqrt{\tau}}\right)>1, \tag{19}$$

*Table 2 does not include data for the SM-2 and HFIR reactors, for which the maximum thermal-neutron fluxes are reached in a comparatively small volume of the neutron traps. For the SM-2 and HFIR the value of J is $5\cdot10^{10}$ neutrons/cm$^2\cdot$sec$\cdot$kW.

then

$$\frac{d\Phi}{dr} < 0 \tag{20}$$

for any value of r > R.

Thus, if water-moderated reactors satisfy inequality (19) (which is true for all known research reactors with beryllium and heavy-water reflectors), then the thermal-neutron flux rises at any point of the reflector on increasing the fuel concentration in the active zone.

Optimum Depth of Fuel Burnup

If the reactor power is N and the average depth of burnup is x, the reactor requires an amount of fuel

$$G \approx \frac{N}{x} \tag{21}$$

per unit time.

It follows from expression (15) that the reactor power is related to the maximum thermal-neutron flux in the reflector by means of the relation

$$N \approx 4\pi \frac{\varepsilon}{\nu_f} D \left[1 - \frac{\tau}{L^2} + \frac{R}{L}\left(1 - \frac{\sqrt{\tau}}{L}\right)\right] \frac{R+\sqrt{\tau}}{e^{-\frac{\sqrt{\tau}}{L}} - e^{-1}} \cdot \frac{k}{k-1} \Phi_{\max}. \tag{22}$$

Since the breeding factor of the neutrons and the radius of the active zone depend on the depth of fuel burnup, the latter also controls the reactor power necessary to produce a given thermal-neutron flux.

If the cost of the fuel included in the fuel elements is α, the cost of chemical treatment for the fuel elements β, and the relative losses in regeneration ε, then the cost of the fuel required by the reactor per unit time is

$$C \approx \alpha \left[x + \varepsilon(1-x) + \frac{\beta}{\alpha}(1-\varepsilon)(1-x)\right] \frac{N(x)}{x}. \tag{23}$$

Three cases are possible: 1) $\beta/\alpha > 1$ (regeneration economically unfavorable); 2) $\beta/\alpha = 1$ (regeneration has no effect on the running costs); 3) $\beta/\alpha < 1$ (regeneration economically desirable).

In any case, as $x \to 0$, $C \to \infty$. If the fuel burnup is very deep, then $k \to 1$, $N \to \infty$, and $C \to \infty$. Hence, too deep burnup is as undesirable as too low.

The optimum depth of burnup depends on the reactor parameters and the values of β/α and ε. The greatest depth corresponds to the case in which there is no fuel regeneration (for this we must formally take $\beta/\alpha = 1$). The smaller the values of β/α and ε, the lower will be the degree of burnup corresponding to the minimum cost of the uranium required. In the limit, with $\beta/\alpha \to 0$ and $\varepsilon \to 0$, the optimum depth of burnup tends to zero. For the case in which fuel regeneration is absent, Fig. 1 shows the U^{235} consumption and reactor power as functions of the depth of burnup for a reactor with a heavy-water reflector and with an active zone having the same composition as that in the SM-2 reactor. The curves are plotted on the assumption that there is no reloading of fuel during the campaign. We see from the figure that the minimum consumption of U^{235} corresponds to a 30 to 40% depth of burnup. Since, however, the cost of a reactor rises with its power, we must select a burnup rather below the value corresponding to the minimum uranium consumption. If the reactor is to operate with cassette-by-cassette reloading of fuel, the uranium consumption falls by almost a factor of two (owing to the increased depth of burnup in the cassettes being unloaded).

In reactors with a neutron trap (SM-2 type) the optimum depth of burnup is lower than for reactors without traps. This is because the thermal-neutron flux in the trap is proportional to the specific power, i.e., the power associated with unit volume. Hence the power of such a reactor is proportional to the volume of the active zone. Figure 2 contains curves analogous to those of Fig. 1 for a reactor with a spherical trap. We see from the graph that the minimum uranium consumption corresponds to a 20% depth of burnup.

In conclusion the author wishes to thank S. M. Feinberg, P. E. Stepanov, and N. I. Laletin for discussing the matters raised.

LITERATURE CITED

1. S. M. Feinberg, et al., In the book: "Transactions of the Second International Conference on the Peaceful Use of Atomic Energy (Geneva, 1958)" [in Russian], Contributions of Soviet scientists, Vol. 2, Moscow, Atomizdat (1958), p. 334.
2. P. Ageron et al., Paper No. 49 presented by France to the Third International Conference on the Peaceful Use of Atomic Energy (Geneva, 1964) [Russian translation].
3. S. M. Feinberg et al., Atomnaya Énergiya, 8, 493 (1960).

CALCULATION OF THE TANGENTIAL STRESSES AT THE WALL OF A CHANNEL AND THE VELOCITY DISTRIBUTION IN A TURBULENT FLOW OF LIQUID

M. Kh. Ibragimov, I. A. Isupov, L. L. Kobzar', and V. I. Subbotin

UDC 621.039.517 : 621.039.517.5

A relationship for the distribution of tangential stresses at the wall of a straight, smooth channel with an arbitrarily shaped cross section (in the fully developed turbulent condition) is derived on the basis of certain concepts regarding the mechanism of the turbulent transfer of momentum. The constants in this relationship are derived from experimental data.

The calculated velocities and tangential stresses at the wall are compared with experimental results for eight forms of complex channels.

Channels of various complex forms are widely used in nuclear reactors, steam generators, and heat exchangers. The heat transfer in such channels depends considerably on the velocity distribution of the heat carrier over the flow cross section. There has been widespread experimental study of the hydrodynamics of complex channels, but it is a very laborious matter to study all the channels found in practice. The few existing methods of calculating velocity fields and hydraulic resistances in channels are based on a number of assumptions and involve laborious computing [1, 2]. There is thus a great need for developing a simpler method of computing the hydrodynamics of complex channels on the basis of physical laws emerging from the analysis of existing experimental data.

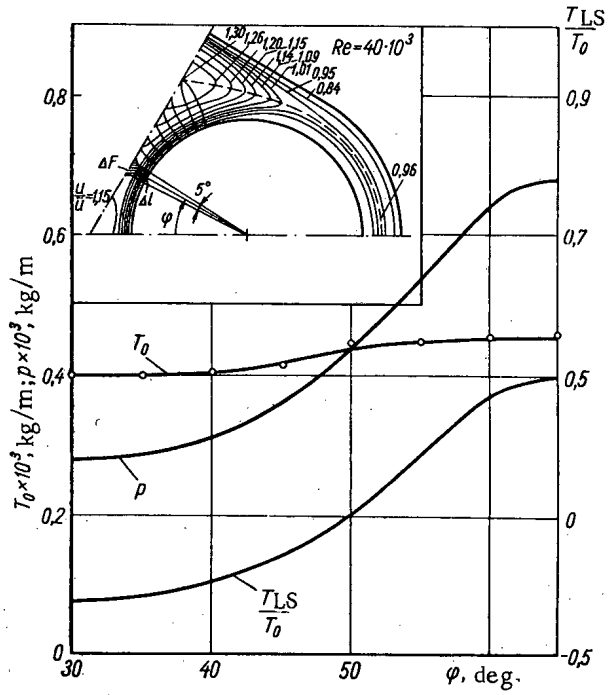

Fig. 1. Relation between the frictional forces T_0 at the wall and the pressure forces p for cells divided by the Deissler-Taylor method.

Translated from Atomnaya Énergiya, Vol. 21, No. 2, pp. 101-107, August, 1966. Original article submitted December 28, 1965.

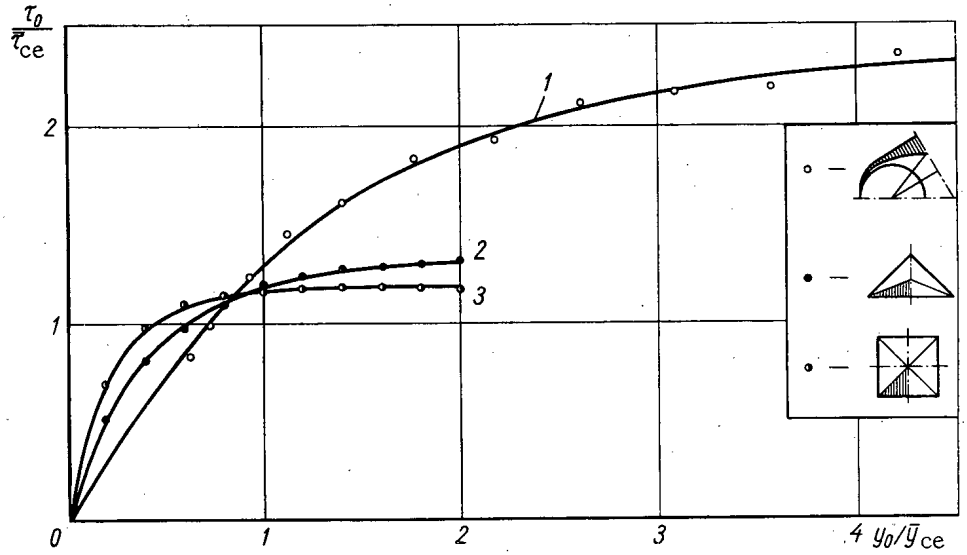

Fig. 2. Distributions of tangential stresses at the walls for various cells: ○) triangular channel with three rods, s/d = 1.41 (data of present paper), Φ_{ce} = 16.9; ●) right-angled isosceles triangle [8], Φ_{ce} = 4.8; ◑) square [9], Φ_{ce} = 2.0; ———) calculation from formula (5); 1) b = 0.8; 2) b = 2.4; 3) b = 4.5.

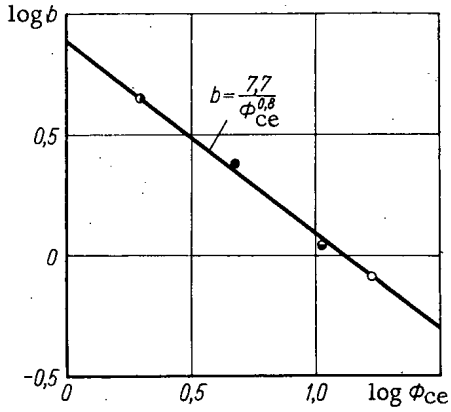

Fig. 3. Variation of the b in formula (5) with the cell shape parameter Φ_{ce}: ○, ●, ◑) see notation in Fig. 2; ◒) cell with close-packed (alternating) rods [6], Φ_{ce} = 10.75, b = 1.1.

In this paper we shall propose a method of calculating tangential wall stresses, velocity fields, and hydraulic resistances in straight, smooth channels with cross sections of various shapes. The calculation is valid for a hydrodynamically stabilized flow of liquid in a developed turbulent condition ($Re > 10^4$). The results of the stress calculations enable us to find the coefficients of turbulent heat transfer required for solving problems connected with the determination of temperature fields and heat-transfer coefficients.

The distribution of tangential stress at the wall is related to the geometrical features of the channel cross section. As a quantitative expression of these features of the cross section we propose using a quantity $y_0(z)$, the distance along the normal from the wall to the line of maximum velocities (LMV). The problem is to find a functional relationship between y_0 and the tangential stress τ_0 at the wall.

There is absolutely no published information on the structure and scale of turbulent eddies in complex channels; hence we must make certain assumptions and introduce empirical quantities in order to establish the $\tau_0 = f(y_0)$ relationship.

The variation of the tangential stress τ_0 over the perimeter of a complex channel is closely connected with the transfer of momentum along the perimeter (z axis). For channels of a form constant around the perimeter ($y_0(z)$ = const), the tangential stress at the wall has a constant value. If, however, $y_0(z) \neq$ const (form of the cross section varies), then there is a transfer of momentum along the z axis, the value of this being a function of $y_0(z)$.

It follows from modern views on the structure of turbulent flows (see, for example, [3, 4]) that the total transfer of momentum is due to two processes: a gradient transfer of momentum due to molecular friction and small-scale turbulent eddies, and a convective transfer of momentum due to the large-scale motion of eddies:

$$\rho\overline{u_x'u_z'} = -\rho(\nu + \varepsilon_\nu)\frac{du_x}{dz} + \rho\overline{u_x'V_z'}, \tag{1}$$

where V'_z is the pulsation velocity of large eddies in the direction of the z axis.

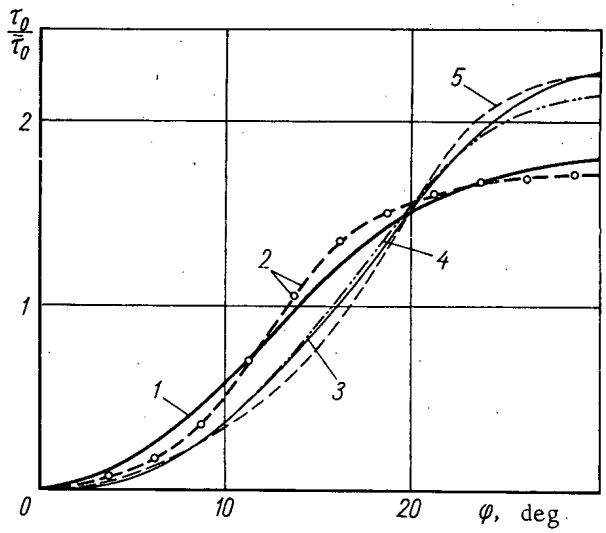

Fig. 4. Comparison between calculated values for the $\tau_0/\bar{\tau}_0$ distribution and experimental data for close-packed (alternating) rods: 1) Calculation by the authors of this paper; 2) experiment [6], $Re = 14 \cdot 10^3$; calculation of L. S. Kokorev: 3) $Re = 24 \cdot 10^3$; 4) $Re = 3.8 \cdot 10^6$; 5) calculation from Deissler-Taylor data [6].

These two forms of momentum transfer differ considerably. Whereas the gradient transfer is determined by the local characteristics of the flow, the convective transfer depends mainly on the geometric features of the channel as a whole.

In complex channels the effect of large-scale eddies on the velocity field should appear most strongly in the directions in which the velocity varies slowly (along the channel perimeter). Along the normal to the channel perimeter (the y axis), however, convective transfer plays a small part, since the velocity gradient is very high and hence so is the gradient transfer of momentum.

Convective transfer should appear more strongly in channels with a sharply varying cross-sectional shape (e.g., close-packed rods), when exchange between eddies of considerably different velocities may occur. In a channel with a slowly varying shape (e.g., an eccentric annular gap) the role of convective transfer is slight. Neglect of the convective transfer of momentum may lead to considerable errors, especially in channels of sharply-varying form. This is clearly shown by the calculations of Deissler and Taylor [2]. For a channel cell bounded by the wetted perimeter and normals to the isotachs (equal-velocity lines), writing the force–balance equation in the form

$$\tau_0 \Delta l = -\frac{dp}{dx} \Delta F, \tag{2}$$

these authors simply reduced the gradient exchange of momentum to zero, neglecting convective transfer. Hence, Eq. (2) and the Deissler-Taylor computing method are only valid for channels of slowly varying shape [5]. Calculation based on the method of [2] gives a considerable deviation from experimental data in the case of channels with rapidly varying shapes [6, 7].

The force balance was checked theoretically in the case of one of the complex channels for which experimental data on the distribution of velocities and tangential stresses at the wall were available [7]. Figure 1 shows the form of the isotachs in part of the channel cross section with unit cells divided up on the Deissler-Taylor principle (the sides of the cells are perpendicular to the isotachs). The pressure $p = \Delta F(dp/dx)$ and friction $T_0 = \tau_0 \Delta l$ forces along the wall were determined for these cells from experimental data. These forces were in fact different, i.e., the balance equation still lacked a term T_{LS}, the resultant force of side friction in the cell. Since the cell is divided in such a way that the component of side friction due to the velocity gradient $\partial u_x/\partial n$ equals zero, the force T_{LS} is the result of large-scale eddies only. Due allowance for T_{LS} in the calculation of [2] would lead to a reduction in the nonuniformity of the τ_0 and velocity distribution, i.e., to better agreement with experiment.

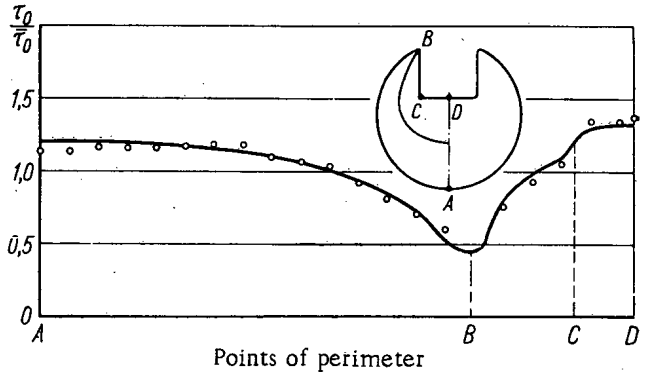

Fig. 5. Comparison between calculated data on the $\tau_0/\bar{\tau}_0$ distribution and experimental data for a grooved tube [8]: ———) calculation; O) experiment [8].

This analysis shows that in complex channels a great part is played by large-scale exchange of momentum. Clearly this transfer is related to the changes in the shape of the channel, i.e., to the variation of y_0. The strongest connection between variations in y_0 and τ_0 should be found for very small y_0 values (narrow gaps into which large eddies from neighboring parts of the channel cannot penetrate and in which the large-scale exchange effect is therefore small):

$$d\left(\frac{\tau_0}{\bar{\tau}_0}\right) \sim d\left(\frac{y_0}{\bar{y}_0}\right), \tag{3}$$

where

$$\bar{\tau}_0 = \frac{1}{L}\int_0^L \tau_0\, dl;\quad \bar{y}_0 = \frac{1}{L}\int_0^L y_0\, dl.$$

With increasing $y_0/\bar{y}_0$ the link between $dy_0/\bar{y}_0$ and $d\tau_0/\bar{\tau}_0$ weakens, since τ_0 is affected by neighboring parts of the channel (with different y_0) on account of exchange by large-scale eddies. In the limit, when $(y_0/\bar{y}_0)\to\infty$, $(d\tau_0/\bar{\tau}_0)\to 0$, i.e., conditions close to external streamlining arise.

These propositions regarding the character of the relationship between $d\tau_0/\bar{\tau}_0$ and $dy_0/\bar{y}_0$ satisfy a functional relation of the form

$$\frac{d\tau_0}{\bar{\tau}_0} = ae^{-b\frac{y_0}{\bar{y}_0}}\frac{dy_0}{\bar{y}_0}, \tag{4}$$

where a and b are empirical quantities depending on the shape of the channel.

Integrating expression (4) and applying the boundary condition $\tau_0/\bar{\tau}_0\to 0$ as $y_0/\bar{y}_0\to 0$, we obtain

$$\frac{\tau_0}{\bar{\tau}_0} = c\left(1-e^{-b\frac{y_0}{\bar{y}_0}}\right). \tag{5}$$

The quantity $c = a/b$ is given by the condition for the normalization of τ_0 over the channel perimeter:

$$\frac{1}{c} = \frac{1}{L}\int_0^L \left(1-e^{-b\frac{y_0}{\bar{y}_0}}\right) dz. \tag{6}$$

In order to give formula (5) a universal form valid for channels of different geometries, we must express b in terms of some parameter of channel shape.

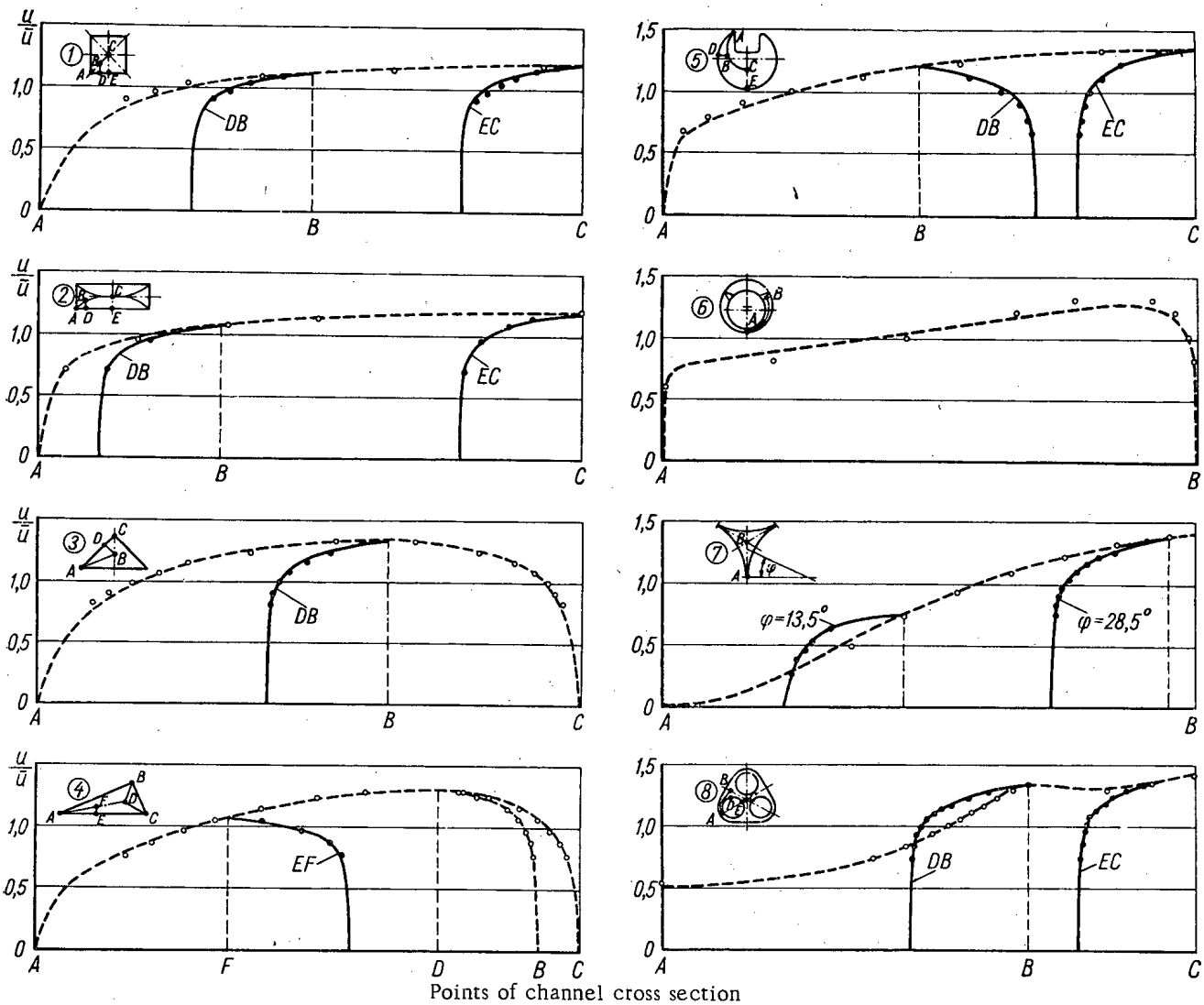

Fig. 6. Comparison between the calculated velocity distribution and experimental data for various shapes (see the table). Along the LMV: -------) calculation; O) experiment. Along the normals to the wall: ———) calculation; ●) experiment.

Starting from our concept of large-scale transfer, it is natural to suppose that the degree of variation of $\tau_0/\bar{\tau}_0$ should be determined not only by that of $y_0/\bar{y}_0$ but also by the ratio of the longitudinal and transverse dimensions of the channel cross section, i.e., its relative spread. It is clear that in a narrow channel the transfer of large eddies along the perimeter (leading to equalization of the field of tangential stresses) is difficult. On the other hand, in a wide channel, large eddies can easily propagate along the perimeter, evening out the value of τ_0. Hence, the relative spread of the channel cross section may serve as a shape parameter. As transverse dimension of the channel cross section we take the quantity $\bar{y}_0$, and as longitudinal dimension $F/\bar{y}_0$, on the principle that the product of the longitudinal and transverse dimensions equals the area of the channel cross section. Then the channel shape parameter is expressed by the relation

$$\Phi = \frac{F/\bar{y}_0}{\bar{y}_0} = \frac{F}{\bar{y}_0^2}. \qquad (7)$$

In order to determine the function $b = f(\Phi)$ we used the experimental distributions of tangential stress at the wall in a variety of complex channels [6-8]. These channels were first split into cells. By "cell" we mean part of the channel cross section bounded by the wetted perimeter, the LMV, and the normals drawn from those points of the perimeter at which the sign of the derivative dp_0/dz changes. For analysis we used isolated cells (i.e., bounded by normals coinciding with lines of symmetry). Clearly these cells may be regarded as independent (iso-

Shapes of Channels for Which Velocity Distributions Were Calculated

No. of channel	Shape of channel cross section	Source of exptl. data	Re No.
1	Square	[9]	$83 \cdot 10^3$
2	Rectangle with side ratio 1:3	[9]	$56 \cdot 10^3$
3	Isosceles right-angled triangle	[8]	$81 \cdot 10^3$
4	Right-angled triangle	[8]	$93 \cdot 10^3$
5	Circular tube with groove	[8]	$109 \cdot 10^3$
6	Eccentric annular gap	[10]	$18.6 \cdot 10^3$
7	Dense packing $\left(\frac{s}{d}=1\right)$	[6]	$14 \cdot 10^3$
8	Triangular shell with three rods $\left(\frac{s}{d}=1.3\right)$	[7]	$40 \cdot 10^3$

lated) channels. In Fig. 2 the experimental distributions of tangential stresses at the wall are presented in coordinates of $\tau_0/\bar{\tau}_{0ce}$, $y_0/\bar{y}_{0ce}$. The cells used for the analysis are shaded.

We see from Fig. 2 that the experimental points are satisfactorily described by an exponential relationship, different shape parameters Φ_{ce} of the cells corresponding to different values of b inequation(5). Figure 3 shows the relation between b and Φ_{ce}, which may be approximated by the formula

$$b = \frac{7.7}{\Phi_{ce}^{0.8}}. \tag{8}$$

Allowing for the empirical function $b = f(\Phi_{ce})$, equation(5) for calculating the distribution of τ_0 in isolated cells of the channel takes the form

$$\left(\frac{\tau_0}{\bar{\tau}_0}\right)_{ce}^{is} = c\left(1 - e^{-\frac{7.7}{\Phi_{ce}^{0.8}} \cdot \frac{y_0}{\bar{y}_{0ce}}}\right), \tag{9}$$

where

$$\frac{1}{c} = \frac{1}{L_{ce}} \int_0^{L_{ce}} \left(1 - e^{-\frac{7.7}{\Phi_{ce}^{0.8}} \cdot \frac{y_0}{\bar{y}_{0ce}}}\right) dz. \tag{9a}$$

In the case of nonisolated cells, interaction takes place between the cells on account of the exchange of large-scale momentum. The effect of a neighboring n-th cell on a given m-th cell may be expressed by means of a mutual function $\Psi_{n \to m}$:

$$(\tau_0)_m = (\tau_0)_m^{is} \Psi_{n \to m}. \tag{10}$$

Clearly the mutual influence of the cells should diminish as the distance between them increases. Regarding the attenuation of interaction as exponential, this effect may be expressed by the function

$$\Psi = 1 + \alpha e^{-\frac{l}{L}}, \tag{11}$$

where l is the distance along the perimeter (along the z axis) from the cell boundary to the i-th point under consideration, and L is the total length of the perimeters of the interacting cells (the interaction between the cells takes place over a section of the channel cross section bounded by the LMV and lines of symmetry).

The interaction of two cells (m and n) is expressed in the interaction functions

$$\Psi_{n\to m}=1+\alpha_m e^{-\frac{l_m}{L}};\quad \Psi_{m\to n}=1+\alpha_n e^{-\frac{l_n}{L}}.$$

The values of the coefficients α_m and α_n may be found from the conditions that τ_0 should match at the boundary of the cells,

$$(\tau_0)_{m/l_m=0}=(\tau_0)_{n/l_n=0} \tag{12}$$

and the normalization conditions for τ_0,

$$\alpha_m\int_0^{L_m}(\tau_0)_m^{is}\,e^{-\frac{l_m}{L}}\,dl+\alpha_n\int_0^{L_n}(\tau_0)_n^{is}\,e^{-\frac{l_n}{L}}\,dl=0. \tag{13}$$

For a large number of interacting cells, τ_0 is first matched for any two neighboring cells, then the latter (now treated as a single cell) are matched with the next cell, and so on.

In Figs. 4 and 5 the calculated values of τ_0 are compared with experimental data [6, 8] and calculations of L. S. Kokorev (Moscow Engineering Physical Institute) and Deissler and Taylor [2] for two complex channels. We see from the figures that the simple calculation of tangential stress by the method here proposed gives better agreement with experiment than do the other more complex forms of calculation. The equation for calculating the tangential stress at the wall does not reflect the effect of the Reynolds number. In general, the value of b in equation (5) must clearly be a function of both Φ_{ce} and Re. There is not enough information at the present time to determine the form of the relationship between b and Re. Apparently the value of b, and hence the ratio $\tau_0/\bar{\tau}_0$, may be taken as independent of Re in the range of Re numbers used in practice (10^4 to $1.5\cdot10^5$). This is to some extent based on the calculations of L. S. Kokorev for piles with different relative spacings and the experiments described in [6].

Knowledge of the tangential stress at any point on the wall of the channel enables us to find the velocity distribution along the normal to the wall at this point, if we assume a definite form of the relationship $u^+=f(y^+)$. The simplest assumption is to take the universal velocity-distribution law for a circular tube [2, 5]. Experimental verification of this assumption was carried out in [6-8]. It follows from these papers that the universal law is acceptable for complex channels and may be used for calculating the velocity distribution along the normals to the wall.

The following scheme of calculation is proposed.

1. An LMV (line of maximum velocity) is plotted on a sketch of the channel cross section as the geometric locus of points equidistant from the walls. If the channel has geometric symmetry, then a symmetrical part is separated our first.

2. The channel cross section is divided into cells. Within each cell the function $y_0(z)$ should be monotonically increasing or decreasing.

3. The values of F_{ce}, $\overline{y}_{0ce}$, and $d_{h_{ce}}$ ($d_{h_{ce}}$ = hydraulic diameter of cell) are found for each cell; the cell shape parameters and normalizing factors c are calculated from equations (7) and (9a).

4. A hydraulic-resistance coefficient λ_c is selected for the channel (to a first approximation, for example, by the Blasius formula) and the mean tangential stress on the channel walls is determined from the given mean velocity $\bar{u}$: $\bar{\tau}_{0c}=\lambda_c\rho\bar{u}^2/8$.

5. For each cell the mean tangential stress at the wall $(\bar{\tau}_0)_{ce}^{is}$ is calculated from the formula $(\bar{\tau}_0)_{ce}^{is}=\frac{d_{h_{ce}}}{d_{h_c}}\tau_{0_c}$, and the distribution of tangential stresses for each cell is calculated from equation (9).

6. For nonisolated cells, the function Ψ of equations (10)-(13) is used to determine the distribution of tangential stresses at the wall with due allowance for mutual interaction.

The correctness of the choice of the LMV as the geometric mean line is verified. In order to do this, the values of τ_0 at corresponding points in the cells adjacent to the LMV are considered (the normals to the perimeter

from these points intersect on the LMV). If the values of τ_0 at corresponding points differ negligibly (< 15%), then the position of the LMV need not be adjusted. For each pair of corresponding points the same arithmetic-mean value of τ_0 is taken and further calculation is carried out. If, however, a substantial difference appears between the tangential stresses at corresponding points, then the position of the LMV must be corrected by moving it in the direction of the cell with the greater τ_0, and the calculation is then repeated.

7. Using the universal law for a circular tube, the velocity distribution $u = f(y)$ is found along each normal y_{0i} to the LMV. In this way the velocity field is determined over the whole cross section of the channel.

8. By integrating the local-velocity distribution, the velocity $\bar{u}_p$ averaged over the channel cross section is found.

9. The calculated mean velocity $\bar{u}_p$ is compared with the given mean velocity $\bar{u}$. The values of these velocities should be close together if the hydraulic resistance λ_c has been chosen correctly.

In order to verify the method proposed, we calculated velocity distributions in various complex channels and compared with experimental data. The table gives a list of the channels for which the hydrodynamic characteristics (distribution of tangential stresses over the channel perimeter, distribution of velocities over the LMV and over individual characteristic normals to the channel perimeter) were calculated. The calculations are compared with experiment for channels of different shapes in Figs. 4-6. In all channels considered, the calculated and experimental velocities agree closely (maximum deviation of local velocities less than 10%).

Explanation of Symbols

u = local average velocity of liquid;
$\bar{u}$ = velocity averaged over channel cross section;
τ_0 = tangential stress at wall;
L = wetted perimeter;
F = through cross section;
d_h = hydraulic diameter ($4F/L$);
x = coordinate along the direction of flow;
y = coordinate along the normal to the wall;
y_0 = distance along the normal to the wall to the LMV;
z = coordinate along the wetted perimeter;
λ = frictional-resistance coefficient $\left(\frac{dp}{dx} d_h \frac{2}{\rho \bar{u}^2}\right)$;
u^+ = dimensionless velocity $\left(\frac{u}{\sqrt{\tau_0/\rho}}\right)$;
y^+ = dimensionless distance $\left(\frac{y\sqrt{\tau_0/\rho}}{\nu}\right)$;
ρ = density of liquid;
ν = viscosity of liquid;
p = pressure.

LITERATURE CITED

1. N. I. Buleev, K. N. Polosukhina, and V. K. Pyshin, Teplofizika vysokikh temperatur, 2, 749 (1964).
2. R. Deissler and M. Taylor, NACA, TN-4384 (1958).
3. A. A. Townsend, Structure of Turbulent Flow with Transverse Displacement [Russian translation], Moscow, IL (1959).
4. I. O. Khintse, Turbulence [in Russian], Moscow, Fizmatgiz (1963).
5. D. Hartnett et al., Trans. ASME, 84(1), 82 (1962).
6. Yu. D. Levchenko et al., Velocity Distribution in a Close-Packed Pile of Rods. In the collection: "Liquid Metals" [in Russian], Moscow, Atomizdat (in the press).
7. M. Kh. Ibragimov, I. A. Isupov, and V. I. Subbotin, Calculation and Experimental Study of Velocity Fields in a Channel of Complex Shape. In the collection: "Liquid Metals" [in Russian], Moscow, Atomizdat (in the press).
8. I. Nikuradze, Ingr-Arch., 1, 306 (1930).

9. H. Leutheusser, Amer. Soc. Civil. Engineers, J. Hydraulics Division, 89, (H4V-3), Pt. 1, 1 (1963).
10. Yu. D. Levchenko et al., Study of the Hydrodynamics of an Annular Gap with Longitudinal Fins. In the collection: "Liquid Metals" [in Russian], Moscow, Atomizdat (in the press).

All abbreviations of periodicals in the above bibliography are letter-by-letter transliterations of the abbreviations as given in the original Russian journal. *Some or all of this periodical literature may well be available in English translation.* A complete list of the cover-to-cover English translations appears at the back of the first issue of this year.

EFFECT OF NEUTRON IRRADIATION ON SOME PROPERTIES OF HEAT-RESISTANT CONCRETES

V. B. Dubrovskii, Sh. Sh. Ibragimov, A. Ya. Ladygin, and B. K. Pergamenshchik

UDC 621.039.538.7

In contrast to the structural materials of nuclear reactors, the radiation resistances of concretes used in biological shielding have not been sufficiently studied. A tendency has recently arisen for the preferential use of heat-resistant concretes in biological shielding instead of materials such as steel, cast iron, graphite, boron, etc., which are costly and in relatively short supply. In this paper we shall indicate the effect of reactor neutron irradiation on certain properties of Porland-cement and liquid-glass heat-resistant chromite concretes. The integral neutron flux used in this investigation was $(2\text{-}2.4) \times 10^{21}$ neutrons/cm^2 and the irradiation temperature up to 550°C.

It was found experimentally that these concretes retain quite high strength and elastic properties. The thermal conductivity and thermal expansion coefficient change very little. It is concluded that such concretes may be recommended for use in the biological shielding of nuclear reactors.

Published information on the radiation resistance of concrete is quite contradictory; it also relates mainly to fairly low integral fluxes of low-energy neutrons [1, 2]. Until recently, there has been no great need for a more intensive study of the radiation resistance of concrete; in thermal reactors, the leakage of neutrons into the shielding is fairly low, and the thermal shielding installed between the reactor tank and the concrete of the biological shielding reduces the flux of radiation passing into the concrete to 10^{11} MeV/cm^2·sec. The latter figure, recommended by a number of authors [3] from considerations of favorable thermal conditions in the shielding (temperature drop 30 to 60°C), clearly limits the integral neutron flux passing into the shielding to values of 10^{18} to 10^{19} neutrons/cm^2 (taking the service life of a reactor as 10 to 20 years).

In view of the development of atomic power-station construction and the development of fast reactors, with an increased radiative load on the shielding, a tendency has recently arisen for costly materials in relatively short supply to be replaced by heat-resistant ferroconcrete [4]. Best of all for this purpose is heat-resistant ferroconcrete with a chromite filler, which constitutes effective shielding even in the absence of water [4]. Structures made of this concrete are used at temperatures up to 1000 or 1100°C and temperature drops up to 600 or 700°C [5]. The radiation flux into the concrete, acceptable from the point of view of thermal conditions, is 10^{13} neutrons/cm^2·sec [4]. Thus in order to solve the problem of the practical use of chromite concrete in shielding we need radiation-resistance data for integral fluxes of 10^{21} to 10^{22} neutrons/cm^2. (In the conclusions of [4], the absence of data on the radiation resistance of concrete is considered the only obstacle to using this material as shielding from intense radiation fluxes.)

TABLE 1. Chemical Composition of the Samples

Concrete	Element, wt. %									
	H	O	Mg	Al	Si	Ca	Cr	Fe	Na	Others
Chromite concrete in Portland cement . .	0,70	37	11,54	5,14	2,64	4,63	30,7	6,45	—	1,20
Chromite concrete in liquid glass	—	32,94	10,12	4,48	6,79	—	27,91	6,79	8,5	1,6

Translated from Atomnaya Énergiya, Vol. 21, No. 2, pp. 108-112, August, 1966. Original article submitted December 8, 1965.

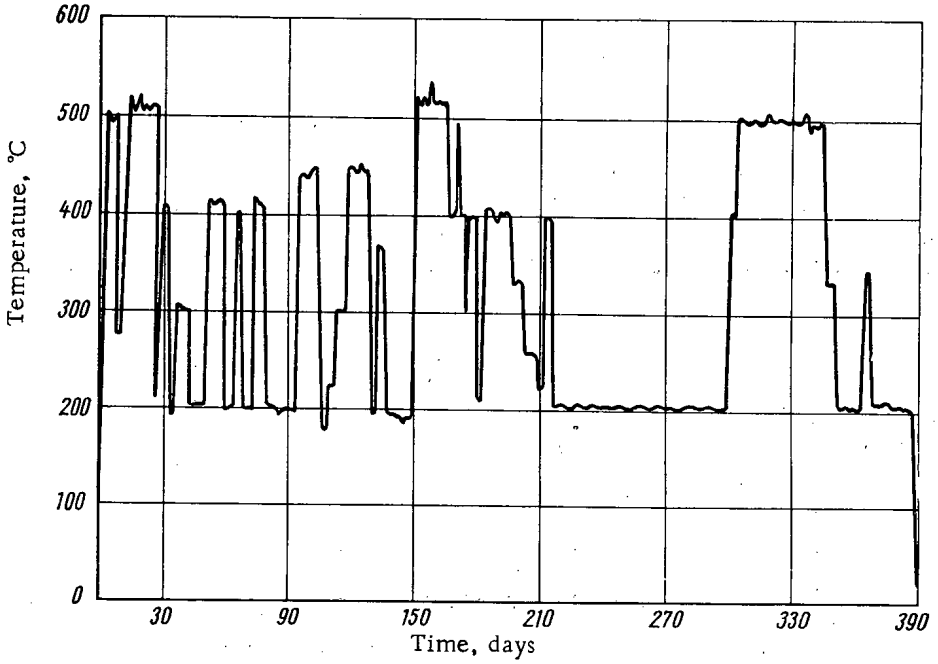

Fig. 1. Temperature variation of the samples during irradiation.

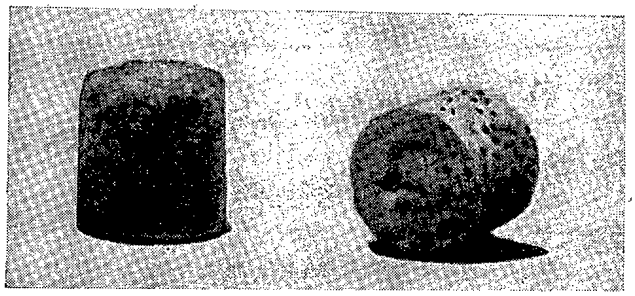

Fig. 2. Samples of chromite concrete in Portland cement after extraction from the ampoule.

TABLE 2. Thermal Conductivity of Chromite Concretes in kcal/m·h·°C

Sample batch	Concrete in Portland cement		Concrete in liquid glass	
	Mean result for the samples	Mean result for the batch	Mean results for the samples	Mean result for the batch
Irradiated	0,880 0,910 0,970	0,920	0,732 0,775	0,754
Hot	0,895 0,946 0,934	0,922	0,787 0,812 0,770	0,790
Cold	0,994 0,880 0,970	0,945	0,990 0,942 1,02	0,978

TABLE 3. Strength and Elastic Properties of Concretes

Samples of chromite concrete in Portland cement			Samples of chromite concrete in liquid glass		
Irradiated	Hot	Cold	Irradiated	Hot	Cold
56,6* / 0,64	110,4 / 0,77	124,6 / 0,817	82,1 / 0,615	90,6 / 0,682	209,5 / —
62,3 / 0,68	95,1 / 0,725	126,3 / 0,885	71,3 / 0,545	134,8 / —	262,7 / 0,885
41,3 / 0,68	81,5 / 0,725	94 / 0,68	74,7 / 0,58	141,6 / 0,853	286,5 / 0,885
53,8 / 0,68	78,1 / 0,634	126,3 / 0,885	—	141,6 / 0,767	207,2 / 0,885
37,4 / 0,612	35,1 / —	126,3 / 0,817	—	—	—
37,4 / 0,68	101,9 / —	78,1 / —	—	—	—
—	51 / 0,578	163,1 / —	—	—	—
Average value					
48,1 / 0,665	79 / 0,686	119,8 / 0,816	76,1 / 0,58	127,9 / 0,767	241,5 / 0,885
Relative value, %					
40 / 82	66 / 84	100 / 100	32 / 66	53 / 87	100 / 100

*Numerator of the fraction gives the strength of the sample in kg/cm^2; denominator gives the slope of the strain curve on the compression diagram.

In this paper we present the results of an investigation into the effects of reactor irradiation on certain characteristics of heat-resistant chromite concrete in Portland cement and liquid glass.* The chemical compositions of the materials studied are given in Table 1.

The samples for study took the form of briquettes 15 mm long and 15 mm in diameter and were prepared in the following way. After placing in demountable metal molds, the prepared mixture was consolidated by vibration for 30 sec. Then the samples of chromite concrete in Portland cement were kept for 7 days under damp conditions and the samples of concrete in liquid glass for 3 days under normal conditions, after which all the samples were dried for 32 h at 100 to 110°C. From then until the beginning of the experiment, the samples were kept at 20 to 25°C in a humidity of 60 to 70%.

Before the experiment, the samples were divided into three batches. The first batch ("irradiated") was placed in special stainless-steel hermetically-sealed ampoules and irradiated in the active zone of a reactor at 200 to 550°C.

The temperature variation is shown in Fig. 1. During irradiation, the samples received an integral neutron flux of $(2\text{-}2.4)\cdot 10^{21}$ neutrons/cm^2 with a mean neutron energy of 0.23 MeV (including 30% of neutrons with an energy greater than 0.7 MeV). The second batch of samples ("hot") was provided in order to eliminate the effects of temperature; these were also kept in hermetically-sealed ampoules, the thermal and humidity conditions being analogous to those of the irradiated batch, i.e., the temperatures and the duration of temperature oscillations exactly corresponded to those of the latter. Samples of the third batch ("cold") were treated as standards and kept under normal conditions of humidity and temperature.

The samples were extracted from the cases and their properties were studied in hot chambers. The samples were viewed through binoculars via a window in the chamber (ten-times magnification). No serious damage or

*Certain data on this were published at the beginning of 1966 [6].

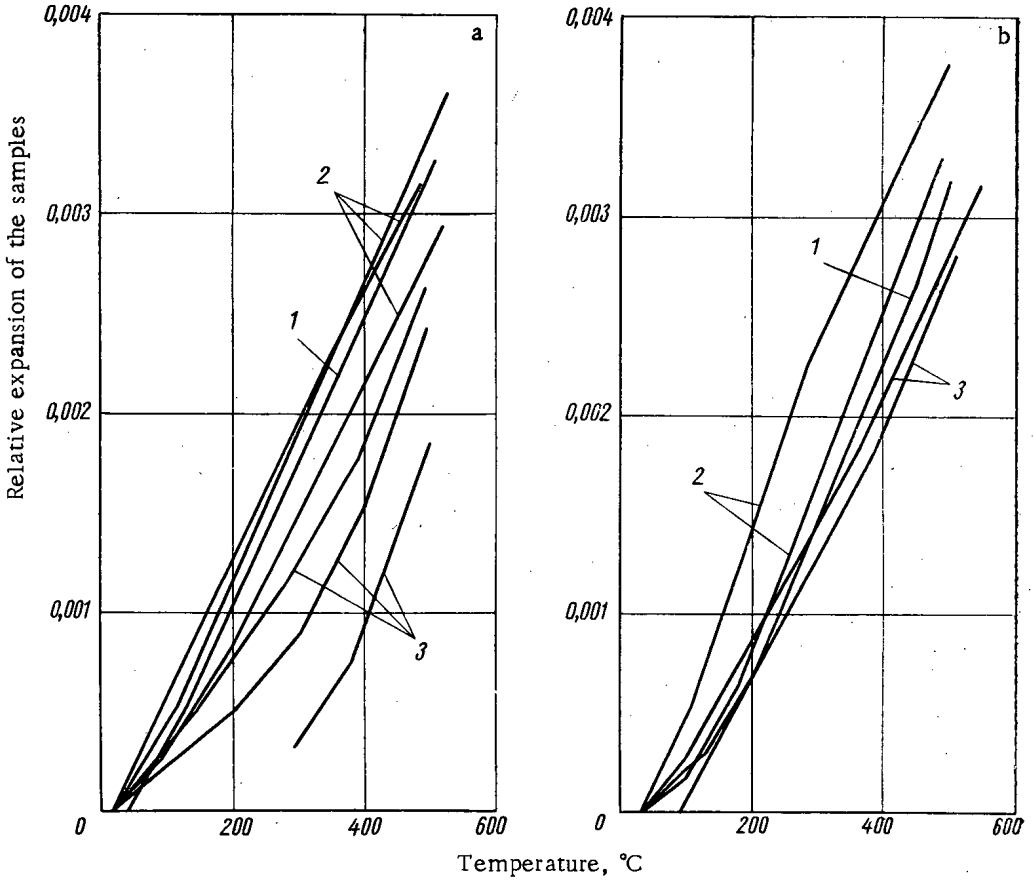

Fig. 3. Relative expansion of the samples as a function of temperature: a) First heating; b) second heating; 1) irradiated samples; 2) hot samples; 3) cold samples.

change in shape was observed. It was noted that in almost all the irradiated and control hot samples one of the end surfaces was more or less rounded (Fig. 2). This may be explained by inadequate consolidation of the mixtures used in forming the samples (loose edges) and the severe conditions of high temperatures and temperature oscillations.

The length and diameter of the samples were measured with a micrometer and sliding calipers (to an accuracy of 0.05 mm). The mean reduction in the linear dimensions (diameter and length) of the hot and irradiated samples as compared with the cold were 0.1 and 0.4% respectively.*

The samples were weighed on an analytical balance to an accuracy of 0.05 g; there was no noticeable change in the weight of the irradiated samples as compared with the hot control samples.

The thermal-conductivity coefficient of the irradiated and control samples was determined in a hermetically-sealed box in the same apparatus by the constant thermal-flux method. The end surfaces of the samples were kept at 20 to 30°C on one side and 120 to 130°C on the other during the measurements, i.e., the mean temperature was 70 to 80°C. Several measurements were made with each sample; three samples were tested from each batch.

The results of the measurements are shown in Table 2, from which we see that the thermal conductivities obtained are close to the values given in [7]; the slightly greater themal conductivity of the cold samples is quite legitimate and is due to the greater humidity of the samples in this batch; within the accuracy of the measurements (5 to 10%), the thermal conductivity of chromite concrete remained unaltered after irradiation by a flux of $(2\text{-}2.4) \cdot 10^{21}$ neutrons/cm^2.

The thermal-expansion coefficient was determined for the chromite concrete in Portland cement. The tests were made with a dilatometer, the expansion of the sample being determined by an indicator with a scale division

*According to data from the Scientific-Research Ferroconcrete Institute, the dimensions of samples of chromite concrete in Portland cement should diminish by 0.2% as a result of shrinkage after heating to 500°C.

of 0.002 mm, and the temperature being measured with Chromel–Alumel thermocouples. The highest temperature of the sample was 500°C and the heating rate 6 to 7 °C/min. The samples were held for 15 min at 100, 200, 300, 400, and 500°C and the expansion was then measured. After the sample had cooled, it was left for 12 h at normal temperature and humidity and the heating procedure was then repeated, together with the measurements.

Figure 3 shows a graph of the expansion of the samples with temperature. The thermal-expansion coefficients calculated from these graphs differ little from those given in [7]. The smaller elongation of the cold samples on first heating (see Fig. 3, a) is due to the fact that shrinkage occurred in the heating process. There are no great differences between the expansions of the irradiated and hot samples.

Strength tests were carried out on the irradiated and hot samples with a remote-control rupture machine at 20°C. The compression rate was 11 mm/min. The (compressive) strain diagram was plotted during the test. The results of the tests are shown in Table 3.

We see from the table that the strength of the irradiated samples of chromite concrete in Portland cement was 60% below that of concrete kept under normal conditions and 39% below that of concrete kept at the irradiation temperature of 200 to 550°C. The reduction in the strength of the samples due to the temperature factor only was 34% [7]. Hence, about 26% of the fall in strength must be attributed to the irradiation.

For samples of concrete in liquid glass, the strength after irradiation was 68 and 40% lower than in the cold and hot samples respectively. The fall in strength due to heating was 47%, i.e., the fall in strength due to irradiation equalled 21% (see Table 3). The 60% reduction in the strength of the concrete after irradiation at 200 to 500°C should not cause any anxiety. Calculations of shielding structures with temperature drops up to 800°C [4, 7] showed that the maximum compressive stresses in the concrete were of the order of 20 to 30 kg/cm^2, i.e., if chromite concrete of type 250 (the poorest allowable under standard requirements) were employed (this having a calculated compressive resistance of 105 kg/cm^2), some 70% of its strength was superfluous.

It is convenient to represent the fall in the strength of the concrete due to irradiation at high temperatures by means of a coefficient. For chromite concrete in Portland cement irradiated by a flux of $2.4 \cdot 10^{21}$ neutrons/cm^2 at 200 to 550°C, this coefficient equals 0.4. Allowing for this, the calculated compressive strength R^p_{com} of 250-type concrete will equal 42 kg/cm^2, which is rather greater than the values of 20 or 30 kg/cm^2 mentioned.

The small dimensions of the samples prevent the compression diagram from being used to calculate the elastic modulus. Changes in this characteristic after irradiation can only be found indirectly from the change in the slope of the compression curve. It follows from Table 3 that the mean slope of the compression curve is much the same for Portland-cement concrete samples belonging to the irradiated and hot batches (0.665 and 0.686 respectively), these values being approximately 20% below that of the cold samples. For liquid-glass concrete the slope is 13 and 34% lower than that of the cold samples for the hot and irradiated samples respectively.

The data presented in this paper show that after irradiation with a flux of $(2\text{-}2.4) \cdot 10^{21}$ neutrons/cm^2 at 200 to 550°C chromite concrete still retains fairly high strength and elastic properties. Such characteristics as the thermal conductivity and linear-expansion coefficient, moreover, hardly change at all. Hence the radiation resistance of this type of concrete does not restrict its use in the thermal shielding of a nuclear reactor.

The effects of irradiation on the shrinkage of concrete and on its strength and elastic-plastic properties are being studied at the present time.

In conclusion the authors wish to thank A. N. Komarovskii, by whose initiative this investigation was conducted, and also A. N. Vorob'ev, V. F. Gulyaeva, M. Ya. Kulakovskii, P. G. Pinchuk, and V. I. Savitskii for help in this work.

LITERATURE CITED

1. D. Clark, Hanford Works, HW-56195 (July 31, 1958).
2. J. Struct, Div. Proc. Amer. Soc. Civil Engrs., NST-I, 123 (1962).
3. B. Price, K. Horton, and K. Spinney, Shielding from Nuclear Radiations [Russian translation], Moscow, IL (1959).
4. V. B. Dubrovskii et al., Atomnaya Énergiya, 19, 524 (1965).
5. K. D. Nekrasov, Use of Heat-Resistant Concrete in Thermal Plant [in Russian], Moscow, Gosstroiizdat (1957).
6. A. N. Vorob'ev et al., Beton i zhelezobeton, No. 2, 11 (1966).
7. A. F. Milovanov, Heat-Resistant Ferroconcrete [in Russian], Moscow, Gosstroiizdat (1963).

RADIOACTIVE SOFT X-RAY SOURCE FOR PHYSICAL RESEARCH, TECHNOLOGY, AND MEDICINE

L. D. Danilin, S. I. Lobov,
A. I. Pavlova-Verevkina, and V. A. Tsukerman

UDC 539.26:615.849

Methods of obtaining x-ray sources containing Fe^{55} are described together with the characteristics of the sources. Applications of the soft characteristic x-rays emitted by this isotope in studying the atomic structure of materials and in contact x-ray microphotography are considered. The possibilities of using powerful Fe^{55} sources in medical and other research are examined.

The iron isotope Fe^{55} belongs to the comparatively small number of radioactive isotopes in which disintegration is accompanied by the emission of the characteristic x-ray spectrum without any hard γ-radiation. Recently, methods of preparing sources with a high specific content of this isotope free from other radioactive impurities have been introduced. This has enabled compact and convenient Fe^{55} sources to be used in research and technology instead of the present cumbersome apparatus with special x-ray tubes having beryllium windows and monochromators.

Characteristics and Methods of Production

The Fe^{55} isotope (half-life $T_{1/2}$ = 2.9 y, transition energy E = 220 keV) transforms into the stable manganese isotope Mn^{55} by electron K capture. In restoring the electron shells of the atom, the characteristic manganese spectrum is emitted. The coefficient of x-ray-quantum formation for one act of electron K capture is 0.3 [1]. The radioactive disintegration on the K-capture principle is accompanied by internal bremsstrahlung, but the intensity of this is much lower than that of the characteristic spectrum. The ratio of the number of emitted quanta of internal bremsstrahlung to the number of K captures for a transition energy of 220 keV is $3.8 \cdot 10^{-5}$ [1], so that Fe^{55} emits a practically pure characteristic x-ray spectrum.

The energy of the characteristic x-radiation of manganese is comparatively low, being 5.9 keV for the K_α-line (λ = 2.103 A). Matter attenuates such soft x rays very considerably. Thus the penetration of 5.9 keV radiation into iron foil (i.e., the distance required for e-times attenuation) is 15 μ.

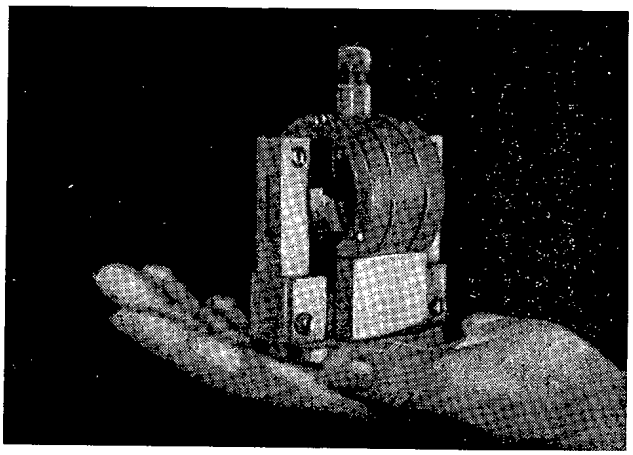

Fig. 1. The "Rada," used in the x-ray structural analysis of polycrystalline samples.

Translated from Atomnaya Énergiya, Vol. 21, No. 2, pp. 112-116, August, 1966. Original article submitted December 10, 1965.

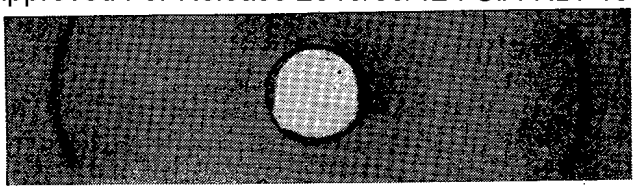

Fig. 2. X-ray diffraction photograph of an iron sample obtained in the "Rada."

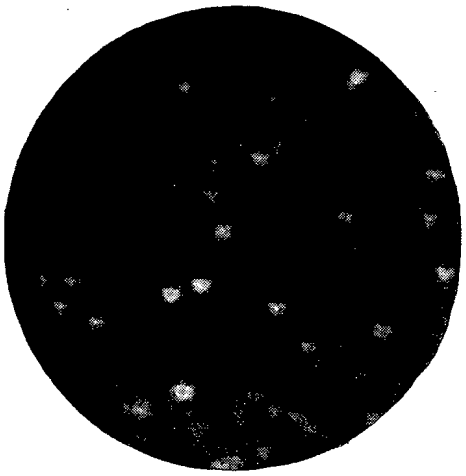

Fig. 3. Reproduction of an x-ray micrograph of an aluminum–zinc alloy. Thickness of template 0.08 mm; light parts correspond to zinc dendrites which severely attenuate the manganese radiation. Optical magnification 30×.

There are various methods of preparing Fe^{55}. By bombarding the stable Mn^{55} isotope with protons having energies of a few MV, radioactive iron is produced in the surface layers of the sample (p – n reaction). Small quantities of Fe^{55} (around 10 μCi) were obtained in an electrostatic generator by this method for the initial stage of our experiments. This method is unsuitable, however, for obtaining radioactive-iron sources of high activity.

A more promising method is the irradiation of iron isotope Fe^{54} with thermal neutrons, using the n – γ reaction. Unfortunately, the production of Fe^{55} is accompanied by an n – p reaction which produces radioactive manganese Mn^{54} ($T_{1/2}$=290 days, γ-radiation energy 835 keV). Although the cross section of this reaction is almost 250 times smaller than that of the n – γ reaction (0.011 and 2.5 b respectively), the activity of the Mn^{54} is around 2% of the activity of the Fe^{55}. In order to realize the main advantage of Fe^{55} as a source of practically pure characteristic x-radiation, the Mn^{54} and other possible radioactive impurities must be removed.

We used an Fe^{54} foil irradiated with a thermal-neutron flux of 10^{21} neutrons/cm^2 integral intensity in our experiments. The Fe^{55} content was about 0.25%, which corresponded to a specific activity of 5.5 Ci/g. The iron was separated from manganese, cobalt, and other impurities chromatographically, and a thin layer was deposited on a substrate. The activity of the resultant sources was about 50 mCi/cm^2. The γ-spectrograms of the purified sources showed a peak in the region of 70 keV, corresponding to the mean energy of the internal bremsstrahlung of the Fe^{55}. According to calculation, the intensity of this radiation should not exceed 0.01% of the intensity of the soft characteristic radiation. There were also two small peaks with energies 1.1 and 1.29 MeV, corresponding to the emission of Fe^{59}. The activity of this isotope did not exceed 10^{-4}% of the activity of the Fe^{55}.

A positive quality of Fe^{55} sources is the comparatively simple radiation shielding. Soft 5.9 keV x-rays are attenuated more than 10^6 times in a 1 mm layer of brass. Titanium is a suitable shielding element, since it selectively absorbs manganese K-radiation. After thorough purification from radioactive impurities, Fe^{55} sources can safely be kept and transported in light titanium or brass cans (wall thickness 1 to 2 mm).

Structural Analysis and X-Ray Microphotography

The characteristic manganese radiation emitted on disintegration of Fe^{55} is especially suitable for use in studying the atomic structure of matter. The calculations and initial experiments of [2] showed that with 5-mCi sources the interference maxima from an iron sample could be recorded in a small Debye camera after an exposure of 5 h. It was shown in [3] that the advantages of the radioactive method of x-ray analysis may be realized most fully in a focusing camera. X-ray diffraction photographs of commercial metals were obtained in a camera focusing widely-diverging x-ray beams with exposures of 18 to 20 h. In the experiments described in [2, 3], an Fe^{55}-containing iron foil not freed from other radioactive impurities was used, so that the main advantage of the method, the absence of extra background on the x-ray photographs, was not realized.

Sources containing Fe^{55} free from foreign radioactive impurities enable apparatus used in radioactive x-ray structural analysis to be improved and simplified. Figure 1 shows a general picture of a camera intended for this

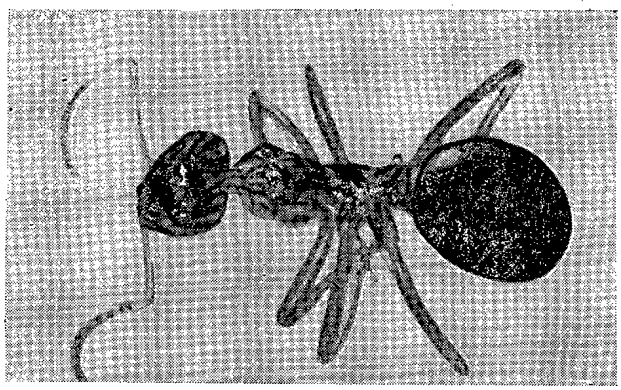

Fig. 4. Print of an x-ray micrograph of an ant. Radiation source Fe^{55}. Optical magnification 13 x.

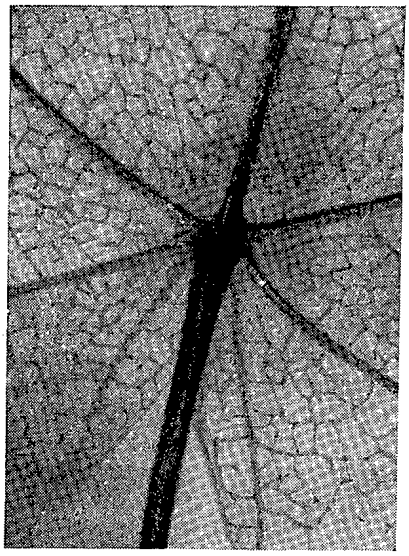

Fig. 5. Print of an x-ray micrograph of a maple leaf. Optical magnification 13x.

kind of work; it was designed by V. N. Funin and V. A. Tsukerman and given the name "Rada." As in [3], the light-concentrating method, involving the axial focusing of widely-diverging x-ray beams (Preston–Al'tshuler [4]), was used. The camera enables x-ray lines corresponding to Bragg angles between 55 and 82°(Θ) to be recorded. This is especially important in precision determinations of atomic lattice spacings.

Figure 2 shows an x-ray diffraction photograph of a well-annealed iron sample obtained in the "Rada." The interference rings recorded constitute reflections from the (112) atomic planes of α-iron. In the geometry taken, the angular resolution exceeds that of standard Debye cameras with a cassette diameter of 57.3 mm by a factor of 1.33.

Radioactive sources of characteristic radiation have a number of advantages over traditional methods for x-ray structural investigations. The size of the radioactive structural camera is many times smaller than that of the ordinary system involving an x-ray tube and high-voltage transformer. Analysis does not call for electrical power sources, so that x-ray photographs can be obtained under field conditions. Structural studies under special conditions are made easier, e.g., at temperatures close to absolute zero, or in inert or aggressive gas media. In such conditions the compact source of radioactive iron is introduced directly into the Dewar or chamber filled with the appropriate gas.

The Fe^{55} isotope is also a convenient source of soft x-radiation for contact x-ray microphotography. This method has become widespread in physical metallurgy, entomology, botany, and histology over the last 15 years. As in structural analysis, the [traditional] source of radiation is an x-ray tube with beryllium windows operating at 5 to 10 kV. By placing a fine object in close contact with a fine-grained photographic plate after irradiation with soft x-rays, a clear high-contrast image of the internal features can be obtained. After developing, the plate is magnified 10 to 100 times by ordinary optical methods.

The replacement of the x-ray tube in contact x-ray microphotography by a purified Fe^{55} source proved entirely satisfactory. The apparatus required for such work was quite simple, comprising a hollow metal cylinder, the lower end of which held a photographic plate with the object pressed firmly against it. The Fe^{55} source, 5 mm in diameter, was placed 10 cm from the photographic plate. With this arrangement, the image spread in the x-ray photograph was no greater than 5 μ for objects up to 0.1 mm thick.

Figures 3 to 5 show some micrographs obtained in the manner indicated. The micrographs were taken with NIKFI photographic plates of the MR type (resolution 250 lines to 1 mm).

In the x-ray micrograph of an aluminum–zinc template the siting and shape of xinc dendrites can be seen quite clearly (Fig. 3). The internal organs of an ant (Fig. 4) and the arrangement of the capillaries near the stalk of a maple leaf (Fig. 5) are also clearly visible.

The characteristic manganese radiation is also especially suitable for x-ray study of bone sections. Owing to the substantial attenuation of the manganese radiation in calcium, clear and high-contrast images of the calcium distribution in bone tissue can be obtained in this way.

Use in Medicine and Technology

Calculations and dosimetric measurements showed that our 1-cm^2 sources containing 0.25% Fe^{55} in direct contact with an irradiated object gave a dose of around 150 R/h. Ways are now clear for preparing sources of higher specific activity. On irradiation with a thermal-neutron flux of integral intensity 10^{22} neutrons/cm^2, the Fe^{55} content rises to 2 or 3%, and the x-ray dose to 1500 R/h. On enriching the source to 20 or 30% Fe^{55}, the radiation does exceed 15,000 R/h.

Such powerful soft-x-ray sources are of special interest in x-ray therapy. In depth of penetration and medicinal effect the 5.9 keV manganese radiation corresponds to the bremsstrahlung of an x-ray tube operating at 10 to 15 kV. X rays of this energy (Bucky rays) are widely used in radiotherapy for healing eczema and other skin diseases. Qualitatively no different from the bremsstrahlung used in Bucky-therapy equipment, radioactive-iron sources present a number of advantages and open new possibilities in medical x-ray technology. There is no longer any need for special therapeutic tubes with windows transparent to soft x-rays. The disk on which the radioactive iron is laid may be introduced into cavities where it is difficult to place an x-ray tube. It is comparatively simple to irradiate eczema and malignant growths in the oral cavity, eyeball, etc. In addition to methods in which the active surface of the source is placed in the immediate vicinity of the irradiated part, other approaches are possible, for example, the introduction of steel needles containing Fe^{55} into the tumor of the patient.

The use of powerful radioactive-iron sources is also extremely convenient for fluorescent x-ray spectral analysis under field conditions. The use of radioactive thulium for this purpose was mentioned in [7], but this has not had any widespread application. Radioactive iron may effectively be used for exciting the K spectra of chromium, vanadium, titanium, scandium, calcium, and other elements with atomic numbers lower than that of manganese. The L_1 spectra of elements with L levels of lower energy than the manganese K spectrum (lanthanum, barium, cesium, etc.) may also be excited.

The Fe^{55} isotope is a convenient source of soft x rays for measuring the thickness of thin plates and coatings. Zirconium–tritium targets were used as radioactive sources for such measurements in [8]. The bremsstrahlung arising from interaction between the β-particles of the tritium and the zirconium atoms either passed directly through the foil being monitored or excited the chracteristic x-ray spectrum of a secondary (fluorescent) target. The intensity of the soft x-rays so obtained is several orders lower than that of the characteristic spectrum given by the Fe^{55} source. Use of the latter in measuring the thickness of thin foils and coatings thus simplifies the recording apparatus, increasing accuracy, and reduces the time spent.

We note finally that, in its diversity of applications to physics, medicine, and technology, Fe^{55} is in no way inferior to such well-known radioactive isotopes as Co^{60} and Cs^{137}. The practical advantages of these materials reduce mainly to the replacement of cumbersome electrical installations in x-ray defectoscopy and radiotherapy by small, compact sources. These advantages are preserved with radioactive iron. In addition to this, Fe^{55} may be used in many investigations calling for a practically pure characteristic x-ray spectrum.

LITERATURE CITED

1. S. V. Starodubtsev and A. M. Romanov, Nuclear Transformations and the Atomic Shell [in Russian], Tashkent, Izd. AN UzbSSR (1958).
2. S. I. Lobov and V. A. Tsukerman, Dokl. AN SSSR, 165, No. 6 (1965).
3. S. I. Lobov, V. N. Funin, and V. A. Tsukerman, Kristallografiya, No. 4, 599 (1966).
4. L. V. Al'tshuler, ZhÉTF, 13, No. 11-12 (1943).
5. D. B. Gogoberidze, Usp. fiz. nauk, 50, No. 4, 577 (1953).
6. V. Cosslett et al., X-Ray Microscopy and Microradiography, N.Y. (1957).
7. K. I. Narbutt, R. L. Barinskii, and I. S. Smirnova, Izv. AN SSSR, Ser. fiz., 24, No. 4, 354 (1960).
8. S. I. Lobov and V. A. Tsukerman, Pribory i tekhnika éksperimenta, No. 4, 164 (1963).

NUCLEONIC DIGITAL SERVOMECHANISM

Pavel Kovanic and Jaroslav Ryhl

UDC 621.039.564

This article describes a digital device designed to measure the relative departure of the pulse count rate from set point. This device can be used in the design of digital servomechanisms intended for work with pulsed detectors, as, for example, in the measurement and automatic control of reactor power output and reactor period.

Detectors of ionizing radiations are most frequently operated in pulsed fashion in nuclear applications: in measuring levels of ionizing radiations to assure safe working conditions; in monitoring nuclear reactor performance, etc. In those cases information on the parameter measured is secured through the pulse count rate. The pulse count rate also provides output information from the devices sensing various physical variables (such as gas pressure, fluid flow rate). It is often not only the average count rate which has to be measured, but also departures of the average count rate from set point, especially when count rate meters are incorporated in the servomechanism. This type of servomechanism is designed for automatic control of a variable characterized by the count rate, or to annunciate departures of the controlled process from the required state. If the average count rate varies over a wide range, it is the relative deviation of the average count rate rather than the absolute deviation from set point which has to be measured, so that the servomechanism gain can be kept independent of the average count rate of input pulses.

Impressive progress has been made in pulse counting rate measurements by the use of digital techniques which improve the precision and reliability of systems, expand the range of available measurements, and bring the system closer to complete automation. These advantages aided the rapid development of special digital devices designed to measure average count rate, replacing the more primitive devices which utilize only input pulse counters or dial type pulse counters.

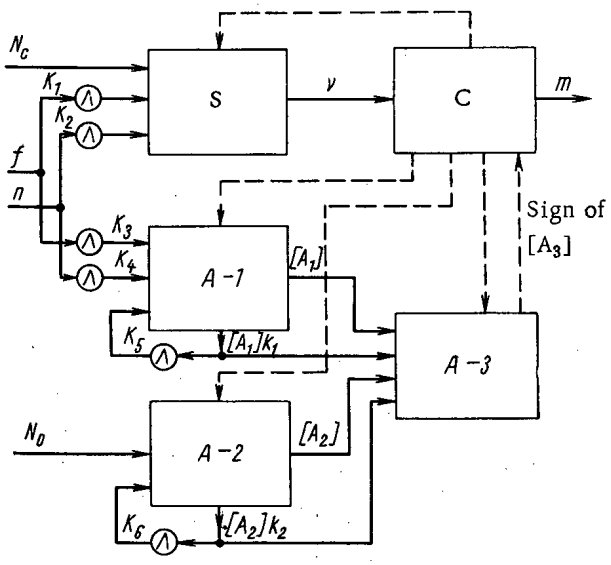

Fig. 1. Generalized circuit diagram of digital rate meter.

Nuclear Research Institute of the Czechoslovak Academy of Sciences, Řež pod Prahou, ČSSR. Translated from Atomnaya Énergiya, Vol. 21, No. 2, pp. 116-120, August, 1966. Original article submitted February 18, 1966.

TABLE 1. Possible Modes of Digital Rate Meter and Performance Data

Operating mode		Device measuring relative deviation of count rate				Log count rate meter			
		1	2	3	4	5	6	7	8
Statistical error		Variable		Constant		Variable		Constant	
Duration of operating interval		Constant		Variable		Constant		Variable	
Switches	K_1	1	1	0	0	1	1	0	0
	K_2	0	0	1	1	0	0	1	1
	K_3	0	0	1	1	0	0	1	1
	K_4	1	1	0	0	1	1	0	0
	K_5	0	0	0	0	1	0	1	0
	K_6	0	0	0	0	0	1	0	1
Coefficient	k_1	k_1	0	k_1	0	k_1	0	k_1	0
	k_2	0	k_2	0	k_2	0	k_2	0	k_2
Formula for specified count rate n_0		$f\frac{N_0}{N_c}$	$f\frac{N_0}{N_c}$	$f\frac{N_c}{N_0}$	$f\frac{N_c}{N_0}$	$f\frac{N_0}{N_c}$	$f\frac{N_0}{N_c}$	$f\frac{N_c}{N_0}$	$f\frac{N_c}{N_0}$
Register contents at start of calculating interval	A-1	$N_c\frac{n}{f}$	$N_c\frac{n}{f}$	$N_c\frac{f}{n}$	$N_c\frac{f}{n}$	$N_c\frac{n}{f}$	$N_c\frac{n}{f}$	$N_c\frac{f}{n}$	$N_c\frac{f}{n}$
	A-2	N_0	N_0	N_0	N_0	N_0	N_0	N_0	N_0

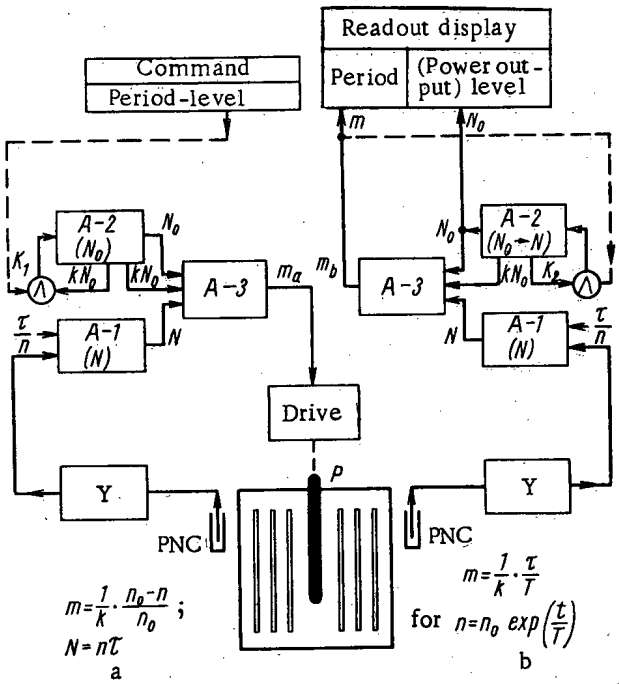

Fig. 2. Block diagram of count rate meter employed in monitoring nuclear reactor performance.

TABLE 2. Formulas Giving Variants in Operation of Rate Meter

State	Formula for m	State	Formula for m
1	$m=\frac{1}{k_1}\cdot\frac{n_0-n}{n}$	5	$m=\frac{\log\left(\frac{n_0}{n}\right)}{\log(1+k_1)}$
2	$m=\frac{1}{k_2}\cdot\frac{n_0-n}{n_0}$	6	$m=\frac{\log\left(\frac{n}{n_0}\right)}{\log(1-k_2)}$
3	$m=\frac{1}{k_1}\cdot\frac{n-n_0}{n_0}$	7	$m=\frac{\log\left(\frac{n}{n_0}\right)}{\log(1+k_1)}$
4	$m=\frac{1}{k_2}\cdot\frac{n-n_0}{n}$	8	$m=\frac{\log\left(\frac{n_0}{n}\right)}{\log(1-k_2)}$

Linear and functional rate meters alike can be built up from digital count rate meter circuits [1-5]; this applies to log count rate meters and log count rate ratio meters.

This article describes an inexpensive digital device which measures the relative deviation of the average count rate from set point and which can be used in servomechanisms (after simple feedback loops are introduced).

Figure 1 shows a generalized block diagram of a rate meter consisting of three binary accumulators A-1, A-2, A-3, a scaler S, and a control device C. Switches $K_1 - K_6$ control various operating modes of the meter by making or breaking connections between the components. (The actual circuitry for a practical rate meter would be decided upon on the basis of the instrument function.)

To get a clearer picture of the operation of this rate meter, consider the state of the switches suited to measurement of the relative departure of the input variable from set point: switches K_1 and K_4 closed, and switches K_2, K_3, K_5, K_6 open.

Input pulses operate on the scaler input at an average count rate f. A previously assigned number N_C is stored in the control device. As soon as the number of pulses recorded equals N_C, a synchronizing pulse ν is transmitted from the output of the control device C, and then the scaler resets. Input pulses operate with average count rate n on the input of the accumulator A-1, and these pulses are recorded from the time the register is cleared to the time the synchronizing pulse arrives. This clock pulse ends the operating interval and begins the arithmetic operations interval.

The number $[A_1]$ stored during the operating interval is transferred to A-3, where the number $[A_2]$, that is, the contents of A-2, is subtracted from the number $[A_1]$. (A specified number N_0 is assigned to the last register when the operation begins.) After the difference $[A_1] - [A_2]$ is taken in A-3, the k_1-th part of the information contained in A-1 is removed from its register, and the k_2-th part of the number $[A_2]$ is taken from A-2. Both of these resulting numbers are added to the contents of the A-3 register or are subtracted from the latter, depending on the sign of the difference $[A_1] - [A_2]$. The numbers stored in A-1 and A-2 are retained during the calculations. Since the registers are designed for a binary system and the numbers k_1 and k_2 equal $2^{\varkappa_1}$ and $2^{\varkappa_2}$ respectively, where $\varkappa_1$ and $\varkappa_2$ are negative integers, the numbers $[A_1]k_1$ and $[A_2]k_2$ can be obtained by shifting the numbers $[A_1]$ and $[A_2]$. The cyclic addition of numbers $[A_1]k_1$ and $[A_2]k_2$ to the contents of A-3 repeats, so that the number $[A_3]$ gradually tends to zero. The control device sends out an output pulse with each cycle adding $[A_1]k_1$ and $[A_2]k_2$ to $[A_3]$. The calculation interval ends at the instant the sign of $[A_3]$ reverses, as annunciated by the A-3 register. The letter m designates the number of output pulses, i.e., the number of cycles required to clear the number $[A_1] - [A_2]$ with the number $[A_1]k_1 + [A_2]k_2$. The following approximate equation is valid at the time the calculation in calculation interval ends:

$$[A_1] - [A_2] \pm m([A_1]k_1 + [A_2]k_2) = 0. \quad (1)$$

The number of output pulses transmitted in a single operating period, consisting of one operating and one calculating interval, is

$$m = \mp \frac{[A_1]-[A_2]}{[A_1]\,k_1+[A_2]\,k_2}. \qquad (1')$$

The number m is therefore proportional to the relative difference of the contents of A-1 and A-2.

After the calculating interval is terminated, the control device C clears the contents of S, A-1, and A-3, and opens the inputs of the scalar and of the A-1 register, which had been closed during the calculating interval. A single period ends at this point and the next one begins. The duration of the arithmetic operations depends on the speed of response of the registers and can be negligibly short compared to the operating interval in many cases. Otherwise loss of input information can be avoided by redundancy in the input registers.

Figure 1 shows how the relative differences are measured. This setup can be used for other purposes after the feedback loops are closed by switches K_5 and K_6 (see Fig. 1). This transfers numbers $[A_1]k_1$ or $[A_2]k_2$ to A-1 and A-2 at the same time they are transferred to A-3.

The information contained in A-1 or in A-2 varies during the calculating interval when switches K_5 and K_6 are closed, and this means a change in the output number m. The register contents are designated by subscript zero when the operating interval terminates. When $k_2 = 0$,

$$m = \pm \frac{\log ([A_2]_0/[A_1]_0)}{\log (1+k_1)}; \qquad (2)$$

and when $k_1 = 0$, then

$$m = \pm \frac{\log ([A_1]_0/[A_2]_0)}{\log (1-k_2)}. \qquad (3)$$

Equations (2) and (3) can be obtained by summing the increments transmitted during the calculating interval to A-3. As mentioned earlier, the sign is determined automatically in Eqs. (1) through (3) from the sign of the difference $[A_1]-[A_2]$ at the start of the calculating interval. Thus, the device shown in Fig. 1 can be used to measure the relative difference of two numbers or the logarithm of the ratio of two numbers.

The exact value of Eqs. (1)-(3) depends on the nature of the input pulse trains and on the concrete way in which the circuit connections are completed. One of the pulse sequences shown in Fig. 1 is made up of strictly periodic pulses, with rate f, and the other consists of pulses whose count rate is unknown and is denoted as n. Depending on the state of switches $K_1 - K_4$, "clock" pulses are sent to C and measured pulses are sent to A-1, or vice versa, K_5 and K_6 are used to close the feedback loops for A-1 or A-2. Table 1 lists some of the possible combinations. The numeral 1 means the switch is open, the numeral 0 means the switch is closed. Formulas for calculating m appear in Table 2.

As Tables 1 and 2 show, modes 1 through 4 correspond to taking measurements of the relative departure of the counting rate n from the set point n_0, and in cases 1 and 4 the output signal of the relative deviation corresponds to division of the deviation by the actual value of the counting rate n, while in cases 2 and 3 it means division of the deviation by the count rate set point n_0. Cases 5 through 8 correspond to measurement of the logarithm of the measured count rate to set point ratio.

An analysis of the operating modes detailed in Tables 1 and 2 shows that the same digital device with its simple structure can be used to measure the relative deviation of the pulse count rate from set point, or to measure the logarithm of the ratio of these count rates at the same time that the count rate is measured, and, in case 6, at the same time that the reciprocal logarithmic derivative of the pulse count rate is measured, as will be shown below. Simple changes in circuit connections between rate meter components make it possible to convert from operation with constant intervals between readouts to operation with constant statistical precision and vice versa, and to bring about a variety of modifications in the operating characteristics of the rate meter. The setup described can also be adapted to variations in counting rate over a broad range.

Figure 2 shows a diagram illustrating the use of digital pulse count rate meters in nuclear reactor control. Pulsed neutron counters PNC are placed in the neutron flux of the reactor P. The pulse count rate is proportional

to this flux. Pulses from the counters are amplified by the amplifier Y, where pulses of low amplitude are discriminated; the discriminated pulses are converted to standard form. Digital count rate meters of the type described above process the pulse data further.

This rate meter is used, in Fig. 2, a, in automatic control of the reactor period and output level. The meter operates in mode 2 (see Table 1) so that the output number m_a is proportional to the relative departure of the count rate n from the set point n_0. This number determines the rate of advance of the control rod or the change in position of the control rod actuated by the rod drive DR. The rate meter keeps the reactor power output level constant when there is no change in the contents of A-2. If the power output level has to be raised or lowered exponentially, the command element closes the feedback loop by means of the logic element K_1, thereby varying the number N_0 exponentially. The change in N_0 brings about a corresponding deviation in m_a, which in turn, through its effects on the reactivity, causes the reactor output level to track the varying contents of the A-2 register. The rereading speed for the number kN_0 plus the absolute value of the number k together determine the assigned reactor period, and consequently the controlled reactor period. The feedback operating time determines by how many times the assigned counting rate (reactor power in this application) will vary with respect to the initial value.

The second part of the arrangement (see Fig. 2, b) shows how a rate meter of this type is applied to measurements of reactor period and reactor power level. In this case the meter is operated in mode 6 (see Table 1). The feedback loop is closed by logic switch K_2 while increments $[A_2]k$ are being added to the contents of the A-3 register, so that the output number m_b is inversely proportional to the reactor period, and the number $[A_2]$ is converted in each calculating interval from the "old" value N_0 to the next value of the measured number N proportional to the reactor power level, i.e., the number stored in A-2 tracks the reactor power level. This makes it possible to obtain information on both power, i.e., $[A_2]$, and on reactor period, i.e., m_b. The relative deviation of the power level from the fixed set point has to be measured when the reactor is operated at constant power level. This is achieved in a simple manner: the appropriate number N_0 is read into the A-2 register by means of the closed feedback loop during the conversion of reactor power output to a constant level. After that it is sufficient to interrupt the feedback by opening switch K_2, which takes the rate meter into mode 2 (see Table 1), and the output number m_b becomes proportional to the measured relative power deviation.

An analysis of the arrangement shown in Fig. 2 shows that the digital device described has the positive qualities inherent in servomechanisms with movable detectors [6, 7] even when it is operated with detectors fixed in place. This derives from the structural similarity of servomechanisms of either type: an exponential type element is used and feedback loops are closed on the device measuring relative deviation of the input variable from set point.

The problem of making digital measurements of the relative deviation of pulse count rate from set point is solved then by means of a comparatively simple digital device. A different mutual arrangement and interconnection of the same components will impart different properties to the rate meter system. The introduction of feedback makes it possible to devise servomechanisms, on the basis of the same general device, for measurement or automatic control of the pulse count rate over a wide range. A digital servomechanism measuring both power level and period of a nuclear reactor, or the relative deviation of the power level from set point, can be devised in this way, and a reactor period-level automatic control servomechanism can be devised with equal facility.

The proposed digital servomechanism can aid the solution of many nuclear engineering problems.

LITERATURE CITED

1. C. Vincent and J. Rowles, Instrum. and Methods, 22, 201 (1963).
2. C. Vincent, J. Rowles, and R. Steels, Nucl. Instrum. and Methods, 26, 221 (1964).
3. J. Schmidt, B. Eriksen, and W. Peil, IRE Trans. on Nucl. Sci., NS-8, No. 3, 1 (1961).
4. Y. Takahashi and S. Tamatsu, Digital Start-up Control of a Research Reactor, Central Research Laboratory, Tokyo (April, 1964).
5. M. Combet, H. Van Zonneveld, and L. Vevbeck, IEEE Trans. on Electr. Computers, EC-14, No. 6 (1965).
6. P. Kovanic and M. Kulka, Atomnaya énergiya, 5, 403 (1958).
7. P. Kovanic et al., Atomnaya énergiya, 12, 350 (1962).

CALIBRATION OF SCINTILLATION COUNTERS WITH ALLOWANCE FOR SCATTERED RADIATION

M. B. Vasil'ev

UDC 539.166:539.16.08

A method is described for calibrating scintillation counters which takes scattered radiation into consideration. Buildup factors for the reflection of radiation from a radium source, and analytic approximations to them, were determined. The formula obtained for the total intensity of direct and scattered γ-rays gives a calibration curve unperturbed by scattered radiation when used for the calibration of scintillation counters.

The γ-ray intensity during the calibration of radiation meters by means of standard radium sources is expressed by the well known formula

$$I = 840 \frac{Q}{r^2} e^{-\mu r}, \tag{1}$$

where 840 is the γ-constant for radium, $\mu R \cdot h^{-1} \cdot m^2 \cdot mg^{-1}$; Q is the radium content of the source, mg; r is the distance between source and detector, m; μ is the linear absorption coefficient for γ-rays in air, m^{-1}. In calibration, one can neglect γ-ray absorption in air [1] so that $e^{-\mu r} = 1$.

Formula (1) makes it possible to calculate the intensity of direct radiation from a point isotropic radium source. However, a detector also records radiation from the radium source which is scattered from the surface of the ground during calibration [2, 3]. The scattered radiation contribution to the total radiation from the source amounts to as much as 50% (Fig. 1). There are various methods for elimination of the scattered radiation which perturbs the behavior of the calibration curve, but they usually require additional apparatus and equipment.

The method proposed below enables one to take into account the radiation from a radium source which is scattered from the surface of the ground. The fraction which is contributed to the total detected radiation by scattered radiation is expressed through a buildup factor for radiation reflection. Numerically, the buildup factor

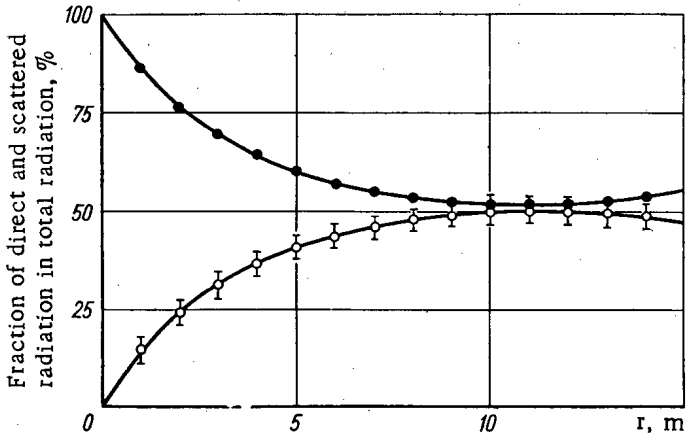

Fig. 1. Fraction of scattered radiation in total radiation as a function of the distance r. ●) Direct radiation; ○) scattered radiation.

Translated from Atomnaya Énergiya, Vol. 21, No. 2, pp. 121-125, August, 1966. Original article submitted January 24, 1966.

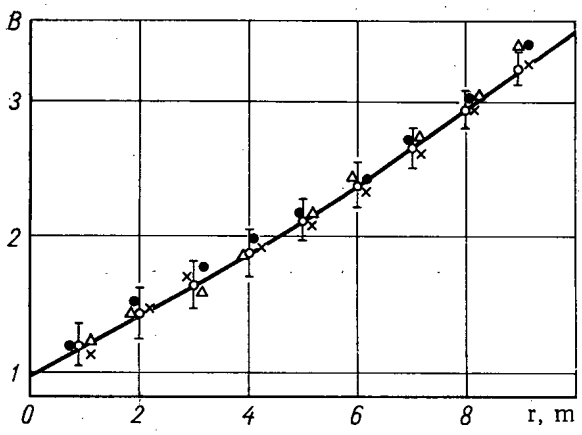

Fig. 2. Variation of buildup (without background subtraction) as a function of distance r for series 1 radium source at different calibration stations. ○) Calculated from the formula $B = 1 + 0.1965r + 0.00582r^2$; experimental data: ×) station 1; ●) station 2; △) station 3.

is the ratio of the effect produced by the total direct plus scattered radiation to the effect of the direct γ-rays, i.e.,

$$B = \frac{I_d + I_s}{I_d}, \qquad (2)$$

whence

$$I = I_d + I_s = BI_d. \qquad (3)$$

Here, I is the intensity of the total recorded radiation; I_d is the intensity of the direct radiation from the source, which is determined by formula (1); I_s is the intensity of the scattered radiation. Thus the total direct and scattered radiation which produces an effect in the detector is determined from the formula

$$I = 840\, B \frac{Q}{r^2}. \qquad (4)$$

In the experimental work, a commercial SRP-2 γ-meter was used. Buildup factors were obtained with and without subtraction of background for series 1, 2, and 10 radium sources containing 0.1, 0.2, and 1 mg of radium, respectively. To determine the value of B, the meter was calibrated at 1.5 m above the ground where the detector records direct and scattered radiation from the source, $I_d + I_s$, and also at a height where the intensity of the radiation scattered from the ground was negligibly small.

In order to select the latter, calibrations were performed at heights of 1, 1.5, 2, 3, 4, 6, 8, and 10 m, and the buildup factors were calculated for each height. The experimental results have been published [4], and they indicate that the detector records mainly direct radiation from the source at heights ≥8 m.

The numerical values of the quantity B were determined in the following manner. Calibration curves were drawn for three ranges of the meter with and without background subtraction and for heights of 1.5 and 10 m. The same scale was used for each range. From the calibration curve taken at 1.5 m height, abscissae were found corresponding to the radiation intensity $I_{1.5}$ for each distance r. The extension of these abscissae to intersection with

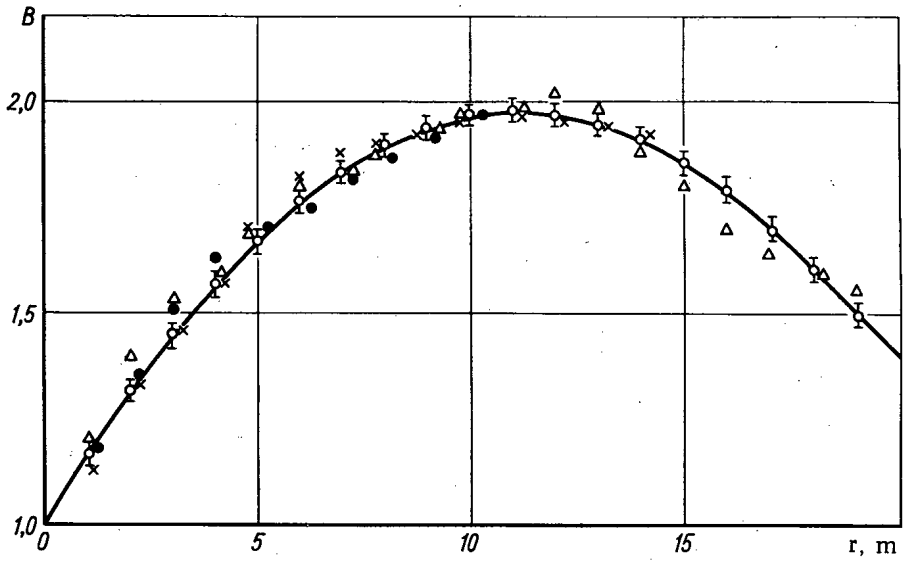

Fig. 3. Variation of buildup factor as a function of distance r for series 1, 2, and 10 radium sources. ○) Calculated from the formula $B = 1 + 0.174r - 0.078r^2$; experimental data: ●) series 1 source; ×) series 2 source; △) series 10 source.

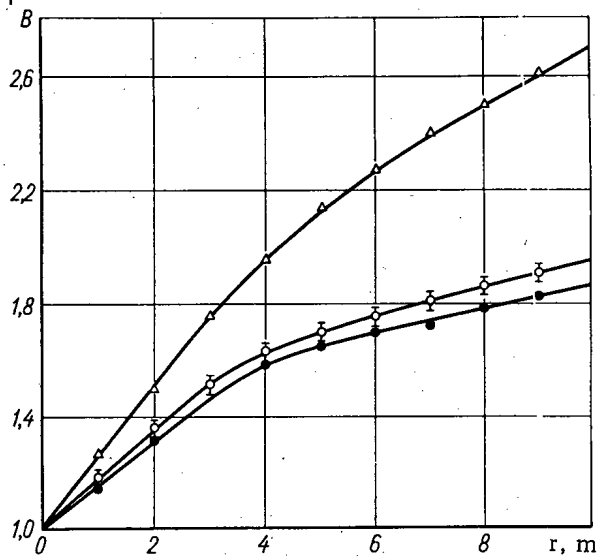

Fig. 4. Variation of buildup factor as a function of distance r above loam, gravel, and water surfaces. △) Water; ○) loam; ●) gravel.

the curve taken at 10 m determined the radiation intensity I_{10} corresponding to the same meter reading as for the 1.5 m height. Division of I_{10} by $I_{1.5}$ produced the coefficients B by means of which the results of meter calibration at 1.5 m were reduced to the 10 m level.

Values of the coefficient B for a series 1 source were obtained without background subtraction at three different calibration stations (1, 2, and 3) located at distances up to 8 km from one another. The values of the effective atomic number Z_{eff} of the reflecting media generally should be somewhat different for the calibration stations listed. The buildup factors obtained at each of the stations agreed with limits of experimental error. This is explained by the fact that the buildup factors for light elements vary insignificantly in the transition from element to element [5, 6]. For a series 1 radium source, the dependence of the factor B (without background subtraction) on distance r is described by the analytic expression

$$B = 1 + 0.1965r + 0.00582r^2. \tag{5}$$

A curve for the variation of the buildup factor as a function of distance r, calculated by formula (5), is shown in Fig. 2. Also plotted on the curve are experimental values of B obtained at calibration stations 1, 2, and 3.

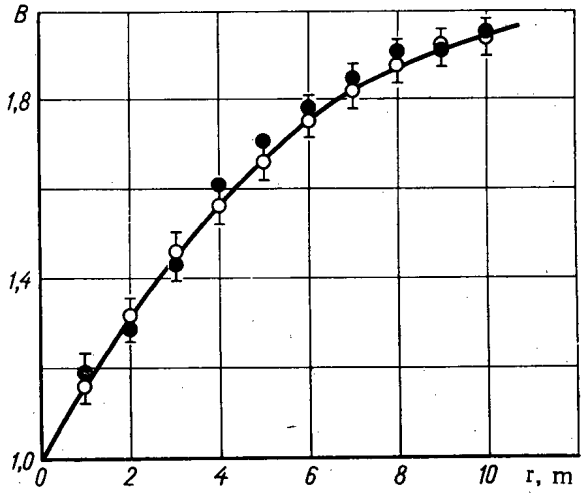

Fig. 5. Variation of buildup factor as a function of distance r for an 18 × 30 mm scintillator. ○) Calculated from the formula $B = 1 + 0.174r - 0.0078r^2$; ●) experimental data.

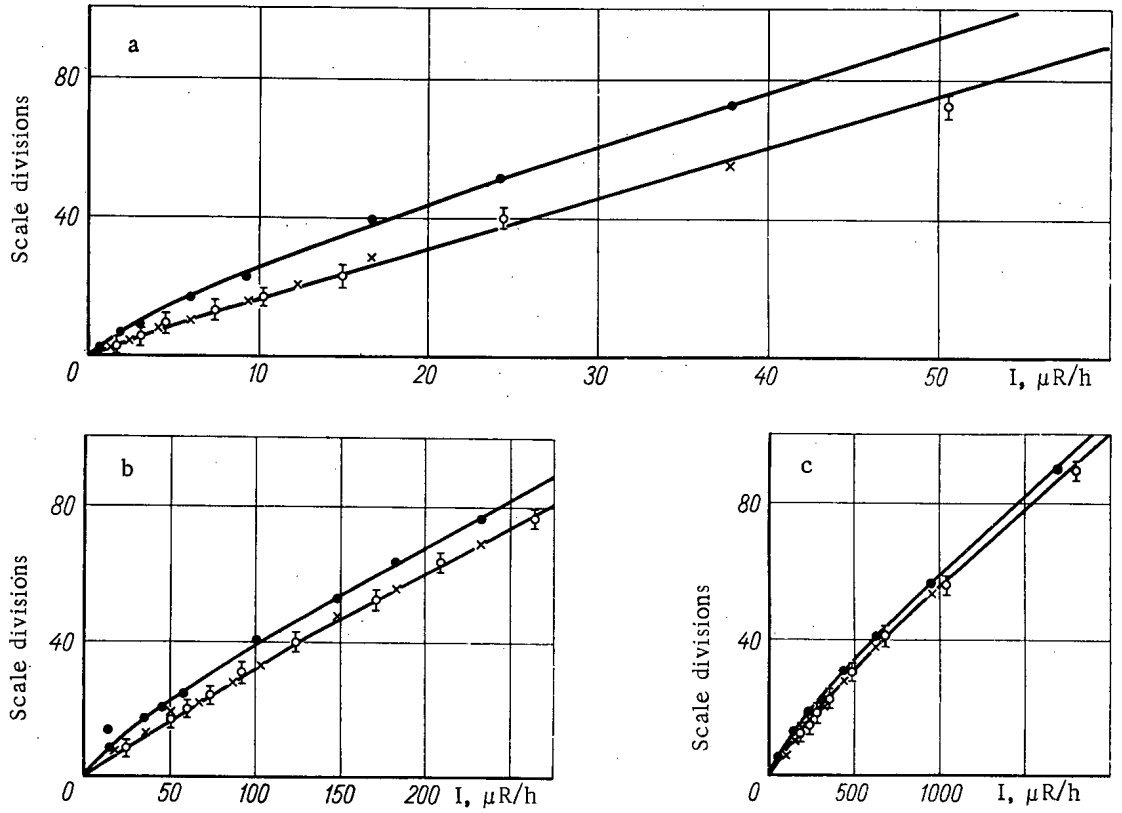

Fig. 6. SRP-2 calibration curves obtained with a series 2 radium source. a)First range; b) second range; c) third range; ●) at 1.5 m (calculated from the formula $8.4 \cdot 10^9\ Q/r^2$); ×) vertical calibration (from the formula $8.4 \cdot 10^9\ Q/r^2$); ○) at h = 1.5 m [from the formula $(1 + 0.174r - 0.0078r^2) \cdot 8.4 \cdot 10^9\ Q/r^2$].

Similar results were obtained also in the determination of the values of B for a series 2 radium source. In this case, the buildup factors can be approximated by the expression

$$B = 1 + 0.148r - 0.005385r^2. \tag{6}$$

Generally, an analytic expression for the calculation of buildup factors (without background subtraction) can be put in the form

$$B = 1 + \frac{I_s}{I_d + I_b}, \tag{7}$$

i.e., the quantity B depends on the fraction of background in the total radiation dose. However, if I_s changes in proportion to I_d, the instrument background, which appears in the denominator of the second term, remains constant. Therefore, the buildup factors for sources of different activities should be different, which was observed in this case. In addition, scintillators with different linear dimensions also have different backgrounds, and thus the buildup factors, obtained without background subtraction, also depend on the dimensions of the scintillation counters.

Consequently, the buildup factors (without background subtraction) for radiation sources of different activities are expressed by different analytic equations. This complicates the practical use of such buildup factors.

Buildup factors obtained with background subtraction are of definite interest. They were calculated for series 1, 2, and 10 radium sources, and had identical values within the limits of experimental error. This is explained by the fact that the buildup factor calculated with background subtraction depends on the primary quantum energy ε_γ, the linear absorption coefficient μ, the atomic number Z of the scattering material, and the measurement geometry (distance r, height h), i.e., $B = B(\varepsilon_\gamma, \mu, Z, r, h)$. For radium sources with different radium content above different scattering surfaces whose effective atomic number Z_{eff} varies within narrow limits, the buildup factor should depend only on the measurement geometry: height h and distance r. For the given geometry used in the calibration of the counters (h = 1.5 m), the buildup factor is a function of the distance r between source and detector.

An analytic approximation to the buildup factor for series 1, 2, and 10 radium sources (with background subtraction) is described by the equation

$$B = 1 + 0.174r - 0.0078r^2. \tag{8}$$

A curve for the dependence of buildup factor on distance r, calculated by formula (8), is shown in Fig. 3, where experimental buildup factors for sources of all three series are also plotted. It has been shown [7] that the buildup factor is also independent of the lower energy threshold of SRP-2 scintillation meters. Substituting the expression for B found in formula (8) into Eq. (4), we obtain the expression

$$I = (1 + 0.174r - 0.0078r^2)\, 840\, \frac{Q}{r^2} \tag{9}$$

for calculating the intensity of the total γ-radiation from radium sources of varying intensities at a height of 1.5 m above a scattering ground surface. Obviously, formula (9) is applicable to various reflecting media consisting of light elements. Indeed, the actual values for the coefficient B obtained during meter calibration above gravel and loam do not differ by more than 5% from one another (Fig. 4). While the density of gravel is much greater than that of loam, its radioactivity is twice as much as that of loam. Consequently, formula (9) is applicable for calibration not only above low-activity quaternary deposits, but also above denser media with increased activity. The value of the buildup factor above water is much larger than the buildup factor above gravel and loam, and increases more rapidly with increasing distance.

All the experiments discussed were performed with NaI(Tl) scintillation detectors 30 mm in diameter and 25 mm high. It is important to ascertain how the buildup factor changes with changes in the linear dimensions of the scintillator. To do this, the coefficient B was determined by the above-described method for an SRP-2k meter in which the scintillation detector has a diameter of 18 mm and a height of 30 mm. The buildup factors obtained in this case (Fig. 5) are well described by the analytic expression (8). Hence it follows that the buildup factor does not change with a change in crystal dimensions from 30 × 25 to 18 × 30 mm. This is in agreement with the concept that the ratio of the effect produced by the total direct and scattered radiation to the effect produced by the direct radiation should not depend on the dimensions of an unshielded scintillator.

In formula (9), letting

$$D(r) = (1 + 0.174r - 0.0078r^2)\, \frac{840}{r^2}, \tag{10}$$

we obtain

$$I = D(r)\, Q. \tag{11}$$

Knowing D(r) and the source content Q (in milligrams of radium), we can determine the γ-ray intensity which must be known for calibration. Values of D(r) are given below for different distances r:

r, m	D (r)	r, m	D (r)	r, m	D (r)
35	2,16	4	82,42	1,0	982,80
30	2,63	3	135,34	0,9	1 192,60
25	3,29	2	277,20	0,8	1 483,13
20	4,27	1,9	352,50	0,7	1 920,0
15	6,92	1,8	334,44	0,6	2 566,70
10	16,46	1,7	369,13	0,5	3 628,8
9	20,01	1,6	416,72	0,4	5 617,5
8	24,81	1,4	527,14	0,3	9 800,0
7	31,37	1,3	601,42	0,2	21 630,0
6	41,07	1,2	700,0	0,1	85 680,0
5	56,11	1,1	819,18		

Practical use of the calculations presented above (Fig. 6) shows that the calibration curve obtained at 1.5 m using formula (9) agrees with the curve obtained at 10 m using formula (1) where the detector is not affected by scattered radiation. Hence it follows that the use of formula (9) for the calibration of scintillation counters makes it possible to obtain calibration curves on whose behavior scattered radiation has no effect.

LITERATURE CITED

1. V. I. Baranov, Radiometry [in Russian], Moscow, Izd-vo AN SSSR (1956).
2. O. I. Leipunskii, B. V. Novoshilov, and V. N. Sakharov, Propagation of γ-Rays in Matter [in Russian], Moscow, Fizmatgiz (1960).
3. B. Price, C. Horton, and K. Spinney, Radiation Shielding [Russian translation], Moscow, Izd-vo Inostr. Lit. (1959).
4. M. B. Vasil'ev, Atomnaya Énergiya, 21, 2, 135 (1966) [this issue].
5. G. V. Gorshkov and S. A. Suppe, In: Radiometric Methods of Uranium Ore Prospecting and Exploration [in Russian], Moscow, Gosgeoltekhizdat (1957).
6. H. Goldstein, Fundamental Aspects of Reactor Shielding [Russian translation], Moscow, Gosatomizdat (1961).
7. M. B. Vasil'ev and M. A. Merkel, Atomnaya Énergiya, 21, 2, 134 (1966) [this issue].

ABSTRACTS

POSITRON GENERATION IN THE TRAVERSAL OF THIN FOILS BY FAST ELECTRONS

A. V. Bautin and V. M. Galitskii

UDC 539.172.2

The angular distributions and yields of photons and positrons resulting from the passage of fast electrons through a layer of material of the order of one radiation unit are discussed. These calculations are required to design converters for cases in which subsequent devices select positrons over a certain anagular range. It is assumed that the electrons have energies on the order of several hundred megaelectron volts. Positrons of sufficiently high energy, $E \geq 0.6E_0$, where E_0 is the energy of the initial electrons, are of interest in beam storage. The process investigated here is described by a system of integro-differential equations taking radiative processes and multiple scattering into account. The exact solution of these equations using Laplace-Mellin transforms leads to formulas for the unknown distribution functions in the form of contour integrals which can be handled only on an electronic computer [1, 2].

This paper develops a technique which enables us to find the total number of photons and positrons over a unit energy interval and the rms angle for particles of a specific energy. The basis of the method is that the number of fast positrons, as well as the number of photons essential to generation of the photons, is modest at depths $t \leq 1$. This allows us to use the first-generation approximation, in which the arrival of electrons due to pair formation and generation of quanta by positrons are neglected. The equations of the cascade theory of showers, written for distribution functions of electrons, photons, and positrons, can be broken up into terms and solved sequentially, once these factors are neglected. As a result, we end up with the first two moments $P_0(t, E)$ and $P_1(t, E)$ with respect to the angular variable for the distribution function $f(t, E, \theta)$:

$$P_0 = \int f(t, E, \theta)\, d\Omega; \qquad P_1 = \int \theta^2 f(t, E, \theta)\, d\Omega,$$

where $\theta^2 = P_1/P_0$; $d\Omega$ is an elemental solid angle.

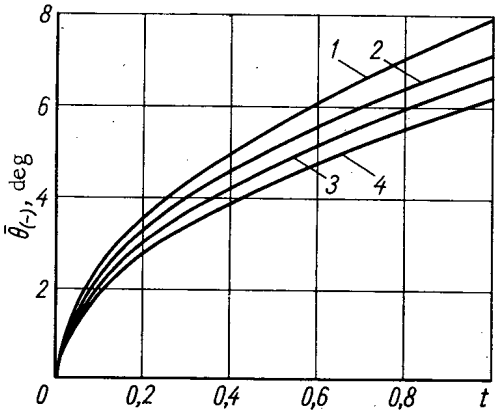

Fig. 1. The function $\bar{\theta}_{(-)} = \sqrt{\theta^2_{(-)}}$, giving the rms angular deviation of electrons for the following values of the ratio E/E_0: 1) 0.6; 2) 0.7; 3) 0.8; 4) 0.9.

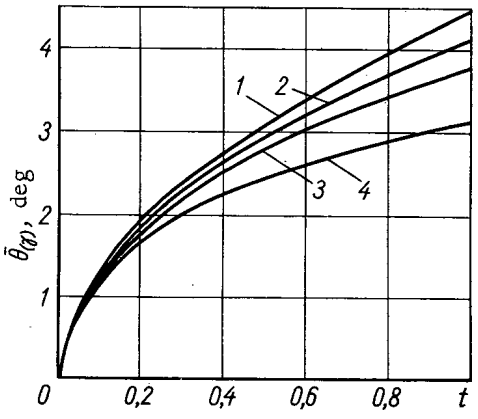

Fig. 2. The function $\bar{\theta}_\gamma = \sqrt{\theta^2_\gamma}$, giving the rms angular deviation of photons for the following values of the ratio E/E_0: 1) 0.6; 2) 0.7; 3) 0.8; 4) 0.9.

Translated from Atomnaya Énergiya, Vol. 21, No. 2, pp. 126-127, August, 1966. Abstract No. 94/3605. Original article submitted February 3, 1966. Complete text 0.9 folio, 4 diagrams, 14 titles in bibliography.

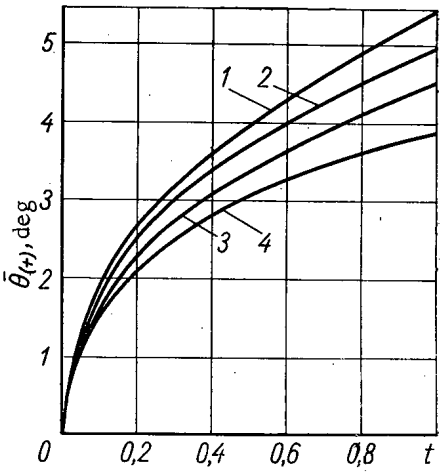

Fig. 3. The function $\bar{\theta}_{(+)} = \sqrt{\theta^2_{(+)}}$, giving the rms angular deviation of positrons for the following values of the ratio E/E_0: 1) 0.6; 2) 0.7; 3) 0.8; 4) 0.9.

The function $\bar{\theta} = \sqrt{P_1/P_0}$ defines the rms angular deviation and is represented graphically in Figs. 1 to 3 for electrons, photons, and positrons respectively. The initial electron energy is 200 MeV.

The results obtained show an excellent fit to the numerical calculations. At shallow depths ($t \ll 1$) formulas for rms angles of deviation of electrons, photons, and positrons exhibit the respective forms

$$\bar{\theta}^2_{(-)} = \frac{E_k^2}{E_0^2}\, t; \qquad \bar{\theta}^2_{(\gamma)} = \frac{E_k^2}{2E_0^2}\, t; \qquad \bar{\theta}^2_{(+)} = \frac{2}{3}\cdot\frac{E_k^2}{E_0^2}\, t,$$

where $E_k = 21$ MeV; t is the depth in radiation units.

LITERATURE CITED

1. V. S. Synakh, Zhur. éksper. i teoret. fiz., 40, 194 (1961).
2. A. V. Bautin and O. S. Koifman, Atomnaya énergiya, 20, 423 (1966).

AN INTEGRAL EQUATION FOR THE STATISTICAL WEIGHTS OF REACTOR COMPONENTS

A. I. Mogil'ner

UDC 621.039.51

It is proved that the sum of the statistical weights of all volume elements of a critical reactor, S, is double the neutron leakage probability with neutron importance taken into account:

$$S \equiv \int \frac{d\varrho}{dv}\Big|_{\rho=0} dv = 2\left(1-\frac{1}{k^*}\right), \tag{1}$$

where the nonleakage probability, with neutron importance taken into account, is

$$p^* = \frac{1}{k^*} = \frac{1}{I_{ND}} \int\int \Phi(\mathbf{r}, u)\, \Sigma_a(\mathbf{r}, u)\, \Phi^+(\mathbf{r}, u)\, du\, dv$$
$$- \frac{1}{I_{ND}} \int\int\int dv\, du\, du' \Phi(\mathbf{r}, u')\, \Sigma_s(\mathbf{r}, u' \to u)$$
$$\times [\Phi^+(\mathbf{r}, u) - \Phi^+(\mathbf{r}, u')]. \tag{2}$$

The quantity k* is a generalization of the concept k extended to an arbitrary reactor, and characterizes the average number of neutrons generated when a single neutron is absorbed in the critical reactor, with the neutron importance utilized as weight factor in the averaging process. Using the formula derived from perturbation theory in diffusion theory, and bearing in mind that the contribution of the volume element dv to the reactivity is made up of the contributions of the materials constituting that volume element, we arrive at the following formula for S:

$$S = 1 - \frac{1}{I_{ND}} \int\int dv\, du\, \Phi(\mathbf{r}, u)\, \Sigma_a(\mathbf{r}, u)\, \Phi^+(\mathbf{r}, u)$$
$$+ \frac{1}{I_{ND}} \int\int\int \Phi(\mathbf{r}, u')\, \Sigma_s(\mathbf{r}, u' \to u)$$
$$\times [\Phi^+(\mathbf{r}, u) - \Phi^+(\mathbf{r}, u')]\, du'\, du\, dv$$
$$+ \frac{1}{I_{ND}} \int\int D(\mathbf{r}, u)\, \nabla\Phi(\mathbf{r}, u)\, \nabla\Phi^+(\mathbf{r}, u)\, du\, dv. \tag{3}$$

The theorem is proved by also using the criticality condition, with neutron importance taken into account, in integral form:

$$-\int\int D(\mathbf{r}, u)\, \nabla\Phi(\mathbf{r}, u)\, \nabla\Phi^+(\mathbf{r}, u)\, du\, dv$$
$$-\int\int dv\, du \Phi(\mathbf{r}, u)\, \Sigma_a(\mathbf{r}, u)\, \Phi^+(\mathbf{r}, u)$$
$$+\int\int\int dv\, du\, du' \Phi(\mathbf{r}, u')\, \Sigma_s(\mathbf{r}, u' \to u)$$
$$\times [\Phi^+(\mathbf{r}, u) - \Phi^+(\mathbf{r}, u')] + I_{ND} = 0. \tag{4}$$

Translated from Atomnaya Énergiya, Vol. 21, No. 2, p. 127, August, 1966. Abstract No. 95/3585. Original article submitted January 21, 1966. Complete text: 0.2 folio; bibliography: 2 titles.

The dependence of k^* on the neutron spectrum and on reactor size should occasion no surprise, since k_∞ is, conventionally, a characteristic not only of the medium but also of the spectrum.

In those reactors where the concept k is defined, the two values k_∞ and k^* are close. The advantage inherent in definition (2) is that only one value of k^*, characterizing, as does k_∞, the nonleakage probability in a critical reactor of finite dimensions, but with the importance $p^* = 1/k^*$ taken into account, corresponds to an arbitrary reactor.

One important advantage of the term k^* is the ease with which it can be measured directly in a reactor.

In conclusion, I express my deep gratitude to V. V. Orlov for highly fruitful discussions of the work.

NEUTRON TRANSPORT IN A MOVING MEDIUM

E. A. Garusov, A. A. Kostritsa,
and Yu. V. Petrov

UDC 539.125.52

The equation of neutron transport in a moving medium can be derived from the transport equation for a fixed medium by using the Galilean transformation of the system of coordinates K($\mathbf{r}$, $\mathbf{V}$) in which the total momentum of all the nuclei distributed over the spectrum $f(v_N)$ is zero to the system L($\mathbf{r}$, $\mathbf{W}$) moving with respect to K at a constant nonrelativistic velocity $\mathbf{U}$. This means replacing the spectrum $f(v_N)$ by the spectrum $f(|\mathbf{W}_N - \mathbf{U}|)$:

$$\frac{\partial N(\mathbf{r}, \mathbf{W}, t)}{\partial t} + \mathbf{W}\nabla N(\mathbf{r}, \mathbf{W}, t) + N(\mathbf{r}, \mathbf{W}, t)\, n_N \times \int \sigma(|\mathbf{W} - \mathbf{W}_N|)\,|\mathbf{W} - \mathbf{W}_N|\, f(|\mathbf{W}_N - \mathbf{U}|)\, d\mathbf{W}_N = n_N \int N(\mathbf{r}, \mathbf{W}', t)\, d\mathbf{W}' \int \sigma_s(|\mathbf{W}' - \mathbf{W}_N|)\,|\mathbf{W}' - \mathbf{W}_N| \times g(\mathbf{W}' \to \mathbf{W};\ \mathbf{W}_N)\, f(|\mathbf{W}_N - \mathbf{U}|)\, d\mathbf{W}_N + Q(\mathbf{r}, \mathbf{W}, t). \tag{1}$$

A translation in velocity space $\mathbf{V} = \mathbf{W} - \mathbf{U}$ alone can be used to derive from Eq. (1) an auxiliary equation* whose solution, while falling short of describing the distribution function measured experimentally, does sometimes simplify the solution of the problem by reducing the collision integral to the same form as in the coordinate system K.

Even solutions of the problem of scattering of neutrons emitted by a monoenergetic source at velocity w_0 on nuclei of infinite mass, ignoring space diffusion, still demonstrate that the neutron angular distribution curve has discontinuities at $\gamma_0 \equiv u/w_0 > 1$. The P_N method is therefore inapplicable in this case, just as in the case $\gamma_0 \ll 1$ in the energy-dependent solutions of Eq. (1). But perturbation theory is applicable when $\gamma_0 \ll 1$ in the case of the solution integrated with respect to energy, and the P_1-approximation is valid.

We can obtain the continuity equation and an expression for the current in the P_1 approximation:

$$\operatorname{div} \mathbf{j}(\mathbf{r}) + \bar{\Sigma}_a \Phi_0(\mathbf{r}) = Q_0; \tag{2}$$

$$\mathbf{j}(\mathbf{r}) = \frac{-1}{3\Sigma_{tr}} \nabla\Phi_0(\mathbf{r}) + \frac{\mathbf{U}}{\bar{w}} \Phi_0(\mathbf{r}) + \frac{Q_s}{\Sigma_{tr}}, \tag{3}$$

where $\bar{\Sigma}_a$ is the absorption cross section averaged over the flux, and $\bar{w}$ is the absolute magnitude of the neutron velocity averaged over the neutron spectrum, for $\Sigma_s(w) = \text{const}$ and in the presence of space diffusion, in a linear approximation with respect to $\gamma \equiv \frac{u}{\bar{w}}$ and $\varepsilon \equiv \left(\frac{\Sigma_a}{\Sigma_s}\right)^{1/2}$

Equations (2), (3) are valid at distances $|\mathbf{r} - \mathbf{r}_0| \ll (\Sigma\varepsilon^2)^{-1} \approx \Sigma_a^{-1}$ from the source. The additional term in the expression for the current, brought in to account for the direction of momentum transfer to neutrons by nuclei of the medium, results in an additional term $\operatorname{div} \frac{\mathbf{U}}{\bar{w}} \Phi_0(\mathbf{r})$ in the diffusion equation.

Boundary conditions on the interface between two media in the P_1 approximation consist in continuity of the neutron flux and neutron current, and the formula for the logarithmic derivative on a boundary with a blackbody contains a corrective factor of the order of γ.

*A. A. Kostritsa, Atomnaya Énergiya, Vol. 21, No. 2, p. 128, August, 1966.

Translated from Atomnaya Énergiya, Vol. 21, No. 2, p. 128, August, 1966. Abstract No. 93/3569. Original article submitted December 30, 1965. Abstract submitted May 13, 1966. Complete text 0.5 folio, with 3 figures and bibliography of 7 titles.

The existence of two diffusion lengths L as implied by the characteristic equation

$$\delta^2 + 3j\delta - 3\varepsilon^2 = 0, \qquad \delta \equiv (\Sigma L)^{-1}, \tag{4}$$

is responsible for the appearance of the factor $\exp\left\{\frac{3\Sigma_{tr}}{2w}\,\mathbf{Ur}\right\}$. in the solution of the diffusion equation. This factor shows that the ratio $\frac{\Sigma_{tr}}{w}$ can be determined experimentally from measurements of the neutron flux intensity at a single point by varying the speed at which the medium moves.

The contribution of coolant motion to the reactivity Δk in highly asymmetric reactors may be approximately γ. When the U are large, Δk may be commensurate with the delayed neutron fractions, and this becomes a hazard if coolant flow is suddenly stopped.

EFFECTIVENESS OF STONE CONCRETE IN ACCELERATOR SHIELDING

V. B. Dubrovskii, L. N. Zaitsev,
V. V. Mal'kov, and V. N. Solov'ev

UDC 621.384.61:621.039.538.7

Penetrating radiation generated by electron accelerators consists of γ-emission and photoneutrons, while ultrafast neutron flux and μ-mesons are generated in the shielding of proton accelerators. Shielding thickness depends primarily on the weight by volume (density) of the grades of concrete in dealing with these forms of radiation. Limitations on shielding thickness place an added demand on the heavier concretes, but this means higher shielding costs. The use of relatively inexpensive high-density concrete is economically justified under these conditions.

A new material, stone concrete, with better performance per cost than ordinary concrete, is obtained by packing a layer of stone (ore or rock) into an underlying layer of concrete mix, and is widely used in the construction of massive lightly reinforced structures.

Studies were made of the conditions under which ordinary concrete and stone concrete with the same filters (hematite ore) can attain maximum density, in order to assess the effectiveness of stone concrete in accelerator shielding. The results are illustrated by tabular and graphical material.

The density range from 3500 to 3900 kg/m^3 (see figure) is of greatest interest for cost and effectiveness comparisons.

The costs of concrete and stone concrete, with respective maximum densities of 3630 and 3900 kg/m^3, are practically identical, but the cost of stone concrete shielding is 10% less when converted to effective thickness. If we assume the densities of concrete and stone conrete to be the same (3900 kg/m^3), the cost of ordinary concrete shielding will be 1.5 times higher, since high-cost steel fillers will necessarily be required in that case.

The cost advantages of stone concrete in accelerator shielding are illustrated by examples in the paper.

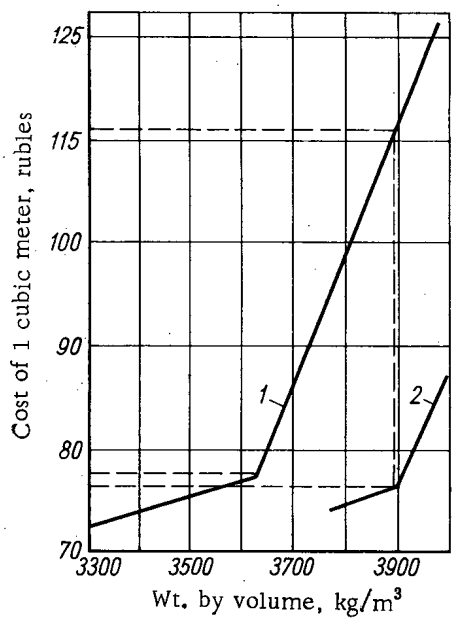

Comparison of costs of prefabricated concrete 1 and stone concrete 2.

Translated from Atomnaya Énergiya, Vol. 21, No. 2, pp. 128-129, August, 1966. No. 96/3686. Original article submitted April 8, 1966. Complete text 0.4 folio, 2 figures, 3 tables, bibliography of 17 titles.

LETTERS TO THE EDITOR

THE VGL-2 CRYOGENIC MAGNETIC TRAP

E. S. Borovik,* F. I. Busol,
B. V. Glasov, V. A. Kovalenko,
E. I. Skibenko, and V. B. Yuferov

UDC 533.9

One method of creating a hot plasma in a magnetic trap is to inject a powerful beam of fast neutral hydrogen or deuterium atoms, some of which, owing to ionization in the magnetic field, can be captured in the trap [1-3]. In this letter we discuss the filling with plasma of a small magnetic trap with a strong magnetic field [3].

Figure 1 is a diagram of the VGL-2 magnetic trap, which differs from previous types in the use of cryogenic techniques. Its main units are as follows: the magnetic system (the trap itself); a vacuum-tight casing with means for evacuation; an injector of fast neutral hydrogen atoms, consisting of an ion source, charge-exchange chamber, and chamber for receiving the beam of neutral particles which have passed right through the system without undergoing ionization. The charged component of the beam is deflected by a capacitor on to a heated target inside the vacuum casing. This enables the charge-exchange chamber to be placed within 0.9 m of the trap.

*Deceased.

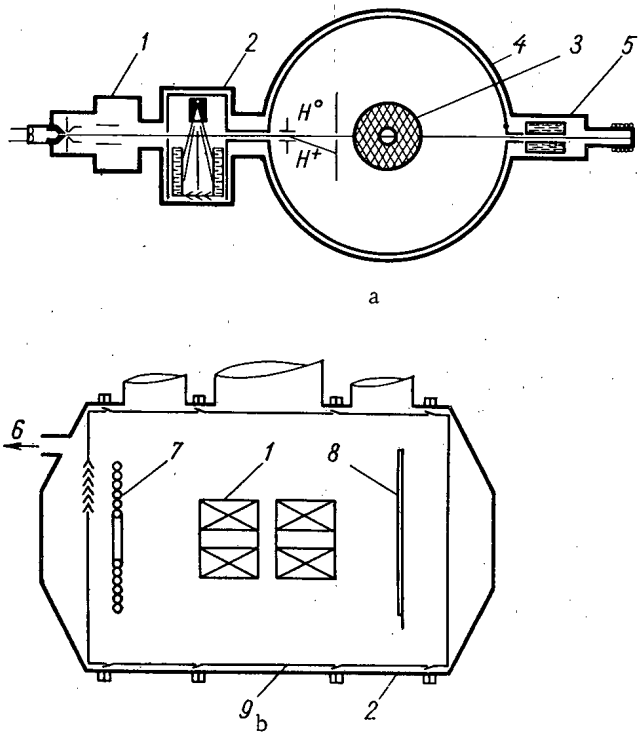

Fig. 1. Diagram of apparatus. a) Cross section along axis of injected particle beam; b) cross section along axis of magnetic field. 1) Ion source; 2) charge exchange chamber; 3) magnetic system; 4) vacuum-tight casing; 5) chamber for receiving beam; 6) outlet to diffusion pump; 7) helium condensation pump; 8) hydrogen condensation pump; 9) nitrogen screen.

Translated from Atomnaya Énergiya, Vol. 21, No. 2, pp. 130-131, August, 1966. Original article submitted April 1, 1966.

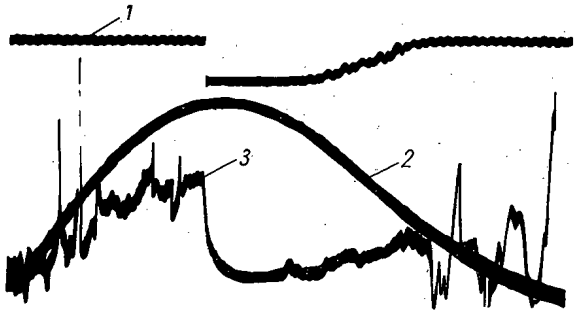

Fig. 2. Time dependence of flux of charge-exchanged particles. 1) Signal from primary-beam detector; 2) magnetic field signal; 3) signal from flux of charge-exchanged particles leaving the plasma.

The magnetic field is created by two long coils with internal diameters of 5 cm. The ratio of the coil length to internal diameter and the ratio of external diameter to internal diameter are both 4.3. The coils are made of copper wire and are cooled by liquid nitrogen or hydrogen. Their volumes are 300 cm^3 each. The magnetic field in the plugs is 105 kilogauss, the plug ratio being 1.5 (but it can be varied by changing the distance between the coils). The time required for the field to reach its maximum was $T/4 = 0.26$ sec. In the central plane of the coil the radial variation of the magnetic field was $\sim 5\%$.

As seen from Fig. 1, the magnetic system is located inside a large vacuum chamber made of ordinary mild steel, of length 1.8 m and with a diameter of 1.2 m. All the detachable connections were packed with ordinary vacuum rubber. The attainable vacuum was $\sim 5 \cdot 10^{-10}$ mm Hg, which was achieved thanks to thorough screening of the vacuum chamber walls by a copper screen cooled to the temperature of liquid nitrogen, and also to the high speed of pumping out (10^5 l/sec).

To get a hydrogen ion beam, we used an Ardenne source without beam separation. The ion injection energy was 30 keV. The ion beam is neutralized in the charge-exchange chamber by a supersonic jet of CO_2 which condenses on a surface cooled to 20.4°K [4]. When the jet density is about 4.10^{14}-5.10^{14} cm^{-3}, the vacuum is about $1 \cdot 10^{-7}$ mm Hg at a distance of 15 cm from the jet.

To calculate the degree of filling of the trap with plasma, we determined the capture coefficient α, i.e., the fraction of the neutral beam which ionizes the operating region of the trap [5]. When the magnetic field at the center of the trap is ~ 60 kilogauss, $\alpha \approx 5 \cdot 10^{-4}$. The plasma density was measured from the intensity of the flux of fast atoms leaving the plasma owing to charge exchange of ions with residual gas. To detect these fast atoms, we used the usual method based on secondary electron emission. The detectors were located outside the coils opposite the ring-shaped gap between them. The neutron flux incident on the detectors was from 0.02 to 0.1 of the total flux of emergent fast atoms. The coefficient of secondary electron emission at the detectors was determined directly in the trap before the experiment, by bombardment with an ion beam. In our experiments, it varied from 3 to 4. The intensity of the primary beam of fast atoms was determined by a detector using secondary electron emission, placed in the chamber for receiving the beam. In the experiments we injected a flux of atoms equivalent to a current of 0.3-0.6 mA. The signals from the primary-beam detectors, the flux of charge-exchanged particles from the plasma, and the magnetic field intensity were recorded by an oscillograph. The lifetime of the plasma was measured with the aid of a device which enabled us to switch off the beam after 10 μsec.

The vacuum was recorded by IM-12 tubes placed in a special sleeve where they were screened from the charged particle fluxes and did not experience the magnetic field during the pulse. Before injection of the beam, the initial vacuum was $\sim (2\text{-}3) \cdot 10^{-9}$ mm Hg, but on switching on the beam the pressure rose to $8 \cdot 10^{-9}$-$2 \cdot 10^{-8}$ mm Hg. We achieved some improvement on the previously attained vacuum [6] by catching the beam on a heated target.

The results of experiments to determine the plasma density in the trap are given by the oscillogram of Fig. 2. The lifetime of the plasma after the beam was switched off was about 10-13 msec at first, and about 20-25 msec after 0.1 sec. This is due to the fact that the vacuum improved after the beam was switched off. Thus the lifetime agrees with that calculated on the basis of vacuum measurements.

The plasma density can be calculated in two ways. The first way is from the current in the neutral-atom detectors and the decay time:

$$n^+ = \frac{i_K \tau}{\gamma \Omega V}, \tag{1}$$

where i_K is the current to the collector; τ is the measured lifetime of the plasma; γ is the coefficient of secondary emission of the detector; Ω is the solid angle subtended by the detector from the plasma; and V is the volume of the plasma (at present the latter is ~ 60 cm^3, because at attainable densities the plasma does not extend along the magnetic field axis out of the region occupied by the beam). The second way is from the injection current J^0, the capture coefficient α, and the decay time τ:

$$n^+ = \frac{\alpha J^0 \tau}{V}. \tag{2}$$

The plasma density value found from the flux of charge-exchanged atoms was $n^+ \approx (3\text{-}4) \cdot 10^7$ cm^{-3}; that found from the current injected into the trap was $n^+ \approx 3 \cdot 10^8$ cm^{-3}. Since there were no observed variations in the density (i.e., no obvious instabilities), we suggest that the low value for the density found from the particles leaving the plasma is explained by a slight redistribution of ion velocities in the plasma. In the geometry which we used, particles with velocities along the field exceeding 10% of their lateral velocities did not fall on the detector.

LITERATURE CITED

1. D. Sweetman, Nucl. Fusion, Suppl., 1, 279 (1962).
2. R. Post, "Proc. of the Fourth Intern. Conf. on Ionization Phenomena in Gases," Uppsala, August, 1959, Vol. II. Ed. by N. Nilsson, North-Holland Publ. Co., Amsterdam (1960), p. 987.
3. E. S. Borovik et al., In symposium: "Plasma Physics and Problems of Controlled Thermonuclear Synthesis," Issue 4, Kiev, Naukova Dumka (1965).
4. F. I. Busol et al, ZhTF, 34, 2156 (1964).
5. E. S. Borovik et al., Nucl. Fusion, 5, 85 (1965).
6. E. S. Borovik et al., Report to the Second International Conference on Plasma Physics and Controlled Thermonuclear Reactions, Kalem (United Kingdom) (September, 1965).

A POLARIZED-ION SOURCE WITH CURRENT STRENGTH OF 1.2 μA

R. P. Slabospitskii, I. M. Karnaukhov, I. E. Kiselev, and A. Ya. Taranov

UDC 539.103:539.121.85:539.128.2

In many laboratories work is being done on polarized-ion sources required for experiments with polarized beams. However, existing sources [1-3] have intensities of 0.3 μA or less.

In this letter we shall describe a source of positive polarized deuterium ions, with a currrent strength of 1.2 μA, differing from the source described in [3] in that the atomic beam is ionized by a more efficient method. The vacuum is also considerably improved by making the whole source of stainless steel and replacing the oil pumps by mercury and titanium pumps.

The source is based on the principle of separating the beam into atoms with different electron spins by means of a strongly non-uniform magnetic field, followed by adiabatic extraction into a region of weak magnetic field.

The figure shows a diagram of the source. The deuterium (or hydrogen) molecules are split up into atoms in a high-frequency dissociator discharge 1. The hf discharge is excited by a resonance circuit connected to an oscillator working at 150 Mc/sec. The inner surface of the dissociator vessel is covered with dimethyldichlorosilane. To increase the yield of atoms in the axial direction, we used a system of microcollimators with 70% transparency.

From the dissociator, atoms pass through diaphragm 2 to magnetic quadrupole 3, where the components of the atomic beam with electron spin projections opposed to the magnetic field are focused, while those with oppositely direct spin projection are defocused. The length of the magnetic quadrupole is 25 cm, and the radius of the magnet channel is 0.4 cm. At the surface of the pole-pieces the magnetic field intensity is $2 \cdot 10^4$ Oe.

Measurements of the intensity of the focused beam and the density of atoms in it revealed that the beam, with an intensity of $6 \cdot 10^{15}$ atoms/sec, is less than 5 mm in diameter and is negligibly spread out at a distance of 200 mm.

The focused beam falls on to ionizer 6, where it is ionized by an electron beam moving coaxially with it. In the ionizer [4], which has a three-electrode electron gun, it is possible to combine the conditions for maximum electron current strength and for optimum gas ionization by the electron beam: it was thus possible to achieve an ionization efficiency of $2 \cdot 10^{-3}$.

Screen 5 screens the ionization region from stray fields from the quadrupole. The uniform magnetic field is obtained by Helmholtz coils 4. The ion current is measured by Faraday cylinder 9.

The tensor polarization of the deuterium beam was found by measuring the differential cross section of the reaction $T(d, n)He^4$. To carry out this reaction, the beam of polarized ions from the ionizer was focused twice in succession by accelerating diaphgrams 7 and 8, accelerated to an energy of 120 keV in accelerator tube 10, and allowed to fall on to target 11. The reaction products were recorded by detectors 12.

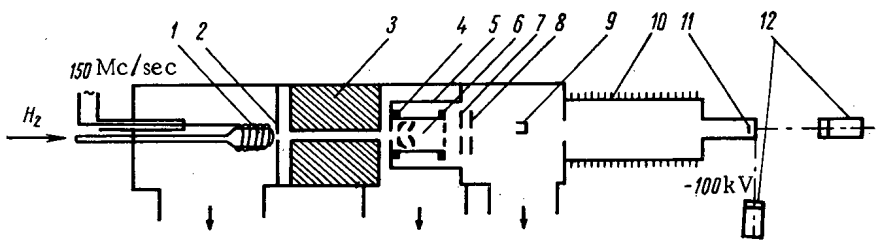

Diagram of apparatus.

Translated from Atomnaya Énergiya, Vol. 21, No. 2, pp. 131-132, August, 1966. Original article submitted April 1, 1966.

The tensor polarization was found to be $P_{33} = -0.274 \pm 0.012$ for current strength of 1.2 μA.

LITERATURE CITED

1. E. Collins et al., Nucl. Instrum. and Meth., 25, 67 (1963).
2. B. P. Ad'yasevich et al., Atomnaya Énergiya, 17, 17 (1964).
3. R. P. Slabospitskii et al., Program and abstracts of reports to Fourteenth Yearly Conference on Nuclear Spectroscopy and the Structure of the Atomic Nucleus (Moscow, 1966), Nauka (1966), p. 128.
4. R. P. Slabospitskii et al., ZhTF, 36, No. 12 (1966).

USE OF AUTORADIOGRAPHY TO MONITOR NONUNIFORMITY IN LAYERS OF ACTINIDE ELEMENTS

A. T. Kazakevich and V. M. Surin

UDC 546.799:621.039.85

Thanks to its simplicity and sensitivity, autoradiography is widely used in scientific research. One use of this method is to study the distribution of radioactive substances on a solid surface [1, 2].

We have used autoradiography to monitor nonuniformity in layers of U^{238}, Pu^{238}, Pu^{239}, and Am^{241} on plane metal substrates obtained electrochemically and by the drop method and having an α-activity of $1 \cdot 10^3$-$4.1 \cdot 10^6$ disintegrations per minute per cm^2.

Method. To obtain the autoradiograms, a "Diavidox" x-ray plate was placed in direct contact with the active layer and exposed for a predetermined time. It was then treated for 4 min with D-19 metol-hydroquinone developer and fixed for 5 min in sodium thiosulfate (250 g/liter). The resultant autoradiograms were measured with an MF-4 microphotometer.

The layer of U^{238} was prepared by reduction of UO_2^{2+} with aluminum in an aqueous solution of uranyl nitrate to sparingly soluble UO_2 [3, 4]. The temperature was 75-95°C and the concentration of $UO_2(NO_3)_2 6H_2O$ was 10-20 g/liter with pH about 2-3. The electrode surface was freed from oxide film by means of fine emery paper. The clean electrode was immersed in uranyl nitrate for 15 min, then washed and dried at 100°C. The UO_2 layer was a non-hygroscopic flat deposit with a black coloration, firmly adhering to the aluminum surface.

Cathode deposits of the fluorides of Pu^{238} and Pu^{239} on nickel disks were obtained by electrolysis of dilute HF solution containing plutonium in the form of $Pu(NO_3)_4$, using a platinum anode. To remove grease, the cathode surface was treated before electrolysis with a paste of CaO + MgO.

Results. Visual inspection of the autoradiograms (Figs. 1-3) showed that the electrochemical method gave a more even deposit than the drop-evaporation method. The latter gave a sharply increased surface density of deposit at the edges.

Nonuniformity of α-Active Layers
(from autoradiography data)

Isotope	α-activity of layer, dis/min·cm^2	A, %	
		Electrochemical method	Drop method
U^{238}	$5{,}0 \cdot 10^3$ $4{,}8 \cdot 10^3$	7,0 6,7	— —
Pu^{238}	$9{,}8 \cdot 10^3$ $2{,}0 \cdot 10^3$	— —	44 66
Pu^{239}	$4{,}1 \cdot 10^5$ $3{,}1 \cdot 10^5$	6,6 7,8	— —
Am^{241}	$2{,}8 \cdot 10^4$ $1{,}3 \cdot 10^4$	— —	26 27

Translated from Atomnaya Énergiya, Vol. 21, No. 2, pp. 132-134, August, 1966. Original article submitted March 20, 1966. Revised April 25, 1966.

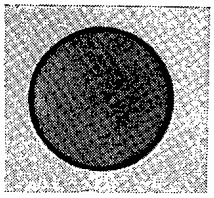

Fig. 1. Autoradiogram of U^{238} layer with a thickness of 3.3 mg U/cm^2 (normal value).

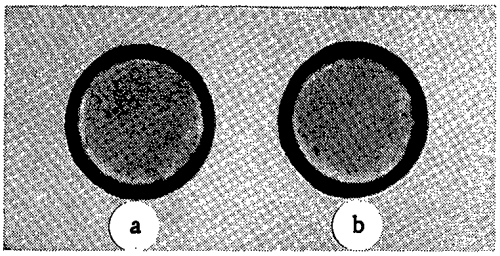

Fig. 2. Autoradiograms of cathode deposits of Pu^{239} fluoride with α-activity of: a) $5.47 \cdot 10^5$ dis/min $\cdot$ cm^2, b) $6.14 \cdot 10^5$ dis/min $\cdot$ cm^2 (normal value).

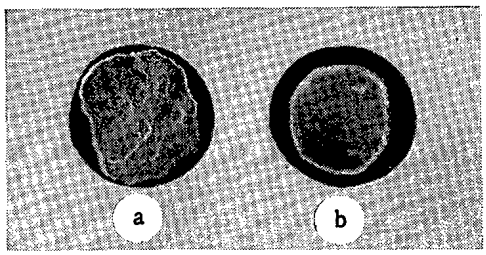

Fig. 3. Autoradiograms of layers produced by the drop method. a) Am^{241}, α-activity $1.3 \cdot 10^4$ dis/min $\cdot$ cm^2; b) Pu^{238}, $9.8 \cdot 10^3$ dis/min $\cdot$ cm^2 (normal value).

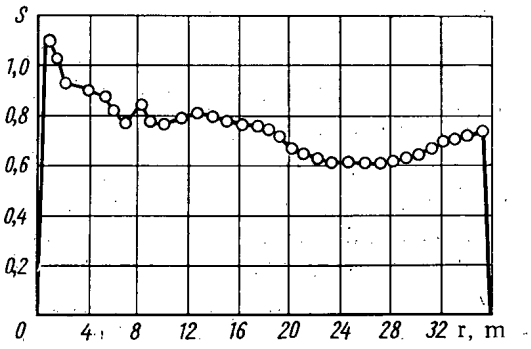

Fig. 4. Variation of film blackening along diameter of autoradiogram of cathode deposits of Pu^{239} fluoride (r is the distance from the edge along the diameter).

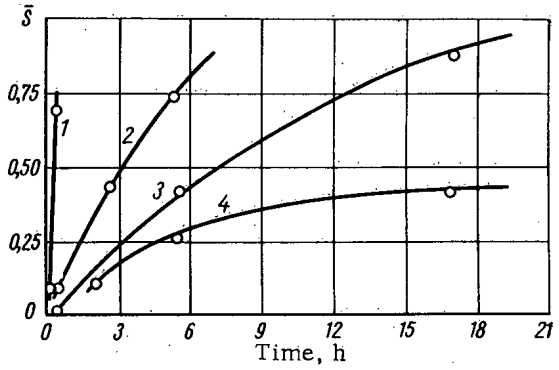

Fig. 5. $\bar{S}$, plotted versus exposure time, for layers of Pu^{239} of the following α-activities, in dis/min $\cdot$ cm^2: 1) $1.1 \cdot 10^4$; 2) $0.7 \cdot 10^4$; 3) $0.5 \cdot 10^4$; 5) $0.3 \cdot 10^4$.

The nonuniformity of the layer was quantitatively assessed by the following formula for the percentage value:

$$A = \frac{S_{max} - \bar{S}}{\bar{S}} \cdot 100,$$

where S_{max} is the maximum blackening, $\bar{S}$ is the mean blackening along a diameter of the layer. The blackening S was determined by the formula $S = \log J_0/J$, where J_0 and J are the intensities of visible light incident on the photographic plate and passing through it, respectively [5].

As an example, Fig. 4 gives the blackening distribution S along one diameter of a layer of Pu^{239} with an α-activity of $3.7 \cdot 10^6$ dis/min $\cdot$ cm^2. The table gives data on the nonuniformity A for layers of various elements.

We studied the relation between $\bar{S}$ and exposure time τ for a series of layers of the same isotope (U^{238}, Pu^{239}, or Am^{241}) with different α-activities. The graphs of $\bar{S}$ versus τ for Pu^{239} are shown in Fig. 5. As τ increases, the rate of film blackening gradually decreases. From these curves we can estimate the time of normal exposure τ_0, for which we can take $S = 1$.

From the values obtained for τ_0 (min and the α-activities N (dis/min) of the layers, we found approximate values for the constant $N\tau_0$. The values found were as follows: for U^{238}, $(1.6 \pm 0.3) \cdot 10^8$ dis/cm^2; for Pu^{239}, $(1.8 \pm 0.4) \cdot 10^8$ dis/cm^2; and for Am^{241}, $(4.6 \pm 1.6) \cdot 10^8$ dis/cm^2. The weighted mean, $\overline{N\tau_0}$, is $(2.4 \pm 1.2) \cdot 10^8$ dis/cm^2. Hence we might calculate a provisional normal exposure time for an α-active layer of known intensity, so as to get a clear picture of its nonuniformity from an autoradiogram.

LITERATURE CITED

1. B. Verkerk, Nucleonics, 14, No. 7, 60 (1956).
2. R. Ko, Nucleonics, 15, No. 1, 72 (1957).
3. S. Skorka, Naturwissenschaften, 40, 605 (1953).
4. W. Gebauhr and J. Martin, Atompraxis, 6, H. 7, 253 (1960).
5. I. P. Bondarenko and N. V. Budarova, Principles of Dosimetry and Radiation Shielding, Moscow, Vysshaya shkola (1962), p. 223.

THE BUILDUP FACTOR FOR REFLECTION OF RADIATION FOR COUNTERS WITH VARIOUS LOWER ENERGY THRESHOLDS

M. B. Vasil'ev and M. A. Merkel'

UDC 539.166

Vasil'ev [1] gives data obtained by studying γ-radiation, from a radium source, scattered from the surface of the earth. From these data he calculated the buildup factors B for reflected radiation from radium sources with various radium contents. He found analytical expressions for the buildup factors and derived formulae for the total (direct plus scattered) radiation, which can be used to obtain calibration curves for scintillation counters, free from the effects of scattered radiation.

However, he did not show how the influence of the buildup factor depends on the lower energy threshold of the counters (on the first discriminating threshold).

The present authors have obtained buildup factors for reflection from the earth's surface of radiation from a point isotropic radium source with 0.1 mg radium at a height of 1.5 m, for first discriminating thresholds of 66, 108, and 167 keV. These thresholds belong to various points on the differential γ-ray spectrum curve obtained from a point radium source in air, for channel width of 15 keV [2]. The table gives the factors found. The geometry of the experiment was described in [1].

The figure plots the buildup factors versus r, calculated [1] from the formula

$$B = 1 + 0.174r - 0.0078r^2. \quad (1)$$

This graph also shows experimental values of B, obtained for counters with various lower energy thresholds.

The table shows that the discrepancies between values of B for the various discriminating thresholds are within the error of observation. Furthermore, as can be seen from the graph, the buildup factors for thresholds 66, 108, and 167 keV agree satisfactorily with the approximation (1). It follows that the buildup factor is practically independent of the lower energy threshold. This can be explained by the fact that energy discrimination simultaneously affects direct and scattered γ-quanta in such a way that their ratio remains constant.

Buildup Factors

Distance between detector and source, r (meters)	B			
	First discriminating threshold, ε_0 (keV)			Cal. from formula $B = 1 + 0.174r - 0.078r^2$ [1]
	66	108	167	
10	2,14	1,91	2,02	1,96
9	2,04	1,87	2,0	1,93
8	1,89	1,83	1,98	1,89
7	1,86	1,80	1,86	1,83
6	1,78	1,76	1,71	1,76
5	1,56	1,73	1,69	1,67
4	1,53	1,62	1,61	1,57
3	1,42	1,45	1,45	1,45
2	1,26	1,33	1,26	1,32
1	1,19	1,20	1,19	1,17

Translated from Atomnaya Énergiya, Vol. 21, No. 2, pp. 134-135, August, 1966. Original article submitted January 24, 1966.

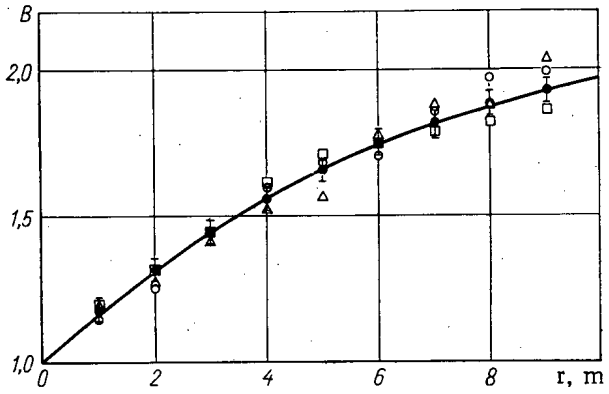

Buildup factor versus distance r for counters with various lower energy thresholds. ●) Calculated from formula $B = 1 + 0.174r - 0.0078r^2$. Experimental data for various values of ε_0 in keV: △) 66; □) 108; ○) 167.

The above results are of practical importance. As the buildup factor B remains constant when the lower energy threshold of the counters varies, the formula for the intensity of total γ-radiation from a radium source,

$$I = 840B\frac{Q}{r^2} \qquad (2)$$

(where 840 represents the γ-constant of radium and Q is the content of radium in the source), is valid for the calibration of radiometers with various first discrimination thresholds.

LITERATURE CITED

1. M. B. Vasil'ev, Atomnaya énergiya, 21, 2, 121 (1966) [this issue].
2. S. G. Troitskii, In symposium: "Topics in Ore Radiometry," Moscow, Gosatomizdat (1962).

SCATTERING OF γ-RADIATION FROM Ra^{226} AND Cs^{137} BY A SURFACE OF EARTH OR WATER

M. B. Vasil'ev

UDC 539.166

The study of γ-radiation scattered from the surfaces of light media such as earth is important in practical radiometry. Several authors [1-7] have studied scattered radiation and buildup factors for reflected radiation.

In this letter we find the build-up factor B for reflection of γ-rays emitted by radium and cesium sources at various heights above earth and water surfaces. The radium source contained 0.1 mg radium, the cesium source contained 0.1 mg-equiv radium. The experimental geometry and method of determining the buildup factors were described in reference [8]. Measurement was by an SRP-2 scintillation γ-radiometer.

Figures 1 and 2 show graphs of the buildup factor of radium sources at various heights h above earth and water surfaces versus the distance r between the source and the detector. They show that at 8 m above earth, or 3 more meters above water, the corresponding buildup factors are equal to unity. For these values of h, the Ra^{226} radiation reaching the detector after scattering at the earth or water surface is negligible.

We carried out similar experiments with γ-radiation from Cs^{137} (Figs. 3 and 4). The figures show that in this case the condition $B \approx 1$ is satisfied at 3 m above earth or 2 m above water.

Figure 5 gives graphs of the buildup factors of radium and cesium sources versus height h above earth or water surfaces. The maximum value of B occurs at a height of 1 m. The shape of the curves does not depend on the nature of the source or the composition of the scattering surface: this is due to competition between the scattering and absorption processes [9]. As the angle of scattering decreases, the intensity of the scattered radiation

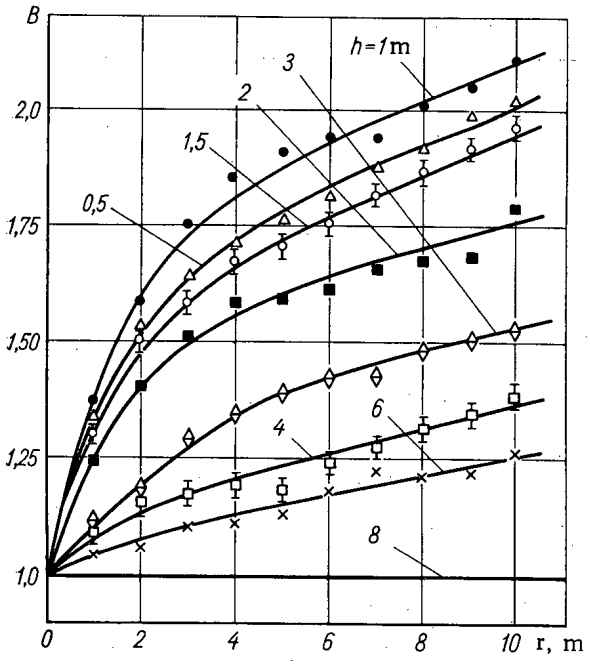

Fig. 1. Buildup factor of radium source at various heights h above earth surface versus distance r between source and detector.

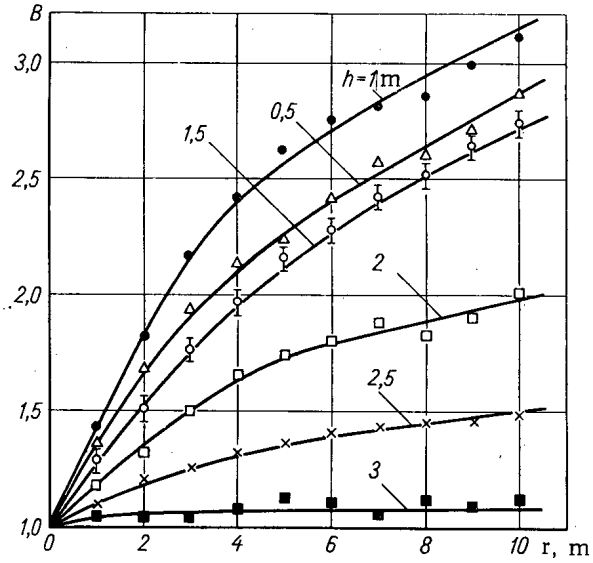

Fig. 2. Buildup factor of radium source at various heights h above water surface versus distance r between source and detector.

Translated from Atomnaya Énergiya, Vol. 21, No. 2, pp. 135-136, August, 1966. Original article submitted January 24, 1966.

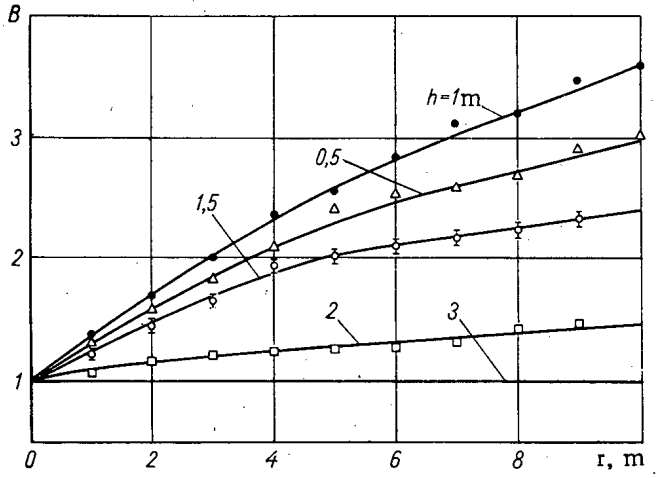

Fig. 3. Buildup factor of cesium source at various heights h above earth surface versus distance r between source and detector.

increases; the probability of its absorption, however, also increases. The competition between these processes leads to the result that, for a given geometry, the scattered radiation recorded by a detector has a maximum intensity at a height of 1 m.

The figures show that the buildup factor above water is greater than that above earth. This is observed both for radium and cesium sources, and is due to the fact that water, being a lighter medium, gives more intense Compton scattering. In addition, the experimental results show that the buildup factor for Cs^{137} is always greater, other things being equal, than that for Ra^{226}.

From the above results, we can in particular conclude that, in calibrating scintillation radiometers, the radiation source and detector must be placed more than 1 m above the earth's surface, because, when h = 1 m, the detector registers maximum scattered radiation and the calibration curve is distorted.

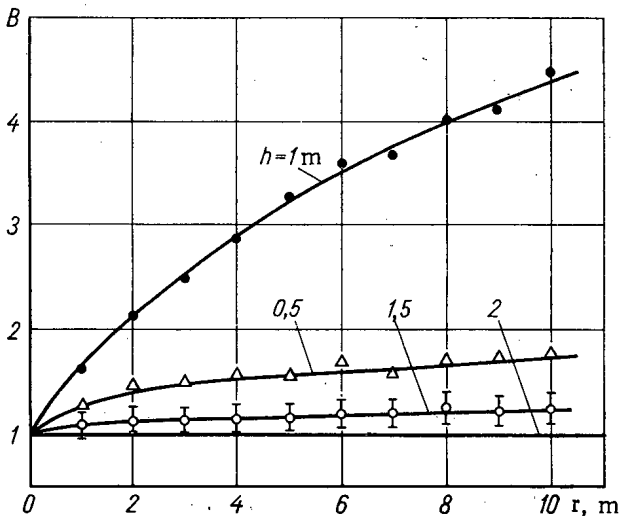

Fig. 4. Buildup factor of cesium source at various heights h above water surface versus distance r between source and detector.

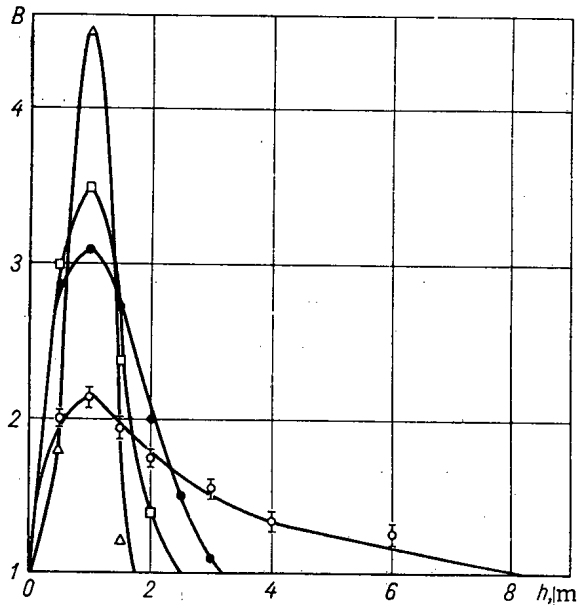

Fig. 5. Buildup factor versus height h. ○) Radium above earth surface; ●) radium above water surface; □) cesium above earth surface; △) cesium above water surface.

LITERATURE CITED

1. O. I. Leipunskii and V. N. Sakharov, Atomnaya Énergiya, 6, 585 (1959).
2. U. A. Ulmanis and N. A. Dubinskaya, Atomnaya Énergiya, 3, 59 (1957).
3. B. P. Bulatov and E. A. Garusov, Atomnaya Énergiya, 5, 631 (1958).
4. B. P. Bulatov, Atomnaya Énergiya, 7, 369 (1959).
5. B. P. Bulatov, Atomnaya Énergiya, 13, 440 (1962).
6. B. P. Bulatov and O. I. Leipunskii, Atomnaya Énergiya, 7, 551 (1959).
7. M. Berger and J. Doggett, J. Res. Nat. Bur. Standards, 56, 89 (1956).
8. M. B. Vasil'ev, Atomnaya énergiya, 21, 2, 121 (1966) [this issue].
9. O. I. Leipunskii, B. V. Novozhilov, and V. N. Sakharov, Propagation of Gamma Quanta in Matter, Moscow, Fizmatgiz (1960).

THE RATIO BETWEEN THE INPUT AND OUTPUT CONCENTRATIONS OF RADIOACTIVE GAS PASSING THROUGH A DZ-70 CHAMBER

I. I. Kornilenko, V. A. Zybin, and A. L. Bochkov

UDC 621.387.422

Bryzgunov [1] gives data on the ratio between the output and input concentrations of radioactive gas passing through a DZ-20 chamber. The present authors have obtained analogous data in experiments with a 70-liter ionization chamber, the DZ-70. The chamber's internal diameter is 40.5 cm, and its length 55 cm. Input and output holes with internal diameters of 0.8 cm are situated at opposite ends of a diameter, 16.7 cm from the chamber axis.

The following method was used to find the change in concentration of the gas when it passed throug the vessel. Air containing Ar^{41} (total activity, 10^{-4}-10^{-3} Ci) is fed from a small rubber balloon to the input of the chamber for a short time (less than 3 sec). A counter is set up at the chamber exit to record the air activity in the measuring space (volume ~ 70 cm^3). The counter is switched on at the moment when the argon is let into the chamber. Before the argon is released, a constant air injection rate is established. Figure 1 gives a graph of the integral Ar^{41} count versus time for a volume injection rate of P = 60 liters/min, after subtraction of background count and allowing for decay. Analysis of the graphs for various values of P showed that the curve for the integral pulse count is given by the formula

$$n = n_\infty (1 - e^{-\lambda' t}), \tag{1}$$

where λ' is the exchange constant for air in the chamber, determined experimentally, and varying with P. Figure 2 plots λ' versus P/V. The points lie on a straight line satisfying the equation $\lambda' = (0.96 \pm 0.02)$ P/V for the range studied (15-110 liters/min). The experimental differential pulse count curve, except for the first few seconds after release of the argon into the chamber, follows an exponential decay curve.

We see that, for a radioactive gas continuously flowing through the chamber and in equilibrium conditions, the ratio between the output and input concentrations of the gas, by (1), is given (as in the case of the 20-liter chamber [1]) by the following formula:

$$\frac{a}{a_0} = \frac{\lambda'}{\lambda + \lambda'}. \tag{2}$$

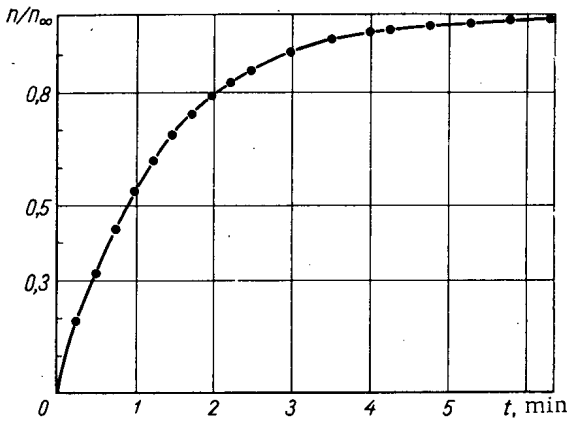

Fig. 1. Integral count versus time.

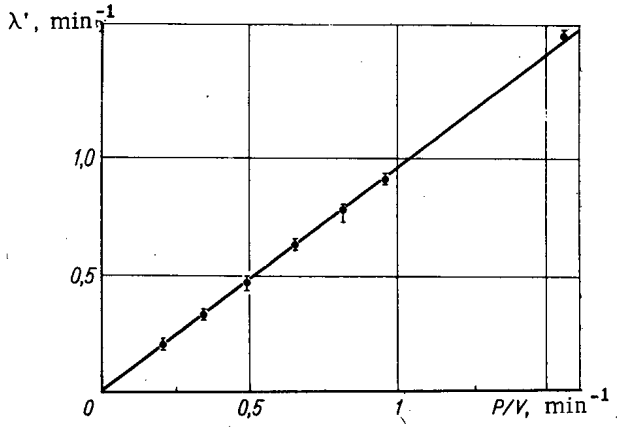

Fig. 2. Exchange constant λ' versus P/V.

Translated from Atomnaya Énergiya, Vol. 21, No. 2, pp. 137-138, August, 1966. Original article submitted February 3, 1966.

For the range of P studied, $\lambda' = 0.96P/V$; thus, for the DZ-70 chamber, we get

$$\frac{a}{a_0} = \frac{0.96P/V}{\lambda + 0.96P/V}. \quad (3)$$

Assuming that there is a mechanism for instantaneous mixing, we can show that the ratio between the output and input concentrations of the gas in the chamber is theoretically given by the formula

$$\frac{a}{a_0} = \frac{P/V}{\lambda + P/V}. \quad (4)$$

This shows that, for the range of air flow velocities considered, the time for total mixing of air in the DZ-70 chamber is much less than the mean residence time of the air in the chamber.

The deviation of the coefficient in (3) from unity may perhaps be due to the presence of a small systematic error in measuring the air flow rate.

In references [2-4], a mechanism of pure displacement of air from the chamber is often assumed. This can lead to incorrect calculations of the concentration changes of short-lived gases, and also to errors in finding the concentrations of gases from the build-up of decay products of these gases on filters after passage through the chamber. For example, it can be shown that, with an air injection rate of ~40 liters/min into a DZ-70 chamber, the error in determining the thoron concentration from build-up of ThB on a filter can reach 30%, according to the assumptions made about the mechanism of air mixing in the chamber.

In conclusion, we may remark that, by making allowance for the mechanism of outflow of radioactive gases from a vessel and for precipitation of solid products of the gases' decay on the vessel walls, we can determine the optimum construction for chambers with two filters and decay tanks for radiometry and reduction of the discharge rates of radioactive gases.

LITERATURE CITED

1. V. A. Bryzgunov, Atomnaya Énergiya, 13, 276 (1962).
2. Yu. P. Burmistenko, Atomnaya Énergiya, 9, 505 (1960).
3. J. Fontan et al., Suppl. Nuovo Cimento, XXIII, Ser. X, No. 1, 132 (1962).
4. A. Bouville et al., Nucl. Instr. and Methods, 27, 329 (1964).

RAPID MEASUREMENT OF THE CONCENTRATIONS OF AEROSOLS OF LONG-LIVED α-ACTIVE ISOTOPES OF THE ORDER OF 10^{-16}-10^{-17} Ci/liter AND AEROSOLS OF THORON DISINTEGRATION PRODUCTS

O. A. Chutkin and V. E. Vishnyakov

UDC 543.52.541.182.3

A pulse ionization chamber (IC) with a large electrode area is the most suitable instrument for simultaneously measuring the isotope compositions and concentrations of aerosols of long-lived α-active isotopes of the order of 10^{-16}-10^{-17} Ci/liter (the maximum permissible concentrations in the air of sanitary zones and populated areas).

The purpose of the present study was to estimate the possibility of determining such concentrations as rapidly as possible when the specimen on the filter contained radon and thoron disintegration daughter products.

The measurements were carried out with a commercially manufactured α-ray ionization spectrometer (type 9014-01) which has a resolution of 1.7% and can be used for measuring flat specimens up to 160 mm in diameter.

The ionization chamber of the spectrometer can be used for separate recording of most α-ray sources with particle energies of up to 9 MeV, including radon, thoron, and actinon products. Since the measurements cannot be made until 20 min after the specimens are extracted, this spectrometer can be used for measuring specimens of long-lived α-ray sources and thoron and actinon daughter products. In order to determine the concentrations of radon disintegration products, we must know the RaA content of the specimen, but this isotope disintegrates almost completely by the time the chamber is charged and filled.

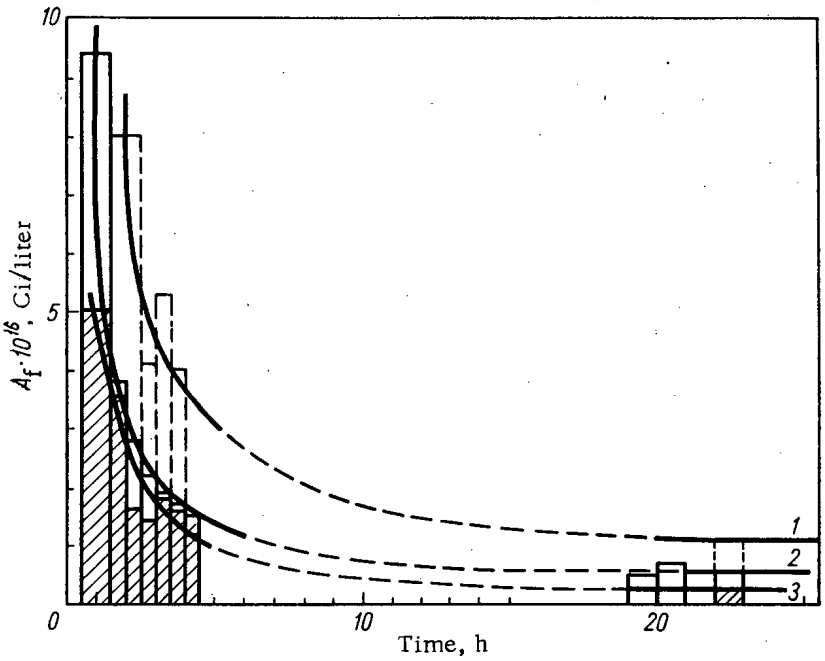

Fig. 1. Average fictitious reading, or sensitivity of measurement of aerosols of long-lived isotopes, with ionization chamber and one-channel discriminator: 1) Channel width = 10 V; 2) 5 V (without collimator); 3) 5 V (with collimator).

Translated from Atomnaya Énergiya, Vol. 21, No. 2, pp. 138-141, August, 1966. Original article submitted November 29, 1965.

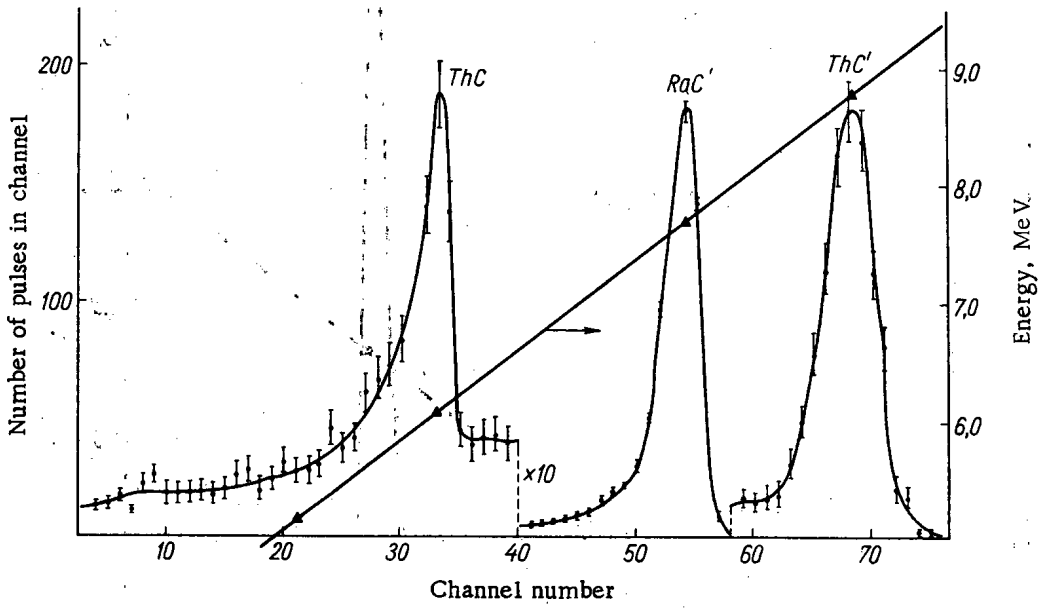

Fig. 2. α-Ray spectrum of natural aerosol particles, obtained by means of an ionization chamber. Volume of specimen 50 m^3, thickness of deposit 0.13 mg/cm^2, storage time 120 min.

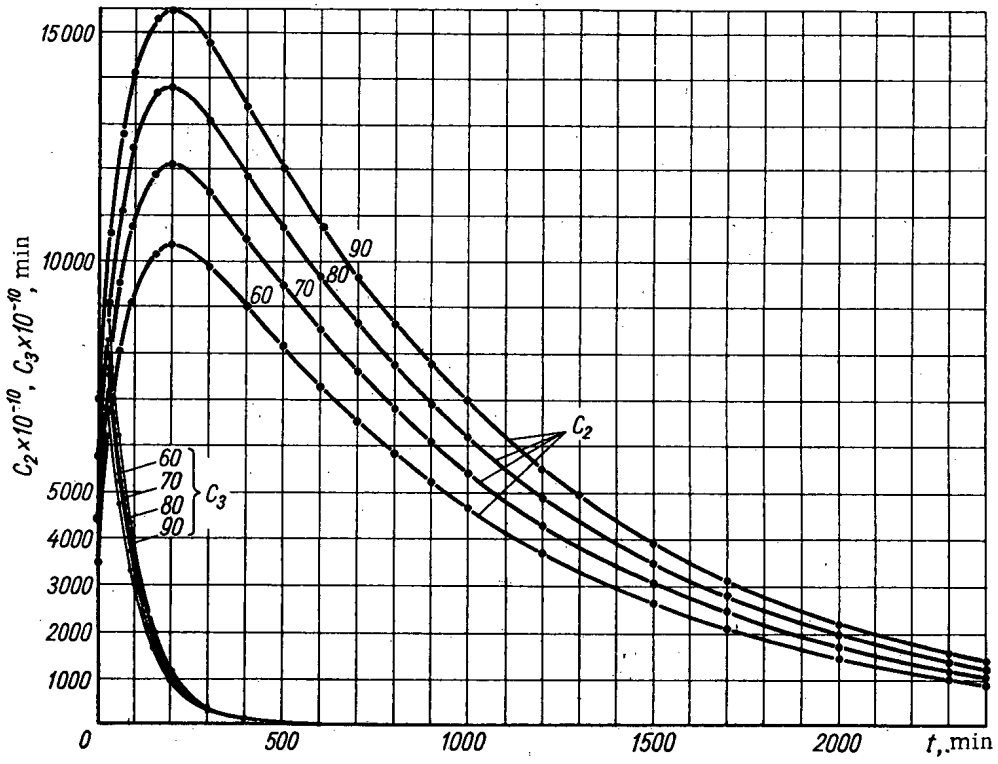

Fig. 3. Coefficients C_2 and C_3 for thoron disintegration products as functions of time. The numbers on the curves indicate the pumping time τ in minutes.

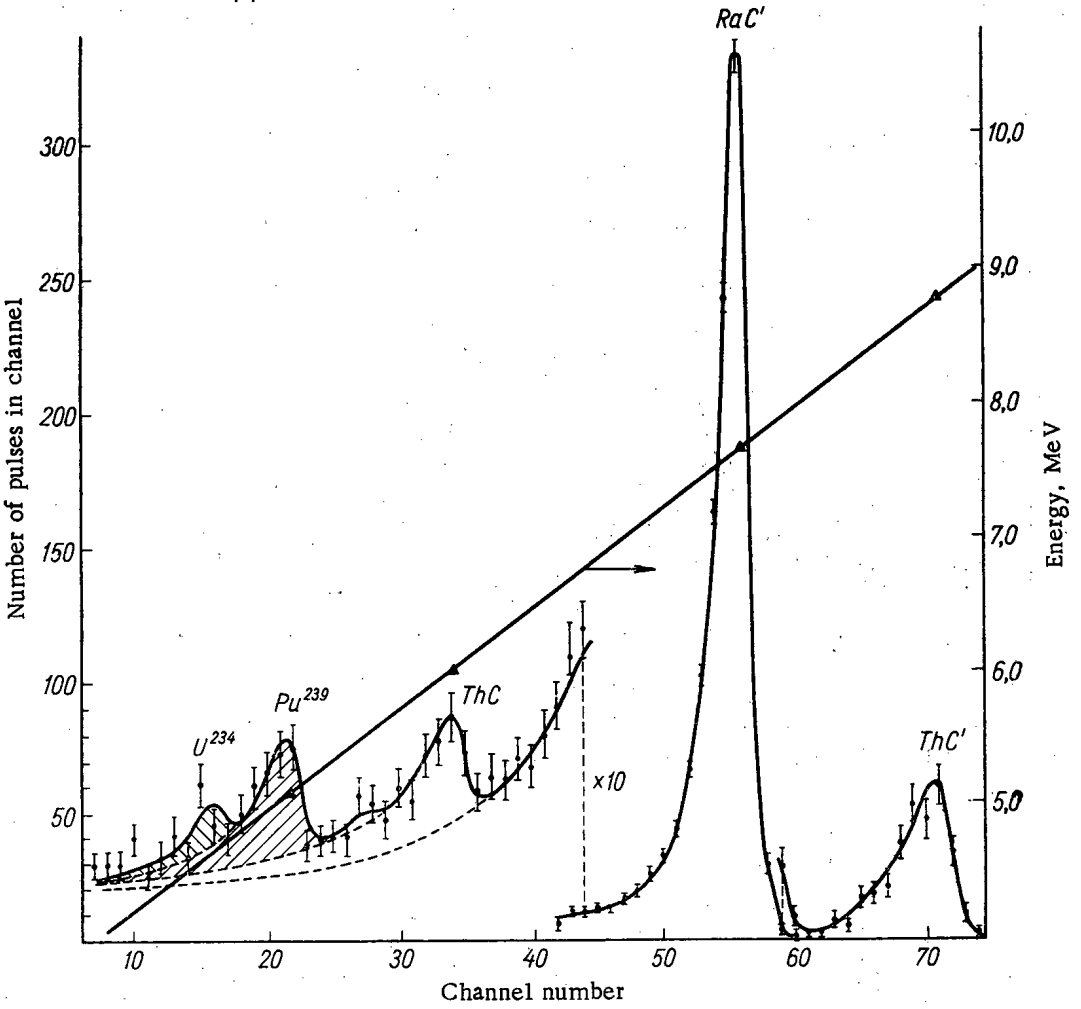

Fig. 4. Determination of the active concentration of plutonium and uranium in the presence of a natural background.

The aerosol particle specimens were taken from the corridor of the laboratory (natural background) under industrial operating conditions. We used disks 140 mm in diameter, made of a foil-type filtering material similar to LFS-1 (with a thickness of 0.4-0.5 mg/cm^2), which is suitable for α-spectrometry of a deposited dispersion phase. The filter did not impair the spectrum resolution by more than 0.5-2%.

In the first series of experiments the window of the BD-2 differential discriminator (5-10 V wide) leading to the instrument was so arranged as to record the α-particles of the long-lived isotopes. When the window was 5 V, we measured the activity of an uncovered specimen and a specimen covered by a collimator. The collimator consisted of a copper mesh of 0.5 mm diameter wires spaced 0.5 mm apart.

For each specimen of aerosol particles we calculated the value of the "fictitious" active concentration of the long-lived α-active isotopes by the formula

$$A_f = \frac{N_c}{\varepsilon v \tau t \eta} 4.55 \cdot 10^{-13} \text{ Ci/liter}, \quad (1)$$

where N_c is the number of pulses in time $t \geq 30$ min; $\eta = 0.96$ is the efficiency of the filter in removing aerosol particles; v (liters/min) is the air pumping rate and τ (min) is the pumping time ($v\tau = 50$-60 m^3); ε is the efficiency of recording of α-particles of long-lived isotopes from the 140 mm diameter source. The values of ε was 36.2% for a window width of 5 V, 43.1% for 10 V, and 12.6% for a window width of 5 V with a collimator.

Figure 1 shows A_f (average of a large number of experiments) plotted against the storage time of the specimen. The thickness of deposit on the filter varied from 0.03 to 0.13 mg/cm^2. The figure shows that the contribution of the natural background in the channel recording the long-lived isotopes is 1/10 to 1/15 of the value

Concentration of Thoron Disintegration Products under Experimental Conditions

Date on which specimen was taken	τ, min	$q_2 \times 10^{14}$, Ci/liter	$q_3 \times 10^{14}$, Ci/liter	$q_2 : q_3$
17/XII 1964	69	0,43	0,42	1 : 0,95
18/XII 1964	90	0,21	0,19	1 : 0,91
6/I 1965	64	0,48	0,38	1 : 0,79
28/I 1965	82	0,25	0,15	1 : 0,60
1/II 1965	68	0,42	0,36	1 : 0,86

obtained with the best aerosol radiometers using α-ray scintillation spectrometers. However, despite its good resolution, the spectrometer is incapable of recording concentrations of the order of 10^{-16}-10^{-17} Ci/liter unless the specimen has been stored for one day.

In our study, during the experiments to estimate the "fictitious" concentrations, we determined the concentrations of aerosols of radon and thoron disintegration products. Since we did not have any sources of radon and thoron disintegration products of known activity, in calculating the concentrations we used the α-particle recording efficiency determined on the basis of Pu^{239}, which in our case does not give rise to any large error.

The concentrations of the radon disintegration products from $1.9 \cdot 10^{-13}$ to $5.8 \cdot 10^{-13}$ Ci/liter were determined from the total activity of the specimen in integral operation taking into account the disintegration of the substance during both the pumping time and the specimen storage time on the assumption that the half-life of the radon products is 40 min.

In order to determine q_2 and q_3 – the concentrations of ThB and ThC – we used an AI-100 amplitude analyzer to record two α-ray energy spectra from each specimen at times t_1 and t_2 (Fig. 2). For each measurement, we used the areas under the ThC and ThC' peaks, which were clearly separated, to determine the total counting rate for the thoron disintegration products, $N(t_1)$ or $N(t_2)$. Since ThC and ThC' are always in radioactive equilibrium, $N(t_1)$ and $N(t_2)$ can also be determined by recording the α-radiation of ThC alone by means of a discriminator.

The concentrations q_2 and q_3 were found from the system of equations

$$N(t_1) = v\eta [C_2(\tau, t_1) q_2 + C_3(\tau, t_1) q_3],$$
$$N(t_2) = v\eta [C_2(\tau, t_2) q_2 + C_3(\tau, t_2) q_3].$$

The coefficients C_2 and C_3 calculated in the present study (which take account of the accumulation and disintegration of the thoron disintegration products) are plotted as functions of pumping time and storage time in Fig. 3. Analogous coefficients for the radon series were calculated by Markov and co-workers.* The resulting values of q_2 and q_3 are shown in the table, from which it is clear that during the experiments the ThB and ThC values in the air were almost in radioactive equilibrium ($q_2 : q_3 = 1 : 0.82$).

When the instrument was tested on artificial aerosols, it was found that the sensitivity of the measurements on specimens without storage may be far too high if the pulses from the α-particles of the long-lived isotopes w are determined not by means of a one-channel discriminator but by decoding the α-particle energy spectra obtained from the specimen by means of a multi-channel analyzer. The background had to be estimated not on the basis of preliminary averaged calibration measurements but separately for each specimen.

Our experiments showed that if the spectrum data were processed 30-40 min after we finished taking the specimens (6-25 m^3 of air), we were able to measure concentrations as low as $1 \cdot 10^{-17}$ Ci/liter with an error of approximately 36%. An example showing the rapid determination of a mixture of U^{234} with a concentration of $5.3 \cdot 10^{-17}$ Ci/liter and Pu^{239} with a concentration of $3.7 \cdot 10^{-16}$ Ci/liter in air is given in Fig. 4. The concentration was found by a formula similar to formula (1), using the shaded areas of the spectrum. The experimental error in the present case is about 25% of the error found when we measured a specimen after prolonged storage.

From the foregoing we may conclude that the ionization spectrometer is the most suitable instrument for measuring small concentrations of aerosols of long-lived α-active isotopes not only after prolonged storage of the

*K. P. Markov et al., Atomnaya Énergiya, 12, 315 (1962).

specimens but also for rapid measurements, and the sensitivity of the method for the latter case is better than $1 \cdot 10^{-17}$ Ci/liter. The ionization spectrometer may also be used for rapidly determining low concentrations of thoron disintegration products in air by the method described in the article.

MEASUREMENT OF THE ACTIVITY OF GASES BY MEANS OF A SPHERICAL IONIZATION CHAMBER

V. A. Bazhenov, V. V. Bochkarev, Yu. M. Golubev, I. V. Levin, T. N. Sokolova, and A. D. Turkin

UDC 543.52.539.107.42

Ionization chambers of various designs are widely used for measuring the concentrations of radioactive gases, and the calibration of these chambers involves considerable difficulties. There are no satisfactory methods for calculating the coefficients which relate the current in the chamber with the activity of the gas being measured. The experimental calibration of chambers for different gases also involves certain difficulties because mass-produced gaseous sample sources are not available.

If we use an ionization chamber of a given design and find with sufficient accuracy the coefficients relating the saturation current value to the activity for a number of gases of practical importance, we can use such a chamber for measuring activity and calibrating other detectors.

The choice of the chamber design for the original calibration is entirely arbitrary. However, the authors decided upon a copper-walled spherical ionization chamber 24 cm in diameter. According to the data obtained by simulation [1] with point sources, such a chamber, when filled with air at atmospheric pressure, in the β-spectrum energy range of 0.15 to 2.2 MeV, has hardness of not more than $\pm$ 10%. Moreover, [2] describes a method for calculating the efficiency of a spherical ionization chamber.

The experiment was carried out for the following gases: Xe^{133}, CO_2, tagged C^{14}, Xe^{131}, Kr^{85}, and Ar^{41}. The chamber was filled with air at atmospheric pressure. The air contained a small admixture of the radioactive gas. The current was measured by means of a Townsend compensation circuit using an SGM-1 string electrometer. The error in the current measurements was no more than 2%.

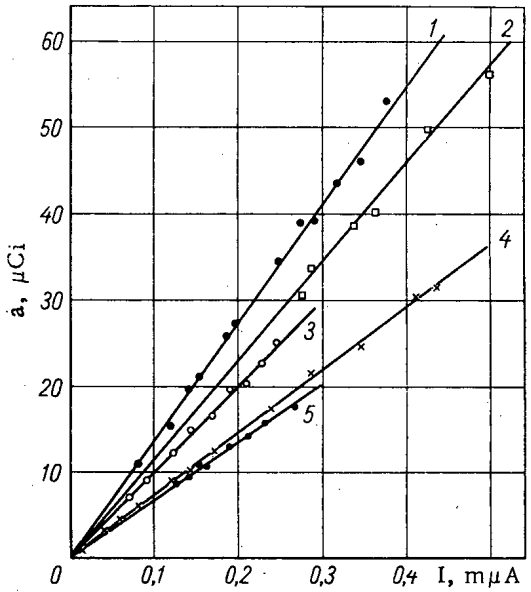

Calibration lines for a chamber 24 cm in diameter, filled with air at atmospheric pressure: 1) C^{14}; 2) Ar^{41}; 3) Kr^{85}; 4) Xe^{131}; 5) Xe^{133}.

Translated from Atomnaya Énergiya, Vol. 21, No. 2, pp. 141-142, August, 1966. Original article submitted July 19, 1965.

Comparison of Calculated and Experimental Values of K

Isotope	$\bar{E}$, MeV	$\frac{I, A}{N, particles/sec}$			
		1	2	3	4
C^{14}	0,053	1,95	1,90	2,12	1,95
Kr^{85}	0,244	2,67	2,12	3,67	1,95
Ar^{41}	0,480	2,34	1,74	3,70	1,95

The activity of the gas in the chamber was determined by means of an apparatus using compensation counters [3]. The measurement error was 2.5%. During the experiment, we extracted a measured quantity of air and radioactive gas from the chamber, passed it into the apparatus with two internally filled counters constituting the compensating vapor, and measured the activity. The counters operated in the proportional range, and the working gas used was methane.

From the value found for the activity of the specimen passed into the apparatus, we determined the total activity of the gas in the ionization chamber by multiplying by the ratio of chamber volume to specimen volume.

After each measurement of the saturation current and the activity of the gas in the chamber, we pumped out a certain quantity of gas, added enough air to restore atmospheric pressure, and mixed the contents so as to obtain a uniform concentration. After this we again measured the current and the activity of the gas in the chamber and continued as before.

The results obtained are shown in the figure. The abscissa axis shows the saturation current I of the chamber, and the ordinate axis shows the total activity a of the gas in the chamber. The following values were obtained experimentally for the coefficient $K = [I(A)/a\ (disintegrations/sec)] \cdot 10^{16}$:

Isotope	K
C^{14}	1.95
Xe^{133}	3.94
Xe^{131}	3.57
Kr^{85}	2.67
Ar^{41}	2.34

Unlike the cases of C^{14}, Kr^{85}, and Ar^{41}, which have simple β-spectra, a considerable part of the radiation from Xe^{133} consists of conversion electrons, and in the case of Xe^{131} the spectrum contains only conversion electrons. Consequently, the method described in [2] for estimating the efficiency of the chamber is applicable only to the first three isotopes.

The average current values per particle in this chamber are shown in the table.

Column 1 shows the experimental values; column 2 shows the current values per particle, calculated by the method of [2], neglecting backscattering, and column 3 shows the average current value when the backscattering of β-particles from the chamber walls is taken into consideration. Column 4 shows the current values that should be expected on the basis of [1].

It can be seen that the values of the coefficient K found in accordance with [1, 2] (neglecting backscattering) coincide with the experimental values within 25-30%. When the backscattering of the β-radiation from the chamber walls is taken into account [2] in determining K, the maximum deviation is 50%.

When more exact measurements are required, one may construct the copper-walled ionization chamber 24 cm in diameter and use the values of K given in the present study.

LITERATURE CITED

1. A. D. Turkin, Atomnaya Énergiya, 11, 60 (1961).
2. M. Yamashita and H. Watanabe, J. Atomic Energy Soc., Japan, 4, 588 (1962).
3. V. A. Bazhenov and V. V. Bochkarev, In: "Techniques of Measurement of Radioactive Specimens" [in Russian], Moscow, Gosatomizdat (1962), p. 115.

VI INTER-UNIVERSITY CONFERENCE ON ELECTRON ACCELERATORS

A. M. Gromov

In February, 1966, the VI Inter-University Scientific Conference on Electron Accelerators was held in Tomsk. About 300 delegates from 64 scientific institutions and industrial enterprises in the country participated in the work of the conference.

Participants in the conference became acquainted with the laboratories and large machines at the Tomsk Polytechnic Institute, the organizer of the conference.

The conference was opened by the rector of the institute, A. A. Vorob'ev, who proposed to dedicate it to the memory of one of the founders of accelerator technology in the USSR, Academician A. K. Val'ter.

A. N. Didenko (NIIYaF TPI, Tomsk) described the present state, and the trends in development, of electron accelerator physics and technology. He emphasized that the basic nuclear physics requirement in the planning of new accelerators and in the improvement of existing ones, in addition to increase in the energy of accelerated particles, is the production of the greatest intensity.

At the conference, 185 reports were given. We shall touch on only those reports which deal with new acclerators, problems of increased intensity, and questions of accelerator use.

I. P. Chuchalin (NIIYaF TPI, Tomsk) reported on the 1965 start-up of a weak-focussing, 1.5 GeV synchrotron. The synchrotron electromagnet consists of four C-shaped sectors separated by straight sections. The radius of the equilibrium orbit is 423 cm, the length of each straight section 157 cm. The magnetic field pulse is a half-sine wave with a repetition frequency of 1 Hz. A 5 MeV microtron serves as injector. Electrons are accelerated by two resonators in opposite straight sections. A maximum energy of 1.1 GeV has been obtained during operation with one accelerating resonator up to the time of the conference. The intensity of the accelerated electrons is $\sim 5 \cdot 10^9$ particles/pulse.

The problem of transverse stability of an electron bunch is of great importance in large, linear electron accelerators. I. A. Grishaev (KhFTI, Kharkov) pointed out the great influence of asymmetric waves in wave-guide decelerating structures on transverse blowup of a bunch. Sources of these waves can be both nonuniformity in iris wave guide and the accelerated bunches themselves. Beam blowup is particularly noticeable in several billion electron volt linear accelerators. It leads to contraction of the accelerated bunch. In order to reduce radial blowup, it is necessary to eliminate transverse nonuniformity in an iris wave guide and to enhance radial focussing by supplementary lenses installed along the accelerator.

Of interest was the report by A. A. Naumov on the results of the start-up of the pulsed B-3M synchrotron with iron magnetic circuit at IYaF SO AN SSSR. The synchrotron can operate with a repetition frequency of 12 Hz and an accelerated particle intensity of $\sim 10^{11}$ particles/cycle. The highest energy of the synchrotron is 200 MeV. Injection into the synchrotron and extraction of the accelerated beam is accomplished by a one-turn circuit. The synchrotron and extraction of the accelerated beam is accomplished by a one-turn circuit. The synchrotron is used for experiments on electron and positron storage.

K. A. Belovintsev and E. G. Bessonov (FIAN, Moscow) discussed work on the achievement of storage of colliding electron and positron beams in the chamber of a 250 MeV synchrotron. They obtained colliding electron-positron beams with energies of about 200 MeV each, and with the production of stored particles numbering 10^{12}. Work is continuing on increasing the number of stored particles.

From the point of view of storage and of production of colliding beams, the strong-focussing accelerator with fixed magnetic field – circular phasotron – is of great interest. Such an accelerator was placed in operation in October, 1965, at FIAN SSSR (Moscow) by a group headed by A. A. Kolomenskii. V. A. Papadichev discussed the start-up of the circular phasotron and the initial results obtained.

Translated from Atomnaya Énergiya, Vol. 21, No. 2, pp. 143-145, August, 1966.

In the Tomsk Polytechnical Institute, an investigation is being made into the possibility of using high-frequency fields for improving focussing in cyclic accelerators. The reports of G. P. Fomenko and A. N. Didenko pointed out that some types of waves which are propagated in a direction opposite to that of particle motion may have a focussing action. If type H waves are propagated along a continuous, closed wave guide located in a magnetic field, these waves can accelerate charged particles. A model of a 10 MeV synchrotron based on this principle was constructed. The dimensions of the wave guide were selected so that the H_{118} wave had a phase velocity equal to the velocity of light at the equilibrium radius. In this synchrotron, the fraction of particles trapped in the acceleration mode depends on the power of the high-frequency accelerating field.

In various laboratories in the country, attempts are being made to increase the intensity of existing accelerators. One of the possibilities for increasing the maximum trapped current, which is determined by space charge, is an increase in injection energy.

The injection energy of betatrons and medium-energy synchrotrons is determined by the potentialities of the electron beam. Recently, a system has come into widespread use in which the electron beam travels outside the limits of the working area, and the electrons are placed in orbit by inflector plates. Furthermore, preliminary acceleration can be used, and, in addition, beam dimensions and electrical stability can be increased.

They have gone such a route at LFTI AN SSSR where the energy of particles injected into a 100 MeV synchrotron was increased to 1.5 MeV. Electrons are accelerated to this energy by an rf resonator operating in the 10 cm range. The introduction of electrons into the chamber is accomplished by means of an iron antimagnetic channel with subsequent bending by electrically pulsed inflectors. As the authors (A. P. Komar, O. P. Korovin) stated, they have succeeded in obtaining an increase in intensity of approximately an order of magnitude. At TPI (B. V. Okulov), they have developed several types of electron beams at voltages to 200 kV with currents/pulse of 10-20 A. A beam with operating voltages to 100 kV and subsequent bending of particles by electric inflectors is used in the circular phasotron at FIAN.

A Moscow electrical factory for medical items manufactures 25 MeV betatrons (B. B. Gel'perin). To increase intensity, the injection energy of this betatron was increased to 60 keV. Extraction of the electron beam was achieved.

For the purpose of increasing the reliability and lifetime of electron beam cathodes, they are investigating plasma electron sources at the Tomsk Institute of Electronics and Electronic Engineering (Yu. E. Kreindel', E. N. Fakhrutdinov, D. A. Noskov). In some sources, they have succeeded in producing a current of about 3 A in a pulse 2-10 μsec long with an electron energy of ~ 20 keV. The density of the current taken from the cathode opening reached 1 A/mm^2. The electrons were extracted from a cold-cathode Penning discharge. Air was the working gas.

Another possibility for increasing the intensity is an increase in the transverse cross section of the chamber. The Tomsk Polytechnic Institute has developed and placed in operation several types of high-current betatrons with large interpolar gaps in the energy range from 3 to 25 MeV for use in various branches of the national economy. In addition, they are developing a series of compact 3-6 MeV betatrons for x-raying articles with a thickness equivalent to 200 mm of steel or less. These accelerators can be used both under shop and field conditions. Of the high-current betatrons, one should single out a 25 MeV accelerator with a dose rate greater than 1000 R/min · m and a 15 MeV double-chamber stereo-betatron with a dose rate of 800-850 R/min · m. The dimensions of the focal spot at the target do not exceed 1 mm.

Automation of accelerator control increases intensity and simplifies maintenance. The latter is particularly important for accelerators used in industry and medicine. The report of A. A. Vorob'ev et al. (TPI, Tomsk) showed that the most advanced circuits for automation of industrial betatrons are extremum circuits. Extremum betatron regulation does not exclude the possibility of stabilizing its intensity at a single level. Such combined control was discussed in the report of I. Vas'kovskii, N. Ya. Makarov, et al. (Tomsk).

The accuracy of physical investigations with a synchrotron is increased if the instantaneous intensity of bremsstrahlung remains constant during an experiment. A system for intensity stabilization was achieved with the 680 MeV synchrotron at FIAN SSSR (Yu. I. Metal'nikov).

The report of B. I. Balyshev et al. (NIIEI, Tomsk) described a technique for simulating a system of extremum betatron regulation on an analog computer. Analog computers can also be used for studying the motion of charged particles in electric and magnetic fields. The report of N. Ya. Trikhanova (NIIYaF, Tomsk) presented a technique for calculating the channel for conveying electrons from the microtron to the 1.5 GeV synchrotron at TPI.

Six reports were presented on electrostatic generators, mainly dealing with studies of charge transport systems using dielectric conveyers having sealed-in conductors.

Great interest was aroused by the report of E. A. Abramyan on work at IYaF SO AN SSSR in the field of dc electron accelerators. A series of high-current electron accelerators has been built. The voltage on the tubes of these accelerators is supplied from commercial power sources through step-up transformers. The portion of the magnetic circuit of the step-up transformer on which the secondary winding is located is divided into sections. The magnetic circuit sections are insulated from one another, and are in the form of an annulus with radial loading. The accelerating tube is located inside the annulus. Such a magnetic circuit significantly increases the electrical stability of the step-up winding, and makes it possible to raise the voltage on the tube to 1.5 MeV. The acceleration tube is also divided into sections, each section being supplied with permanent focussing magnets to increase current transmission. The electron beam has a cathode electrode which makes it possible to regulate the intensity and energy spread of the accelerated beam. With this accelerator, which has received the designation ELT-1.5, they have produced an electron beam 3-5 mm in diameter with an energy of 1.5 MeV, average power to 20 kW, and energy spread from 15 to 1%. The efficiency of the machine amounts to 90%.

A 1 MeV (ELIT-1) pulsed high-current electron accelerator has also been built. In this accelerator, they have used a Tesla transformer with a coupling coefficient between windings of about 0.6. A condenser bank is discharged into the primary winding through a thyratron. With a properly selected coupling coefficient, the highest voltage in the secondary winding, which is used for electron acceleration, occurs during the second half-wave. Regulating the electron current in a given manner by means of the cathode electrode, one can obtain monoenergetic beams by changes in loading. An electron beam with an energy of 1 MeV and 10 nsec duration was produced with the ELIT-1. Beam current reached 100 A/pulse. The energy spread was 1%. At the present time, they are preparing for commercial manufacture of such equipment.

A report presented by a group of authors from VNIIYaG (Moscow) discussed the possibility of using betatrons for the analysis of minerals. It was demonstrated that the γ-activation method can be used for the analysis of the composition of rock and ore samples. When using scintillation counters as detectors of induced activity, the sensitivity is 10^{-3}-10^{-2}% weight content of the analyzed element.

About 30 reports dealt with the use of electron accelerators in medicine and biology. Basically, the reports were concerned with beam therapy for cancer and the effect of γ-radiation on various biological objects.

A 25 MeV linear accelerator has been placed in operation at the Institute of Biophysics (Moscow) for studying he biological effects of radiation. Reports were presented giving a description of the basic characteristics of the accelerator and its beam.

O. A. Val'dner (MIFI, Moscow) delivered a report at the final plenary concerning the V International Accelerator Conference, which was held at Frascati in September, 1965. I. A. Grishaev (KhFTI, Kharkov) discussed the linear accelerators which are available at the Kharkov Physicotechnical Institute. At the present time, four accelerators are operating: at 5-40 MeV, 30-90 MeV, 100-300 MeV, and 400-2000 MeV.

The proceedings of the conference will be published in a separate volume.

XVI ANNUAL CONFERENCE ON NUCLEAR SPECTROSCOPY AND NUCLEAR STRUCTURE

N. A. Voinova

The regular conference on nuclear spectroscopy and nuclear structure was held during January, 1966, in Moscow. Physicists from the Soviet Union and from the socialist, and some capitalist, countries participated in the work of the conference. The scientists worked in plenary sessions in the following sections: properties of specific nuclei, properties of the lightest nuclei, theory of deformed nuclei, theory of spherical nuclei, β-and γ-processes, nuclear resonance reactions, photoreactions, neutron spectroscopy, nuclear fission, Coulomb excitation, applied nuclear spectroscopy, techniques of nuclear spectroscopy, and also in seminars on high-energy processes, on radiochemistry, etc. It is clear from this list that the group of problems which was discussed at the conference was very extensive. More than 300 papers were presented at the conference; approximately half of these papers were concerned with studies of the properties of specific nuclei. At the present time, nuclear theory involves three fields: the theory of finite Fermi systems as applied to the calculation of nuclear properties, which is being developed by A. B. Migdal's group (Moscow Engineering Physics Institute); the theory of the superconducting nucleus, which is being developed by V. G. Solov'ev's group (JINR); and the theory of the axially asymmetric nucleus, which is being developed by A. S. Davydov's group (Institute of Physics, AN UkrSSR). In all the theoretical papers, it was pointed out that in both light and heavy nuclei mixtures of wave functions were possible which represented both spherical and aspherical parts in a single state.

The conference sessions began with a review report by Migdal in which he discussed the application of the theory of finite Fermi systems to the calculation of nuclear properties: calculation of nuclear masses, calculation of magnetic moments, consideration of the effect of closely-spaced levels, etc. All the previous work of the Migdal group should be considered as the construction of a theoretical apparatus, and only now is this group turning to the "construction of a theory of the nucleus." The majority of the papers of this group which were presented at the conference was related to the substantiation of the method; however, also presented and compared with experiment were calculations of magnetic moments (V. M. Osadchiev and M. A. Troitskii) and of the probability of μ-capture in heavy nuclei (a paper by G. G. Bunatyan in which he obtained remarkable agreement with experimental data). The papers of the Solov'ev group were concerned with the analysis of mixtures in the ground and excited states of odd nuclei. It was shown that in states which are ordinarily considered single-quasiparticle, there is a significant admixture of collective-one-phonon states. This admixture often amounts to several tens of percent, which has an important effect on all the properties of these states, particularly on transition probabilities and on Coulomb excitation cross sections. The decoupling parameters "a" were calculated for nuclei with $K = 1/2$, and qualitative agreement with experiment was obtained. Some of the work of the group involved the investigation of the properties of isomeric states of transuranic elements having anomalously high fission probability. These isomers were discovered several years ago by S. M. Polikanov in the laboratory of G. N. Flerov (JINR) and ever since a search has been going on for the most accurate description of them. Solov'ev and his associates have calculated the properties of type 11^- and 12^- isomeric states, they have learned in which nuclei these states should occur, and they have calculated the properties of these states with respect to electromagnetic deexcitation; it has been established that these isomers must have deformation parameters approximately 30% greater than those of the ground state.

In the Davydov group, Davydov and V. I. Ovcharenko have completed work on the investigation of the effect of deformation in odd-odd nuclei during transitions to excited states on the probability of E-2 transitions between quadrupole collective excited states and on the average value of the electric quadrupole moment in excited states. As an example, calculated data for the Gd^{154} nucleus was compared with experimental data. R. M. Diamond (USA) reported interesting results which confirm Davydov's theory in the transition region from iridium to mercury.

Many papers were presented which dealt with the classical fields of α-, β-, and γ-spectroscopy. In the rare-earth region, fine structure of α-spectra was first observed on the JINR α-spectrometer (V. G. Chumin et al.).

Translated from Atomnaya Énergiya, Vol. 21, No. 2, pp. 145-146, August, 1966.

This fact is not unexpected since excited states exist in the daughter nuclei. However, the intensity of the transitions has not been calculated before. The ratio $\alpha_1/\alpha_0 = 1/1600$ found for α decay can serve as a check on the theory of α decay.

At the last conference, the work of L. A. Sliv's group (A. F. Ioffe Physicotechnical Institute, Leningrad) showed that isotopic spin was a good quantum number in both light and heavy nuclei. Therefore $0^+ \rightarrow 0^+$ β-transitions, which are allowed by spin and parity, should be completely forbidden by isotopic spin, and log ft $\rightarrow \infty$ for them (instead of 5 for allowed transitions). However, there are few β-transitions of this type. Two of them, in Lu^{170} and Eu^{156}, were studied by O. E. Kraft (LGU) and P. G. Hansen (Denmark). It was shown that log ft was 9-10, i.e., the forbiddenness from isotopic spin was not absolute; it is possible that the observed transition occurs because of a mixture of isotopic spins.

Two reports were presented at the conference, one by G. Scharff-Goldhaber (USA) and one by V. M. Lobashov (LFTI), which dealt with the problem of parity conservation in electromagnetic transitions, i.e., with the problem of the possibility of the mixing of a state I^- in an I^+ state. If such mixtures exist, they are undoubtedly very few. Scharff-Goldhaber, studying $L_I : L_{II} : L_{III}$ conversion in a Hf^{180} transition, observed a variation in the ratio for E1 transitions, which can be interpreted as a small mixture of an M1 transition, i.e., some nonconservation of parity. The existence of the effect is undoubted; however, other explanations of it are not excluded. Lobashov's group studied the circular polarization of γ-rays during the decay of unpolarized nuclei by the method of forward Compton scattering from magnetized iron using resonance discrimination and build-up of the periodic signal. Control experiments were performed which demonstrated the absence of an effect for clearly unpolarized Sc^{46} γ-rays (E2), and the presence of an effect of the expected magnitude with polarized γ-rays which were produced by scattering from magnetized iron or as electron bremsstrahlung. The circular polarization of γ-rays from the Ta^{181} nucleus (M1 transition, $h\nu = 482$ keV) was measured. Negative circular polarization was observed which, on conversion to activity of the Hf^{181} source, gives an estimate of the contribution to polarization from bremsstrahlung ($P = -0.5 \cdot 10^{-5}$). In addition, circular polarization of Lu^{175} γ-rays was studied. The value of circular polarization obtained was $+(4 \pm 1) \cdot 10^{-5}$. Additional control experiments were performed which showed that the addition of unpolarized γ-rays to a bremsstrahlung source did not change the results.

More than one hundred papers were devoted to a study of the properties of specific nuclei; in the majority of them, nuclei from lanthanum to iridium were investigated, and only a quarter of the papers were devoted to other nuclei. Considerable complication in the interpretation of experimental data was characteristic of the papers.

In the section on nuclear reactions, a very extensive development of optical model analysis of the nucleus was noted. It is important that the constants which are introduced in this theory formally become more physical; for example, one can now calculate the constants for the deuteron from the constants for neutron and proton. Considerable progress was noted in understanding the similarities in the behavior of the (n, γ) and (d, p) reactions, as well as (n, n') and (d, d'). The paper of Ferguesson (England, work done in Copenhagen) on the latter two reactions in U^{238} was of interest.

Tremendous progress was observed in the field of γ-spectroscopy. R. L. Gresham (Canada) and J. M. Hollander (USA) reported on measurements of γ-spectra using 154 cm^3 germanium detectors with very high efficiency and high resolution. Semiconductor spectrometers in the Soviet Union have considerably smaller germanium–lithium detectors: volume ~ 5 cm^3, and depth of active layer ~ 6 mm (Ya. Ya. Urbanets, JINR); nonetheless, there now exists the possibility of studying γ-rays from weak sources of ~ 0.01 mCi, particularly the γ-radiation from many neutron-deficient isotopes in which the conversion spectra have been well studied.

During recent years, β spectrometers have been built which have very high resolution: chiefly the new $\pi\sqrt{2}$ instrument of K. E. Bergquist (Sweden) with electrical compensation and the instrument of H. Daniel (FRG) which was reported on at the conference.

Several interesting reports were given in the plenary session on the last day of the conference. The review by A. F. Tulinov (MGU) covered a study of the effect of the crystal lattice on the nature of the motion of fast charged particles in monocrystalline specimens – the channeling effect – and the angular distributions of charged products of nuclear reactions when using a monocrystal as a target – the shadow effect. He discussed the possibility of using the effects produced by the interactions of fast charged particles with monocrystals in nuclear research and using the shadow effect in solid state physics. The report of O. I. Sumbaev (LFTI) described measurements of isotopic shifts in K_α x-ray lines for a group of neodymium and samarium isotopes. The values obtained were used to determine a quantity characterizing the compressibility of the nucleus. The value found, $\gamma_N = 1.05 \pm 0.08$, corresponds to the uncompressed nucleus.

In his closing remarks, the chairman of the conference, B. S. Dzhelepov, noted the rapid development of experimental techniques in nuclear spectroscopy which has taken place in the past year, the even more rapid complication of data interpretation, and the requirement for future improvement in experimental methods and in the development of nuclear theory.

GAMMA RAYS AND CAROTIN

A. S. Nikolaeva

As the result of many years of experience in our country, a large amount of factual material has been accumulated on the economic prospects for the technique of pre-sowing irradiation of seed, which makes it possible to increase the yield of crops, to accelerate ripening and improve the quality of agricultural products grown from irradiated seed.

In order to exchange operating experience in the field of atomic energy applied to agriculture, Glavatom in conjunction with the Krasnodar agricultural board held a conference in March, 1966, which was attended by 280 individuals including agronomists from State farms, experimental farms, and test plots, and representatives from scientific institutions of the USSR Academy of Science, the USSR Ministry of Agriculture, and VASKhNILa.

During the past three years, a considerable amount of work on the practical use of ionizing radiations in agriculture has been carried on by institutions in the Krasnodar region. The Krasnodar combine for biochemical and vitamin preparations is developing a very important carotin vitamin preparation from vegetable raw materials. Because of pre-sowing γ-irradiation of carrot seed for a number of years, the yield has been increased and the carotin content increased. For example, in 1965, an additional 439 tons of carrots was obtained from 145 hectares sown with irradiated carrot seed.

At the State test plot for the Krasnodar region, experiments have been carried out on pre-sowing irradiation of seed from VIR-156, VIR-42, and Krasnodar 309 corn. After three years, the average experimental increase in gain was 200-360 kg/ha. In 1965, the experimental grain yield in the Abinsk test plot was 9400 kg/ha (the control yield was 6800 kg/ha); in the Labinsk test plot, the experimental yield was 9490 kg/ha (the control yield was 8300 kg/ha), i.e., 1190 kg/ha higher.

The green weight yield from experimental plots exceeded that from the control plots by 2200 and 3300 kg/ha for yields of 26,100 and 41,300 kg/ha, respectively.

From the data of the Institute for Oil- and Volatile-Oil-Producing Crops, an 18% additional yield of coriander and an 22% additional yield of linseed oil was obtained because of pre-sowing γ-irradiation of seed. By irradiation of the seed of Bezostaya winter wheat with a single 1000 R dose 10 days before sowing, an additional wheat yield of 340 kg/ha was obtained (data from the Krasnodar Agricultural Research Institute). Pre-sowing irradiation of early cabbage seed with a 2000 R dose increased the cabbage yield by 16-19% with earlier ripening of the heads and improved quality of yield (data from the Krasnodar Agricultural Institute).

The average yield of tomatoes during a six-year period at the North Caucasus Institute of Horticulture and Viticulture was 13,350 kg/ha. The highest yield, in 1964, was 28,600 kg/ha. In 1965, 33,800 kg/ha of tomatoes was obtained from an 8 ha plot sown with irradiated seed. Participants in the seminar pointed out that it was necessary to work on refinement of some of the factors influencing radiation effects (time interval between irradiation and sowing, radiation dose, moisture content of the seed, and method of storage of irradiated seed).

The collected reports of the conference will be published in 1966 by the Kolos press.

Translated from Atomnaya Énergiya, Vol. 21, No. 2, pp. 148-149, August, 1966.

THE MSh-P-5 BALL-AND-SWIVEL MANIPULATOR

G. I. Lukishov, V. P. Smirnov,
and K. D. Rodionov

Ball-and-swivel manipulators are general-purpose devices by means of which various operations with radioactive materials can be performed remotely in shielded boxes.

For the simplest operations, ball-and-swivel manipulators with manual tongs are usually used, and for more complicated work, ball-and-swivel manipulators with wrist units. Until recently, MShL-05 manipulators with wrist units were mainly used in radiochemical laboratories; they had important deficiencies: low load-lifting capacity (up to 0.5 kg), unsatisfactory operating reliability (frequent cable breakage), breakdown of box integrity during replacement of the sheath.

The deficiencies mentioned have been eliminated to a large extent in the construction of the new, MSh-P-5 ball-and-swivel manipulator developed by the State Planning Institute of the State Committee for the Utilization of Atomic Energy. The MSh-P-5 manipulator (Fig. 1) consists of a shaft, ball, sealing sheath with fastening collar and instruments (a collection of interchangeable working units and holders for them). The designed 5 kg load-lifting capacity of the manipulator is assured by including in the construction of the shaft rigid mechanical elements instead of cables. The manipulator has five independent motions: 1) longitudinal motion of the shaft in the ball; 2) rotation of the shaft around the longitudinal axis; 3) tilting of the shaft in the ball within the limits of a 70° solid angle; 4) bending of the wrist from 0 to 90°; 5) motion of the plunger for controlling the working units (closing or opening the jaws of the clamp).

The shaft and ball can be fixed in any position. The manipulator shaft, which is of tubular construction, has a control level at one end and a wrist with working units at the other. By rotating the wheel for bending the wrist,

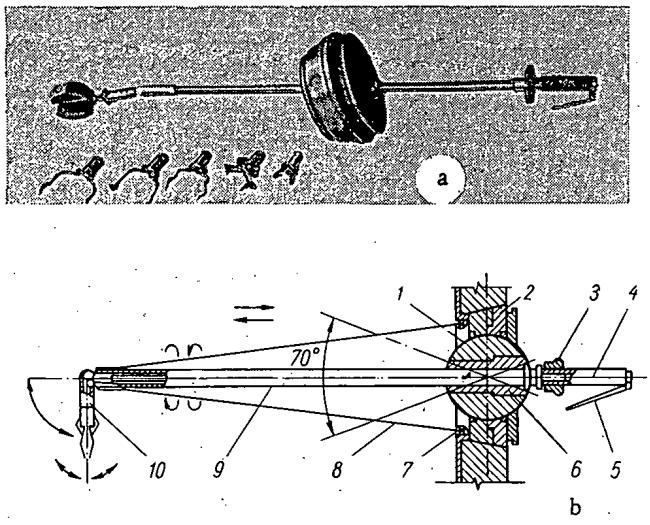

Fig. 1. MSh-P-5 ball-and-swivel manipulator: a) General view; b) mechanical diagram. 1) Ball; 2) ball housing; 3) wheel for bending wrist; 4) control handle; 5) lever for opening clamp jaws; 6) adapter; 7) sheathing installation collar; 8) sheathing; 9) shaft support tube; 10) wrist unit.

Translated from Atomnaya Énergiya, Vol. 21, No. 2, pp. 149-150, August, 1966.

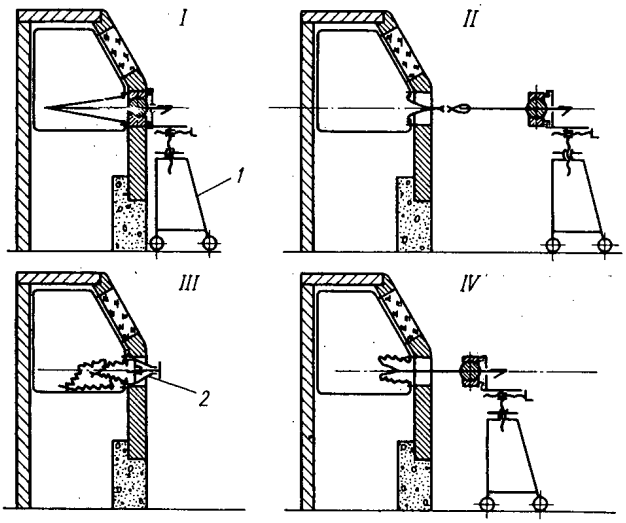

Fig. 2. Sequence of operations for replacement of manipulator (sheath): I) Original position before removing manipulator. Ball is disconnected from box and fastened to faceplate on cart; II) manipulator removed, sheath hermetically sealed and cut off; III) new sheath pressed into place, old one dropped inside box; IV) sheath fastened to shaft of manipulator, after which manipulator is installed in box opening. 1) Cart; 2) appliance.

the tubular rod produces a longitudinal displacement along the shaft through the mechanical action of a nut and screw combination, and bends the wrist to the corresponding angle. Closure of the clamp jaws is produced forcibly by springs installed in the wrist unit, and opening by pressure on the lever of the control handle. All motions of the shaft are easily performed with one hand.

The ball has a demountable housing in which the ball is mounted in bearing rings. A demountable bushing is provided inside the ball for installing the shaft.

Typical balls are designed to be equivalent to shield (cast iron) thicknesses of 50, 75, 100, and 150 mm in accordance with the standardized series of thicknesses for the front walls of shielded boxes [1]. All the balls have standardized seating dimensions assuring the installation of standard gloves in place of manipulators when necessary.

The manipulator is isolated from the box environment by a special conical sheath. The narrow end of the sheath is fastened to the wrist of the shaft, and the wide end has an elastic collar and is fitted on a special ring which is installed in the box opening. In this way, the sheath is maintained in position by the elastic forces of the collar. Such a sheath fastening makes it possible to replace it by means of simple equipment without disturbing the integrity of the box. Figure 2 shows the sequence of operations for replacing a sheath or changing manipulators. The installation of gloves in place of a manipulator is done in similar fashion. In that case, a glove is pressed into place instead of installing a sheath in carrying out operation III. A special cart is provided for operational convenience in changing manipulators.

A typical group of working instruments for a manipulator consists of interchangeable clamps, pincers, and hooks which are in special pockets normally located on the rear wall of the box. Furthermore, the pockets are arranged along the axis of the shaft making it easy to do remote replacement of these instruments during operation.

The MSh-P-5 ball-and-swivel manipulator is commercially manufactured by the Red Tool-Making Factory (Kirov), and can be obtained through the All-Union Isotope Association.

LITERATURE CITED

1. G. I. Lukishov et al., Ball-and-swivel manipulators, Department Standard ON-10, 5-65 (State Planning Institute, State Committee for the Utilization of Atomic Energy).

FRENCH EXHIBITION OF MEASURING INSTRUMENTS AND ELECTRONICS

Thirty-two French companies showed the results of their efforts in the production of measuring and electronic instruments from May 12 to May 21, 1966, in Leningrad. A considerable part of the displays was instruments and equipment used in nuclear engineering and also for use with radioactive isotopes in industry, medicine, and science.

In particular, one ought to mention the display of the Nucleometer company which showed radioisotope instruments for automatic monitoring and control of technological processes, including gauges for thickness, level, and sulfur content in petroleum products, which had interesting structural features. For example, the thickness gauge X, which was designed for monitoring the thickness of cold-rolled metallic sheets of steel and copper in the range from 0.1 to 8 mm and of aluminum from 0.02 to 10 mm, uses an isotopic source of x-radiation operating on the principle that x-radiation is produced by the deceleration in metal targets of β-particles emitted by Pm^{147} or tritium.

The radiation is detected by means of a scintillation counter. Accuracy is 2-5% of the monitored value. The source is fastened in a special head above the rolled strip, and can be swung around the axis of the tube to which the head is fastened making it possible to soften the shock produced, for example, with rupture of the rolled strip. The instrument is supplied with readouts on digital lights, strip charts, and meters. The firm also manufactures and installs radioisotope thickness gauges for paper, film, coatings, etc. During the years of its existence, the firm has manufactured and installed more than 300 different thickness gauges, including an instrument for measuring the thickness of zinc plated on iron. In this case, control of coating thickness is accomplished by recording the intensity of the characteristic radiation of zinc excited by a source of soft γ-radiation from Am^{241}. The firm has developed a laboratory instrument, the PR-2 Profilograph, by means of which the profile of sheet materials having weights of 1-2000 g/m^2 is measured. The instrument detects changes in material weight per m^2 from established values within a time of not more than 2 min.

The Intertechnic company demonstrated multichannel and multiparameter analyzers with 400 and 4096 channels having magnetic memories and various devices which are well known to our readers.*

Various devices for the detection of α-, β-, γ-, and neutron radiation were demonstrated by the Snap firm; of interest was a single-channel transistorized spectrometer providing a measurement of counting rate and of count in a set energy region of the radiation, spectrometers with automatic recording of results, and an instrument to determine the activity of solid and liquid samples. The resolving time of the scaling circuit of an analyzer with a capacity of 10,000,000 counts is more than 1 μsec, and for the entire instrument 5 μsec. For treatment of results and for analysis of results in the case of the existence of a definite signal at noise level, an ART-1000 electric signal analyzer having 1024-channel memory with ferrite cores is used. The analyzer has four standard programs which facilitate the handling of measurements.

The Thomson-Houston combine presented several dosimetric instruments, an electron-optical converter for x-ray images, and high-output power tubes and ignitrons used in accelerator engineering. A distinguishing feature of the dosimetric instruments was ionization chambers with tissue-equivalent walls made of polymer materials. An extremely interesting TN-9431 electron-optical converter had an entrance field diameter of 300 mm and exit field diameter of 22 mm, and produced an increase in image brightness of 8000.

The Sojev company showed various vacuum devices, including a PEB absolute differential interference manometer system. Fabry-Perot plates and the free surface of a liquid form a wedge for which the spacing between sides is very small and changes as a function of pressure with a resulting change in the interference pattern produced by a monochromatic source. In the presence of oil and mercury, the instrument makes it possible to measure pressure in the 10^{-4} to $2 \cdot 10^{-1}$ mm range with an accuracy of $2.4 \cdot 10^{-5}$ mm.

*Atomnaya Énergiya, 17, 232 (1964).

Translated from Atomnaya Énergiya, Vol. 21, No. 2, pp. 151-152, August, 1966.

Photodosimeters, emulsions for recording nuclear particles, and films for industrial radiography and roentgenography were shown by Kodak-Pathé.

Visitors were greatly interested in the general-purpose A-110 analog computer of the Analac company, which was designed for the solution of various equations or systems of equations. The machine has an input device, a two-coordinate recorder with 12 recording channels, and an automatic readout device with an accuracy of $1 \cdot 10^{-4}$ on six digital lights.

One ought to mention the MS-46 probe microanalyzer of the Kameka company with auxiliary equipment which enables one to analyze the content of low atomic number elements starting with boron ($Z = 5$).

All the apparatus and instruments shown at the exhibition were characterized by attractive appearance and high-quality assembly.

BRIEF COMMUNICATIONS

Collaboration of socialist countries. At Dubna, in June, 1966, there was held the tenth session of the SEV permanent commission on the use of atomic energy for peaceful purposes in which representatives from Bulgaria, Hungary, GDR, Poland, Rumania, the Soviet Union, and Czechoslovakia participated.

The commission discussed problems of collaboration in the fields of reactor science and engineering, nuclear power, nuclear instrument construction, shielding technology, and isotope production and use.

Rumanian exhibition in Moscow. At the economic exhibition of the Rumanian Socialist Republic in Moscow, which was held from May 4-17, 1966, a set of shielded laboratory equipment for working with α- and β-active isotopes in medical and scientific institutions was shown.

The set consisted of an EMS-2 shielded box, which was made of plastic, with two working positions, a special rack for decontamination of laboratory glassware and pipettes, manual manipulators, remote pipettes, a collection of containers for storing and transporting isotope preparations, and various devices for facilitating the use of radioactive isotopes in medical practice. The apparatus present made it possible to accomplish such operations in the box with liquid radioactive materials as titration, dilution, analysis, etc.

For a maximum contamination of 50 mCi of I^{131} on the front wall of the EMS-2 box, the maximum dose rate with shielding present was 0.25 mR/h.

The box was installed on a special stand, and the combination had the following external dimensions: height, 1485 mm, length, 1860 mm, and maximum width, 610 mm.

At the Swedish industrial exhibition, which was held in Moscow during May, 1966, the firm of Landis and Geer showed a series of instruments designed for working with isotopes in science and industry, including a paper thickness gauge and spectrometers. Among the instruments shown, mention should be made of a device for automatic monitoring of air contamination by radioactive materials. This device makes it possible to measure Sr^{90} concentrations down to $5 \cdot 10^{-17}$ Ci/liter and Pu^{239} concentrations down to $2 \cdot 10^{-17}$ Ci/liter. Detection is carried out by means of a counting tape 80 mm wide through which air is pumped. The tape is 30 m long, and moves with speeds of 1-16 mm/h. With a tape speed of 1 mm/h, the detector registers 16 cts/min corresponding to a Sr^{90} concentration of 10^{-16} Ci/liter. The device operates at environmental temperatures from -20 to 45°C.

In the demonstration hall of the Isotope store, Swedish specialists gave a lecture on the industrial uses of isotopes and nuclear radiations.

Collaboration is increasing. A delegation of the directors of the French Atomic Energy Commission headed by B. Goldschmidt arrived in the Soviet Union on April 30, 1966 at the invitation of the USSR State Committee on the Utilization of Atomic Energy. The delegation came to discuss problems of collaboration in high-energy physics.

As the result of two exchanges of delegations during 1965, Soviet and French physicists concluded that there was mutual interest in collaborating on research at the Serpukhov accelerator using the French 6-m^3, large liquid-hydrogen bubble chamber.

French and Soviet representatives discussed the following questions: 1) collaboration in high-energy physics (installation of the French 6-m^3, large liquid-hydrogen bubble chamber at the 70 GeV accelerator in Serpukhov); 2) the performance of joint research using the accelerator beam in the liquid-hydrogen bubble chamber.

They agreed that the French should set up a liquid-hydrogen chamber in the USSR along with the necessary equipment for its operation, and that French specialists, with the participation of Soviet engineers and technicians, should assemble and adjust the chamber. The Soviet was made responsible for the production of intense beams from the 70 GeV accelerator.

Both sides agreed that collaboration between the scientists at Serpukhov and the Laboratory for High-Energy Physics at Saclay ought to be carried out within the framework of a protocol in addition to which there will be set up a technical appendix explaining the technical and engineering aspects of the collaboration.

Translated from Atomnaya Énergiya, Vol. 21, No. 2, pp. 154-155, August, 1966.

In concluding remarks, B. Goldschmidt expressed satisfaction with regard to the atmosphere at the negotiations. He also expressed the wish that the protocol on collaboration in high-energy physics be signed in Paris, and invited the directors of the USSR State Committee for the Utilization of Atomic Energy to come to France for the signing.

Italian physicists in the USSR. During March, 1966, a delegation of Italian scientists concerned with the problems of controlled thermonuclear reactions and plasma physics was in the Soviet Union. This was the first delegation coming to the USSR in accordance with the agreement signed October 22, 1965 in Moscow on collaboration in the peaceful use of atomic energy between the USSR State Committee on the Utilization of Atomic Energy and the National Committee for Nuclear Energy of the Italian Republic. The delegation was headed by Professor Bruno Brunelli, Director of the Laboratory of Ionized Gases at Frascati.

During their stay in this country, the delegation visited the I. V. Kurchatov Institute of Atomic Energy and the P. N. Lebedev Institute of Physics, USSR Academy of Science, in Moscow, as well as other research institutes in the cities of Sukhumi, Kharkov, and Novosibirsk.

Through their visits to the institutes and laboratories, the visitors became familiar with the work in plasma physics being carried on in the USSR. Thus, at the Sukhumi Physicotechnical Institute, the Italian scientists were shown the results of work on plasma behavior in combined high-frequency and steady fields of toroidal and rectilinear configuration, various plasma diagnostic methods used at the institute (microwave, optical, and laser), studies of Raman scattering of electromagnetic waves in plasma, studies of plasma heating under bunch instability conditions, and other work. At the Kharkov Physicotechnical Institute, the delegation heard about studies of collective processes in the interaction of electron beams with plasma, work on the interaction of plasma bunches with magnetic fields, and experiments on high-frequency heating of plasma. At the Institute of Physics, USSR Academy of Science, in Moscow, the Italian scientists were shown equipment with which experiments were being performed on the injection and confinement of plasma in stellerator magnetic fields, and experiments on the production of plasma by means of lasers. In Novosibirsk, the visitors were acquainted with work on plasma heating with shock waves and the production of very-high-intensity fields by explosive methods.

At the I. V. Kurchatov Institute of Atomic Energy, the scientists learned about experiments on the storage of hot plasma in the PR-5 and Ogra-II composite traps, about studies of ohmic heating and plasma confinement in toroidal devices like Tokamak, high-frequency methods of plasma stabilization, etc.

At the institutes, discussions and seminars were held at which the Italian and Soviet scientists gave interesting reports. For example, Dr. Hugo Ascoli Bartoli spoke of recent results in his work on plasma production by irradiating deuterium ice with a laser and on the use of lasers for plasma diagnostics.

A return visit to Italy by a delegation of Soviet scientists in order to learn of the work of the Italian scientists is planned for the end of 1966.

BIBLIOGRAPHY

Molecular Beams. Edit. by John Ross. New York–London–Sydney. Interscience Publ., a division of J. Wiley and Sons, 1966, 420 pages.

This is the 10th volume in a series entitled "Advances in Physical Chemistry" published by Interscience. It contains review articles on research covering collisions of molecules, atoms, and ions in beam methods. Two articles deal with elastic scattering, two articles with reactions involving neutral atoms and molecules, two articles with ion reactions, two articles with charge transfer phenomena and with ion-neutral reactions. There are also articles on inelastic scattering of metastable atoms, determinations of atomic polarizabilities, and supersonic beam techniques. The literature covered in the articles extends to 1964 inclusive. The volume will be of unquestionable value for systematic survey and reference.

Progress in Nuclear Techniques and Instrumentation. Edit. by F. Farley. North-Holland Publ. Co., Amsterdam.

This book is the first volume in a proposed series on experimental techniques in nuclear physics. The editing staff and the panel of authors hope that the publication will be of interest not only to specialists in the field, but to a wider audience as well. It is for this reason that each article is tailored to cover the topic fully, from the basic principles to the latest developments. This volume will be devoted to techniques in the physics of the nucleus and to high energy physics, but will also serve as a guide to experimental techniques per se, so that the object of the research is relegated to the background and is treated only for illustrative ends.

This approach, which contrasts sharply with the classic type of references such as E. Segre's Experimental Nuclear Physics, seems to be a welcome innovation. The unavoidable use of cumbersome, expensive, and complicated instrumentation in experiments has meant that a large number of physicists and engineers have to become totally occupied with the invention, development, and improvement of the equipment, and are left at a certain distance from the very experimental physics for which the equipment is being designed in the first place. (It is sufficient to recall accelerator physics in this context, a pursuit which has become an independent field in its own right.) We can assume that the book being reviewed here will become a useful reference filling a need felt most acutely by precisely this group of specialists.

The book consists of six extended tutorial review articles written by known European and American scientists. It is important to note that the first review articles,"Sector-focused cyclotrons" (J. Richardson), departs somewhat from the basic contents of the volume. This article is written on a high scientific level and reflects the latest progress in the field (up to 1964). But accelerators are deserving of an entire volume reserved for that field alone in this series, since they are the basic instruments of experimental physics. It is not clear from that standpoint why the first article in the first volume would be reserved precisely for sector-focused cyclotrons, which occupy a rather modest place in the family of accelerators.

Richardson's article is written more or less along the lines indicated above: a historical survey, a concise presentation of focusing theory, and coverage of the engineering features of machines of several types. The fairly detailed sections on magnetic field measurements, beam properties, and particle extraction are noteworthy. Negative ion cyclotrons are one of the latest modifications of this type of accelerator reviewed in the article. Meson factories are mentioned only in passing, and this is one shortcoming of the article. The author concludes with detailed tabular material on sector-focused cyclotrons under construction or presently commissioned, and with a catalog of computer programs for details in the design of this type of facilities.

The next two articles are "Polarized ion sources and acceleration of polarized beams" (J. Dixon) and "Polarized targets" (G. Shapiro). These two entries deal with one of the most difficult problems in present-day experimental technique. The first article describes only one method for separating polarized beams by the use of nonuniform magnetic fields; this method is now in practical use. A strong point of this article is the detailed treatment of many engineering problems and the detailed description of equipment in use in various laboratories.

Translated from Atomnaya Énergiya, Vol. 21, No. 2, pp. 156-159, August, 1966.

Beam depolarization in cyclic accelerators is also touched upon but only cursorily. The article is indubitably useful as reference material, but one should expect a broader treatment of the physical concepts underlying, at least in principle, alternative methods for separating polarized beams. Shapiro's article is interesting in this respect, with its laconic but quite lucid survey of the widest variety of methods for fabricating polarized targets, starting from the most advanced high-frequency technique and ending with optical pumping of gaseous targets and suggestions on the possible use of superconductors. On the other hand, the author was obliged to abridge much of the portion devoted to targets now in use, even though one of these, the one used at the Lawrence Radiation Laboratory (Berkeley, Calif.,USA), is described in close detail.

The article "Computing systems for processing experimental data" (R. Spinrad) goes a long way in filling the present gap in review literature on this topic. The use of automatic data processing systems for handling experimental data is not only desirable, but simply indispensable, particularly in work with very-high-energy accelerators of the latest designs. The author sketches the overall problems encountered in the use of computers and in the choice of computer parameters in a brief article, with a style accessible to the nonspecialist. The value of the article is enhanced by the treatment of specific computer systems now in practical use, but the data on which the article is based takes us only to 1963.

The concluding two articles in the volume are devoted to recording techniques. The first (G. de Carvalho) describes techniques for fabricating and processing nuclear photographic emulsions in detail, with attention to specifics in the recording of different species of particles. The main burden of the article is preceded by a detailed review of facts related to photochemical processes. The last article(G. Charpac, L. Meusonnier, J. Favier) discusses various aspects of the performance of bubble chambers, which have lately become a major tool in the experimental physics of elementary particles.

A brief rundown of the main topics covered makes it clear that the choice of materials, except for the leading article, is mot fortunate. The articles come with a generous bibliography up to data as of the end of 1964. Work carried out in the USSR is adequately reflected and covered. There are no similar books of a review type in our literature on experimental techniques. Translation of this book with an expansion of the bibliography to cover later work, and possibly with some abridgment of the test, would be both timely and rewarding.

Shielding for High-Energy Electron Accelerator Installations. US National Bureau of Standards Handbook 97; Department of Commerce, 1964, 166 pages.

New recommendations by the US NBS consist of five principal sections. Section 1 gives a brief rundown on primary and secondary ionizing radiations occurring when electron accelerators are operated, and formulates radiation safety problems to be coped with in the building and operation of accelerators. Section 2 presents a concise account of basic shielding requirements. Most of the factual material is presented compactly in section 3, dealing with the characteristics of the primary beam and the secondary emissions. An ample array of graphs and tables for different energies and beam currents of accelerated electrons impinging on targets of a wide variety of materials offers data on the intensity of the resulting ionizing radiations and on their energy and space distributions. The presentation is separate for electrons, bremsstrahlung, neutrons, and residual radioactivity in irradiated materials. Section 4 assembles recommendations on techniques for measurement of primary electron beams and secondary radiations, with a separate subsection devoted to units of measurements. Section 5 offers data on interactions of radiation with matter pertinent to shielding against electrons, protons, and neutrons. Special subsections deal with explosion hazard and incendiary hazard in irradiated materials and with radiation damage to electrical protection systems. The brochure ends with a list of notation and symbols and a list of related literature (mainly from British and American periodical literature) of 54 titles.

Secondary Shutdown Systems of Nuclear Power Plants. C. S. Walker.

This report is the seventh on the program of the Oak Ridge National Laboratory information center on nuclear safety, set up in 1963 with the participation of the USAEC. The author separates the reactor control and protection system into two distinct systems: the primary system for normal operative control and shutdown, and the secondary system for scram shutdown and stoppage of the reactor in a variety of emergency situations.

The bulk of the report is devoted to a discussion of emergency shutdown systems in existing (mainly power) reactors. The reactors are grouped by type (PWR, BWR, channel type reactors, gas-cooled graphite-moderated reactors, organic-moderated organic-cooled reactors, sodium-cooled graphite-cooled reactors) and by country (Great Britain, France, Canada).

Protection systems for plutonium production reactors at Hanford and Savannah River are also described. Boron steel pellets loaded in the reactor channels are employed for scram shutdown in the old Hanford reactors; the NPD reactor uses samarium oxide pellets. The Savannah River reactors use a fluid scramming system which employs gadolinium nitrate solution. In general it is the fluid system which has been developed to the fullest extent in foreign reactor practice, and this is reflected in the report.

The material is descriptive and schematic on the whole, and the report constitutes in essence an attempt to classify the reactor protection systems currently in use by their general features and to describe them in general outline. From this standpoint the material cited in the appendices to the basic report is more practically oriented. The appendices furnish information on scramming systems for the basic USA reactors (30 reactors). Some of the technical data for those systems is presented. There is an extended list of reports and publications on this and related subjects.

Despite the somewhat schematic treatment and descriptive approach, the information contained in the report will be of use to reactor control specialists.

The Technology of Nuclear Reactor Safety. Vol. 1. Reactor Physics and Control. Edit. by T. I. Thompson and I. G. Beckerley. Cambridge, MIT press, 1964, 743 pages.

This book, written by a special team of scientists set up on the initiative of the USAEC, consists of 11 chapters and two appendices.

The second chapter (the slender first chapter is purely introductory) deals with physical aspects of nuclear reactor safety. It discusses relationships between cause and effect and the nature of the physical processes leading to emergency situations of different types.

The reasons for several emergencies and accidents occurring at reactors now shut down or still in operation are analyzed, and the effect of physical characteristics and of different reactor design elements on reactor safety is demonstrated. A wealth of useful information of a reference nature is presented, reactivity effects vital to reactor safety are discussed, and an analysis is made of the design of several operating reactors from the vantage point of operational safety.

The contents of this chapter supplement the concluding chapter of the book, which analyzes reactor accidents and critical facility accidents in detail, and discusses some accidents occurring with nonreactor equipment. Here we find, collected and generalized for the first time, practically all accidents occurring in the operation of nuclear reactors over the past two decades, with a minute analysis of the reasons and consequences of the accidents.

Chapter 3 deals with mathematical models and experimental techniques important in reactor dynamics research. Linear and nonlinear equations of reactor dynamics are discussed, as well as the programs most generally employed in computer solutions of these problems and techniques for measuring dynamic response of reactors.

Chapter 4 describes resonance neutron absorption in thermal and fast reactors. The temperature variation of the absorption of resonance neutrons in U^{238} and in Th^{232}, which is of importance for stable and safe reactor operation, is studied in detailed fashion, and there is an interesting review of theoretical and experimental data on resonance absorption of neutrons in fast reactors.

Chapter 5 is devoted to operating experience with subcritical and critical assemblies and zero-power reactors, as well as nuclear safety in the storage and reprocessing of nuclear fuel. There is a good deal of factual material and the effect of delayed neutrons on reactivity in various multiplying assemblies is examined.

Chapter 6 describes instruments for measuring neutron flux, for hydraulic and heat transfer measurements, various dosimetric devices, etc., plus a variety of monitoring and reactor control arrangements.

The chapter "Mathematical models of fast transients" discusses various reactor operating transients in response to different changes in reactivity common to reactors of all types, and techniques for investigating the behavior of reactors applicable equally when using simplified models with a linear variation in the energy liberated during the transient and models with a nonlinear variation of energy release, the latter providing a more accurate description of real processes.

The next three chapters (chapters 8-10) are devoted to the dynamics of water-cooled water-moderated reactors (pressurized water reactors and boiling water reactors), solid-moderated reactors, and fast reactors. Various methods of reactor control are examined for each of these reactor types, and an analysis is given by the dynamics

equations presented in a form typical of the reactors of a given type. Recommendations are offered on the resonance of control systems and on the requirements imposed on actuators in control systems. Chapter 10 is the most thorough coverage of fast reactor dynamics. The chapter on the dynamics of PWR and BWR (chapter 8) makes scant use of the rich experience available in the design and operation of those reactor types.

The two appendices store information of basic reactor parameters pertinent to safety in most power reactors around the world, and the reactor abbreviations used in the book.

The book is liberally illustrated and contains extensive bibliographic information at the end of each chapter.

In-Pile Dosimetry. Report of a panel held in Vienna, July 13-17, 1964. Vienna, IAEA (Technical reports, series No. 46), 1965, 108 pages.

This is an official report of a conference of experts on the topic, and the texts of 23 papers submitted on dosimetry of ionizing radiations in the reactor core. A brief official report (15 pages) contains clearly formulated descriptions of the most efficient flux and absorbed dose measurement techniques for work with gamma rays, thermal neutrons, intermediate-spectrum neutrons, and fast neutrons.

The papers presented are grouped in two sections. One contains reports on the present status of in-pile dosimetry country-by-country (Hungary, Great Britain, Canada, Netherlands, USSR, USA, West Germany, France, Yugoslavia), plus Euratom and the International Organization of Measures and Weights. The second section includes compressed reviews of papers on specific topics in in-pile dosimetry, such as investigations of radiation damage, techniques for recording gammas and neutrons (flux and dose recording), activation analysis techniques in neutron dosage determinations, and so forth.

The brochure ends with a list of the experts who attended the conference, and a list of authors.

Application of the Mössbauer Effect in Chemistry and Solid-State Physics. Vienna, IAEA, 1965, 267 pages.

This collection of articles includes 30 papers read at the symposium on applications of the Mössbauer effect in chemistry and in solid state physics. Most of the reports deal with the study of the structure of chemical compounds, the nature of chemical bonds, and measurement of isomeric shifts and quadrupole splittings in a large number of compounds.

Some of the reports describe the procedure and technique used in Mössbauer experiments. Some papers discuss applications of the Mössbauer effect to the study of magnetic properties of certain materials, and applications in analytical measurements. Of special note are two tutorial papers on observation of the Mössbauer effect in the actinides and in noble gases.

Some of the papers also deal with recoil of nuclei in various Mössbauer sources.

Pulsed Neutron Research. Vienna, IAEA, 1965. First Volume 698 pages, second volume 918 pages.

This two-volume edition collects the papers presented at the Karlsruhe May 1965 international symposium on pulsed neutrons sponsored by IAEA. The reports are grouped in seven sections.

The first section, on experimental investigations of nonmultiplying assemblies, opens with a review paper by K. Beckurts (West Germany), discussing the present state of the art in pulsed neutron research, some new investigative techniques, and giving the diffusion characteristics of some moderator materials. A paper submitted by L. Pal et al. (Hungary) analyzes techniques for processing experimental data to minimize the error in determinations of the diffusion characteristics by the pulsed method. The other papers in this section deal with measurements of various diffusion characteristics of moderators: ordinary water and heavy water, beryllium oxide, graphite, benzene, toluene, etc.

Papers in the following section discuss the theory of the propagation of pulsed neutrons in nonmultiplying systems. Transients in the measurement of the space, time, and energy distributions of neutrons are discussed (N. Korngold, USA). Techniques for calculating nonstationary spectra of neutrons obtained from pulsed neutron sources when different scattering models are employed are covered (J. Wood, Great Britain; S. Purohit, Sweden). Theoretical findings are compared to experimental data. Papers by R. Bednarz (Poland) and S. Albertoni et al. (Italy) provide a mathematical analysis of transport equations and take note of special aspects of their application to the study of compact specimens. Papers submitted by A. Stepanov (USSR) develop a graphical method for solving the problem of neutron transmission through a moderator with time-varying and space-varying scattering properties, and take up the transmission of cold neutrons through matter with quantum-mechanical effects con-

sidered. M. Kazarnovskii and Sh. Kenzhebaev (USSR) proposed a method for investigating the analytical relationship between neutron distribution and the variables of the scatterer nuclide. A report by H. Honeck (USA) presented a method for calculating the neutron diffusion coefficient for an anisotropic plane lattice, and a paper by G. De Uren (USA) offered a pulsed technique for determining the diffusion characteristics of moderators with neutron leakage effects taken into account.

Most of the papers in the third section deal with experimental studies of nonstationary and asymptotic spectra of slow neutrons in various pure and poisoned moderators (V. Mostovoi et al., S. Ishmaev et al., USSR; R. Creeter et al., E. Gertner, USA; M. Poole et al., Great Britian), and the moderator temperature dependence of the neutron spectra (L. Maiorov et al., USSR; R. Sinclair and P. Williams, Great Britain; G. Kahlfelz et al., West Germany, J. Neil et al., USA). The papers cite the diffusion characteristics of moderators and thermalization parameters of neutrons. Experimental data are compared to theoretical predictions based on various neutron scatterer models. Neutron spectra in multiplying systems (R. Slovaczek et al., USA; D. Rossberg, West Germany) are also taken up. A paper by J. Yang (USA) discusses physical models and calculating methods in widespread use to describe slow neutron scattering in moderators, and a paper by M. Poole (Great Britain) discusses applications of pulsed neutron sources in the measurement of neutron spectra in moderators and in reactor lattices. A review paper by A. Bergman (USSR) takes up moderation of pulsed neutrons and neutron slowing-down-time spectroscopy.

Application of pulsed neutron techniques to the measurement of the characteristics of thermal-neutron multiplying assemblies is the subject of several papers in the fourth section (volume II). Application of pulsed techniques to reactivity determinations, with deep subcriticality measurements included (E. Utzinger et al., Switzerland; M. Petrovic, Yugoslavia; T. Gozani and P. Demarmels, Israel and Switzerland), was discussed in many reports. Results of a determination of other important characteristics of reactors and critical assemblies were also made available: neutron multiplication factor, neutron age, diffusion coefficient and diffusion length, control rod worth, to name a few (B. Joshi, India; S. Chwaszczewski et al., Poland; J. Debreux, Belgium; S. Fousterre, France). Most of the experimental findings were compared with calculated data.

The next section dealt with aspects of the application of pulsed neutron techniques to the study of fast and intermediate systems (F. Storrer and M. Cadillac et al., France), results of measurements in fast neutron systems, rate of decay of neutron flux after the pulse (V. Cato et al., USA; G. Borgwaldt et al., West Germany; V. Patterson et al., Great Britain), and some characteristics of fast assemblies: neutron lifetime, subcriticality, neutron balance, kinetic characteristics (A. Bergstrom et al., Sweden; R. Comte et al., France). A few papers discussed fast neutron spectra in certain materials (D. Hayter et al., Great Britain; J. Russell et al., L. Gebian and S. Wilensky, USA).

The sixth section is on pulsed neutron sources. Here we find treatment of the design, performance, and experimental potentialities of fast pulsed reactors such as GODIVA (T. Wimet, USA), the fast pulsed reactor SORA developed by Euratom (W. Rajewski et al.), and the thermal pulsed reactor POLESTAR (J. McPea and R. Lamb, USA). The remaining papers deal with the design and characteristics of various neutron generators capable of producing a simulated neutron flux of varied intensity (up to $3 \cdot 10^{13}$ neutrons/sec) at regulated frequency and regulated pulse width.

The papers in the concluding section deal with research on the physical characteristics of moderators and multiplying media based on studies of different types of nonstationary processes (R. Uhrig, R. Perez, R. Booth, USA), a theoretical analysis of experiments using pulsed and modulated neutron sources (M. Cadillac et al., France; S. Carno, Italy). Results of an experimental determination of various characteristics of multiplying systems by recording and analyzing reactor noise are also treated (M. Edelmann et al., West Germany; S. Biermann and E. Clayton, USA), as well as modulated and pulsed neutrons (J. Wuhl et al., USA; W. Rotter, Belguim; R. Haas et al., Italy).

HANDBOOK OF GENERALIZED GAS DYNAMICS

By R. P. Benedict and W. G. Steltz

Westinghouse Electric Co., Steam Divisions and Drexel Institute of Technology

With the help of this book, all one-dimensional gas dynamics problems involving compressible and constant density fluids can be solved. Stressing a fundamental approach, this complete treatment of one-dimensional gas dynamics embodies a new recognition of the common bonds that unite separate flow processes. A unified description of the subject is achieved by means of a single table or chart for the particular gas under study which combines separate treatments for the various processes into one all-encompassing analysis.

243 pages 1966 $12.50

17 ill., 208 pages of tables

PLENUM PRESS DATA DIVISION 227 West 17th Street, New York, New York 10011

A DIVISION OF PLENUM PUBLISHING CORPORATION